

CHIRAL SEPARATIONS AND CHIROPTICAL SPECTROSCOPIC STUDIES

By

Peng Zhang

Dissertation

Submitted to the Faculty of the  
Graduate School of Vanderbilt University  
in partial fulfillment of the requirements  
for the degree of

DOCTOR OF PHILOSOPHY

in

Chemistry

August, 2006

Nashville, Tennessee

Approved:

Professor Prasad L. Polavarapu

Professor David M. Hercules

Professor David E. Cliffel

Professor Charles M. Lukehart

To My Family

## ACKNOWLEDGEMENTS

I would like to express my gratitude to my research advisors: Dr. Prasad L. Polavarapu and Dr. Tingyu Li for their support and guidance during my graduate study. I thank my committee members: Dr. David M. Hercules, Dr. David E. Clifffel, and Dr. Charles M. Lukehart for their constant encouragement and inspiration to my research work.

I appreciate the dedication of my research collaborators. Without them, some of my research work would not have been done. They are Dr. Junmin Huang from Mississippi State University, Mississippi state, MS (Chapter III); and Dr. Joseph Gal from University of Colorado, Denver, CO (Chapter VI).

I thank our group members: Dr. Yan Wang, Dr. Junmin Huang, Amanda Norick, Dr. Jordan Blodgett and Dr. Wenjian Lao in Li group and Ana Petrovic, Dr. Ganesh Shanmugam, Dr. Jiangtao He and Dr. Feng Wang in Polavarapu group for helpful discussion about various projects.

I also want to thank all faculty and staff members in the chemistry department for all kinds of support.

This work was supported by NSF (CHE0092922) and Vanderbilt University.

## TABLE OF CONTENTS

	Page
DEDICATION.....	ii
ACKNOWLEDGEMENTS.....	iii
LIST OF TABLES.....	vi
LIST OF FIGURES.....	viii
Chapter	
I. INTRODUCTION.....	1
Chirality .....	1
Chiral separation by HPLC.....	2
Chiroptical techniques .....	2
Instruments.....	7
Calculation .....	8
References.....	8
II. EVALUATION OF NEW L-PROLINE BASED CHIRAL STATIONARY PHASES FOR THE RESOLUTION OF ENANTIOMERS .....	10
Introduction.....	10
Experimental .....	14
Results and discussion.....	18
1. Influence of structural components on separation abilities of CSPs .....	19
2. Mobile phase .....	46
3. Comparison of CSP-7 with commercial CSPs.....	49
Conclusion.....	55
References.....	56
III. SPECTROSCOPIC RATIONALIZATION OF THE SEPARATION ABILITIES OF DECAPROLINE CHIRAL SELECTOR IN DICHLOROMETHANE-ISOPROPANOL SOLVENT MIXTURE .....	57
Introduction.....	57
Experimental.....	62
Results and discussion.....	64
1. Optical rotation .....	64
2. Electronic circular dichroism spectra.....	65



3. Infrared absorption spectra .....	67
4. Vibrational circular dichroism spectra.....	70
5. Rationalization of separation abilities of the decaproline chiral selector .....	71
Conclusion.....	75
References.....	76
IV. VIBRATIONAL ABSORPTION, VIBRATIONAL CIRCULAR DICHROISM AND SPECIFIC ROTATION STUDY ON DIALKYL TARTRATES AND THEIR CYCLODEXTRIN COMPLEXES.....	77
Introduction.....	77
Experimental.....	80
Results and discussion.....	85
1. VA and VCD study of dialkyl tartrates.....	85
2. Optical rotation study of dialkyl tartrates .....	89
3. DFT calculatiks.....	91
4. study of dialkyl tartrate cyclodextrin complexes .....	120
Conclusion.....	126
References.....	127
V. VIBRATIONAL CIRCULAR DICHROISM OF MATRIX ASSISTED AMINO ACID FILMS IN THE MID-INFRARED REGION.....	130
Introduction.....	130
Experimental.....	132
Results and discussion.....	136
Conclusion.....	150
References.....	151
VI. EXPERIMENTAL VERIFICATION OF THE VALIDITY OF VAN'T HOFF'S PRINCIPLE OF OPTICAL SUPERPOSITION.....	153
Introduction.....	153
Experimental.....	154
Results and discussion.....	156
Conclusion.....	160
References.....	160
Appendix	
A. MASS SPECTRA .....	162
B. NMR SPECTRA .....	167

## LIST OF TABLES

Table	Page
2-1 Comparison results for CSP-1 and CSP-2.....	21
2-2 Comparison results for CSP-3 ~ CSP-6 .....	27
2-3 Comparison results for CSPs with different number of L-proline units .....	31
2-4 Comparison results of CSP-5, CSP-6, CSP-9 and CSP-10 .....	35
2-5 Comparison results of CSPs with different end groups.....	42
2-6 Comparison results of CSP-7 and CSP-2 in two types of mobile phase systems ..	47
2-7 Comparison results of CSP-7 and three commercial CSPs .....	51
4-1 Geometries and electronic energies of the 22 conformers at B3LYP/6-31G* level .....	93
4-2 4B3LYP calculated Gibbs energies; populations, and specific rotations of five conformers of Isolated dimethyl ( <i>S, S</i> )-tartrate .....	96
4-3 Calculated frequencies ( $\nu_i$ ), dipole strengths ( $D_i$ ) and rotation strengths ( $R_i$ ) of five conformers of isolated dimethyl ( <i>S, S</i> )-tartrate at B3LYP/6-31G* level .....	100
4-4 Calculated frequencies ( $\nu_i$ ), dipole strengths ( $D_i$ ) and rotation strengths ( $R_i$ ) of five conformers of isolated dimethyl ( <i>S, S</i> )-tartrate at B3LYP/ aug-cc-pVDZ level .....	101
4-5 B3LYP/ 6-31G* calculated Gibbs energies; populations, and specific rotations of conformers of dimethyl ( <i>S, S</i> )-tartrate in CCl <sub>4</sub> .....	103
4-6 Calculated frequencies ( $\nu_i$ ), dipole strengths ( $D_i$ ) and rotation strengths ( $R_i$ ) of four conformers of dimethyl ( <i>S, S</i> )-tartrate in CCl <sub>4</sub> at B3LYP/6-31G* level .....	104
4-7 Experimental absorption and VCD band positions <sup>a</sup> of diethyl D-tartrate in CCl <sub>4</sub> and their correlation to B3LYP predicted values of isolated dimethyl ( <i>S, S</i> )-tartrate and the molecule in CCl <sub>4</sub> .....	106
4-8 B3LYP predicted specific rotation( $[\alpha]_D$ ) of dimethyl ( <i>S, S</i> )-tartrate and experimental intrinsic rotation( $\{\alpha\}_D$ ) of dimethyl D-tartrate .....	107

4-9	B3LYP/ 6-31G* calculated Gibbs energies; and specific rotations of conformers of clusters of dimethyl ( <i>S, S</i> )-tartrate with DMSO .....	112
4-10	Experimental absorption and VCD band positions of dimethyl D-tartrate in DMSO-d <sub>6</sub> and their correlation to predicted values of dimethyl ( <i>S, S</i> )-tartrate in DMSO .....	118
4-11	B3LYP/6-31G* predicted specific rotation( $[\alpha]_D$ ) of dimethyl ( <i>S, S</i> )-tartrate and experimental intrinsic rotation( $\{\alpha\}_D$ ) of dimethyl D-tartrate in DMSO .....	118
4-12	Comparison of intrinsic rotations between dialkyl tartate- cyclodextrin complexes and their corresponding 1:1 ratio mixtures.....	122
4-13	Binding constants of diethyl L-tartrate and cyclodextrin in solutions .....	126
5-1	Amino acids, their solubilities, concentrations and volumes of stock solutions used for solution and film VCD studies.....	135
5-2	VCD bands of amino acid films in the 1800-1200 cm <sup>-1</sup> region.....	148
6-1	Comparison of the experimental rotations with those predicted with the principle of optical superposition .....	159

## LIST OF FIGURES

Figure	Page
1-1 A block diagram of a conventional ECD instrument .....	4
1-2 A block diagram of a FT-VCD spectrometer .....	5
2-1 Structures of CSP-1 and CSP-2 .....	19
2-2 Structures of CSP-3 ~ CSP-6 .....	26
2-3 Structures of CSPs with different number of L-proline units .....	30
2-4 Structures of CSP-5, CSP-6, CSP-9 and CSP-10 .....	34
2-5 Structures of CSPs with different end groups .....	39
2-6 Chromatograms of TFAE separated by CSP-7 and three commercial CSPs .....	54
3-1 Structure of the decaproline oligomer (Boc-(Pro) <sub>10</sub> -OBn) .....	61
3-2 The chemical structure of the CSP with the decaproline oligomer as chiral selector .....	61
3-3 Specific rotation, $[\alpha]_D$ , of the decaproline oligomer in IPA/DCM solvent mixtures .....	64
3-4 ECD spectra of the decaproline oligomer in IPA/DCM solvent mixtures .....	67
3-5 Infrared absorption spectra of the peptide C=O groups of decaproline oligomer in IPA/DCM solvent system .....	68
3-6 Frequencies of peptide carbonyl band of the decaproline oligomer in IPA/DCM solvent system .....	68
3-7 IR spectra of the C=Os of Boc groups of the decaproline oligomer in IPA/DCM solvent system .....	70
3-8 VCD spectra of the peptide C=O groups of the decaproline oligomer in IPA/DCM solvent system .....	71
3-9 Representations of PPI (left) and PPII (right) structures constructed from six proline residues .....	72

3-10	Structure of 2,2,2-Trifluoro-1-[10-(2,2,2-trifluoro-1-hydroxy-ethyl -anthracen-9-yl) – ethanol (DiTFAE) .....	74
3-11	Retention factors (left panel) and separation factor (right panel) of DiTFAE achieved in the decapoline column in IPA/DCM solvent system.....	74
4-1	Vibrational absorption(bottom) and VCD(top) spectra in the Mid IR region in CCl <sub>4</sub> solution of both enantiomers of diethyl tartrate(0.017M).....	87
4-2	Vibrational absorption(bottom) and VCD(top) spectra in the Mid IR region in DMSO-d <sub>6</sub> solution of: (a) dimethyl D-tartrate(0.046M), (b) diethyl D-tartrate(0.040M), (c)both enantiomers of diisopropyl tartrate(0.035M).....	88
4-3	Vibrational absorption(bottom) and VCD(top) spectra in the C=O stretching region in D <sub>2</sub> O solution of: (a) dimethyl D-tartrate(0.048M), (b) diethyl D-tartrate(0.041M).....	89
4-4	Optical rotation ( $\alpha_D$ ) and specific rotation ( $[\alpha]_D$ ) of dimethyl D-tartrate, as a function of concentration in CCl <sub>4</sub> , DMSO and H <sub>2</sub> O solutions .....	90
4-5	The three principle conformations of dialkyl ( <i>R,R</i> )-tartrate around the C* -C* bond .....	91
4-6	The five lowest energy conformers of dimethyl ( <i>S,S</i> )-tartrate at B3LYP/6-31G* level in our study.....	94
4-7	The simulated absorption (top) and VCD (bottom) spectra with B3LYP/6-31G* for individual conformers of isolated dimethyl ( <i>S, S</i> )-tartrate and for the isolated molecule .....	98
4-8	The simulated absorption (top) and VCD (bottom) spectra with B3LYP/aug-cc-pVDZ for individual conformers of isolated dimethyl ( <i>S, S</i> )-tartrate and for the isolated molecule .....	99
4-9	Comparison of the experimental absorption (top) and VCD (bottom) spectra of diethyl D-tartrate in CCl <sub>4</sub> with predicted absorption spectra of isolated dimethyl ( <i>S, S</i> )-tartrate and the molecule in CCl <sub>4</sub> .....	105
4-10	Comparison of experimental ORD of dimethyl D-tartrate in CCl <sub>4</sub> and predicted ORD for isolated dimethyl ( <i>S,S</i> )-tartrate .....	107
4-11	Structures and electronic energies(with B3LYP/6-31G* basis set) of TransCOOCH <sub>3</sub> -(DMSO) <sub>2</sub> -0 and TransCOOCH <sub>3</sub> -(DMSO) <sub>2</sub> -1 .....	109
4-12	Structures of 6 conformers of clusters of dimethyl ( <i>S,S</i> )-tartrate with 2 DMSO molecules with hydrogen bonds between OH and S=O .....	111

4-13	The simulated absorption (top) and VCD (bottom) spectra for conformers of cluster of dimethyl ( <i>S, S</i> )-tartrate with 2 DMSO and for the molecule in DMSO (population weighted sum of conformer spectra) with B3LYP/6-31G*. ....	113
4-14	Comparison of the experimental absorption (top) and VCD (bottom) spectra of dimethyl D-tartrate in DMSO-d <sub>6</sub> with the simulated absorption spectra of Trans-COOCH <sub>3</sub> -(DMSO) <sub>2</sub> -1 and Trans-H-(DMSO) <sub>2</sub> -2 conformers and the predicted absorption spectra of dimethyl ( <i>S,S</i> )-tartrate in DMSO.....	117
4-15	Comparison of experimental ORD of dimethyl D-tartrate in DMSO and predicted ORD for dimethyl ( <i>S,S</i> )-tartrate in DMSO .....	119
4-16	Vibrational absorption(bottom) and VCD(top) spectra in the C=O region in D <sub>2</sub> O solution of diethyl L-tartrate α-CD complex(0.044M) .....	121
4-17	Vibrational absorption(bottom) and VCD(top) spectra in the C=O stretching region in DMSO-d <sub>6</sub> solution of (a)diethyl tartrate β -CD complex(0.040M); (b)diisopropyl tartrate β -CD complex(0.040M ) .....	121
4-18	Calorimetric titrations of (a) diethyl L-tartrate (100 mM) with α-CD (2 mM) in H <sub>2</sub> O; (b) diethyl L-tartrate (100 mM) with β-CD (2 mM) in H <sub>2</sub> O; (c) diethyl L-tartrate (450 mM) with α-CD (20 mM) in DMSO; (d) diethyl L-tartrate (150 mM) with β-CD (20 mM) in DMSO .....	125
5-1	Absorption and VCD spectra of L-proline at lower absorption.....	137
5-2	Absorption and VCD spectra of L-proline at higher absorption.....	138
5-3	Absorption and VCD spectra of films and of aqueous solutions (Left panel: alanine; right panel: proline) .....	142
5-4	Absorption and VCD spectra of films (left panels) and of aqueous solutions (right panels) for L-methionine and L-histidine.....	143
5-5	Absorption spectra of films (top) and of aqueous solutions (bottom) for L-phenylalanine and L-tryptophan.....	144
5-6	Absorption (bottom) and VCD (top) spectra of L-methionine, L-histidine L-phenylalanine and L-tryptophan in the film state.....	149
6-1	Structures of compounds <b>1-5</b> .....	156
6-2	Observed rotation ( $\alpha_{589}$ ) and specific rotation ( $[\alpha]_{589}$ ) of compound <b>1, 2, 4</b> and <b>5</b> as a function of concentration in CH <sub>2</sub> Cl <sub>2</sub> solutions.....	157
6-3	Two fragments of compound <b>4</b> .....	159

A-1	Mass spectrum of Compound <b>1</b> .....	163
A-2	Mass spectrum of Compound <b>2</b> .....	164
A-3	Mass spectrum of Compound <b>4</b> .....	165
A-4	Mass spectrum of Compound <b>5</b> .....	166
B-1	NMR spectrum of Compound <b>1</b> .....	167
B-2	NMR spectrum of Compound <b>2</b> .....	168
B-3	NMR spectrum of Compound <b>4</b> .....	169
B-4	NMR spectrum of Compound <b>5</b> .....	170

## CHAPTER I

### INTRODUCTION

#### **Chirality**

Chirality, the existence of mirror-imaged “right-“ and “left-handed” forms of an object, exists in many types of matter, from elementary particles and atoms to natural objects and galaxies. Molecular chirality is of particular importance because of its relevance to life. More than 90% of natural biomolecules are chiral and more than 70% of drugs in the market are chiral. Right-handed and left-handed molecules, known as enantiomers, often possess drastically different biological functions. In an extreme example, as in the notorious case of thalidomide, one could be beneficial and the other harmful.<sup>1a</sup> Since 1992, the US Food and Drug Administration (FDA) has been enforcing the policy of "racemic switch." If only one enantiomer has medical efficacy, either this enantiomer must be used singly, or the other enantiomer must be proved harmless before marketing.

So it is very important to develop methods to obtain single enantiomers, and to develop analytical techniques for determination of enantiomeric purity. It is also very necessary to develop analytical methods to determine the configuration and conformation of chiral molecules.



## **Chiral separation by HPLC**

Chromatography is the fastest, most expedient method to obtain the pure enantiomers of a racemate. Chiral chromatography is also the most widely-used analytical method to determine enantiomeric purity in the pharmaceutical industry.<sup>1b</sup>

Among all the chiral separation chromatographic techniques, HPLC has proven to be the most convenient, reproducible and widely applicable method. Most of the HPLC methods employ a chiral selector as the chiral stationary phase (CSP). There are basically five types of chiral stationary phase in common use in HPLC<sup>2</sup>: protein CSP, brush type CSP, cellulose and amylase CSP, macrocyclic glycopeptides CSP and cyclodextrin CSP.

Brush type chiral stationary phase has a lot advantages over other types of CSPs: a large number of choices of chiral selectors, excellent column durability, stability in both the reversed phase mode and the normal mode and universal solvent compatibility. Another advantage is that for a targeted analyte, specific structure of CSP can be designed and optimized to achieve very high enantio-selectivity.

In our study, we are focused on the development of new brush type CSPs with high efficiency and versatility.

## **Chiroptical techniques**

Chiroptical techniques<sup>3</sup> refer to optical techniques which use refraction, absorption or emission of anisotropic radiation for investigating chiral substances. Chiroptical techniques mainly include optical rotation at a fixed wavelength, optical rotatory dispersion (ORD), electronic circular dichroism (ECD), vibrational circular dichroism (VCD), Raman optical activity (ROA), and circular polarization of luminescence (CPL).

In our research, we have combined the use of optical rotation, ECD and VCD techniques and DFT calculations for conformational analysis of chiral molecules.

### ECD and VCD

Circular dichroism (CD) spectroscopy measures differences in the absorption of left-handed polarized light versus right-handed polarized light which arise due to structural asymmetry. The electronic transitions of a chiral molecule give rise to circular dichroism (CD) in the visible ultraviolet (VIS-UV) spectral region, which is called ECD, while vibrational transitions give rise to CD in the infrared region, which is VCD.

One of the earliest and most elegant papers dealing with various instrumental approaches for the measurement of ECD was published by Cotton in 1896.<sup>4</sup> In 1960 Grosjean and Legrand<sup>5</sup> introduced modulation technique to the measurement of CD. ECD spectrometers have been widely available for routine measurements since then. A diagram of a conventional ECD instrument is shown in Figure 1-1.<sup>6</sup>

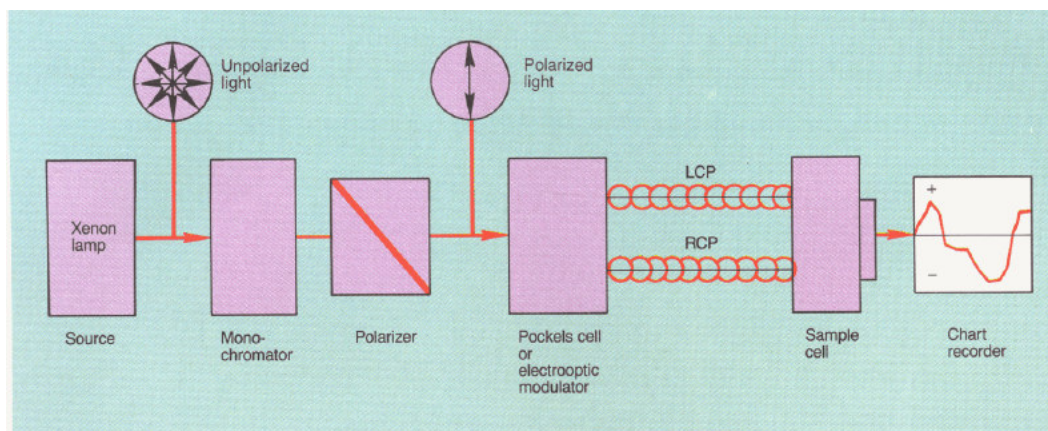


Figure 1-1 A block diagram of a conventional ECD instrument<sup>6</sup> (LCP and RCP are left and right circularly polarized light beams, respectively.)

The first VCD spectrum was measured on a dispersive instrument around 1975.<sup>7</sup> The first Fourier Transform (FT) VCD instrument was built around 1979.<sup>8</sup> The FT-VCD

instrument has throughput and multiplex advantages compared to a dispersive instrument. The application of dual polarization modulation technique further improves the baseline in VCD measurement.<sup>9</sup>

Figure 1-2 shows a general diagram of FT-VCD instrument. The infrared radiation passes through an interferometer and the light is then polarized by a linear polarizer and a photoelastic modulator (PEM), which is used to generate the circularly polarized radiation.. The circularly polarized light then passes through the sample and a second PEM, which cancels out the linear birefringence intensity. The light is finally focused on the detector. The signal is amplified by the pre-amplifier and separated by the electronic filter to a low frequency DC signal, which is a normal absorption spectrum, and a high frequency AC signal, which is related to the VCD spectra. Two lock-in-amplifier (LA) are used in measurement of the differential signal. The Fourier transform is done by the computer and the raw signal is demodulated to get the absorption and VCD spectrum.

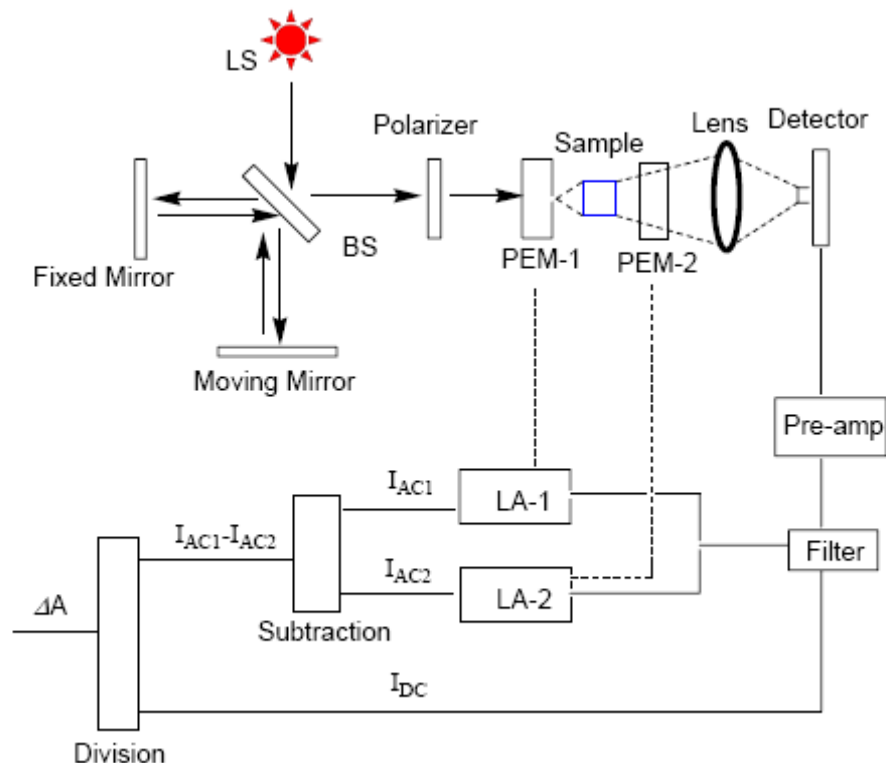


Figure 1-2. A block diagram of a FT-VCD spectrometer<sup>9</sup>

The interpretation of ECD and VCD spectra has greatly benefited from the development of theoretical chemistry, especially the development of density functional theory (DFT).<sup>10</sup> The theoretical quantity which corresponds to the normal absorption is dipole strength ( $D_{01}$ ) and the theoretical quantity which corresponds to the CD is rotational strength ( $R_{01}$ ). Their expressions are listed in Equations 1-1 and 1-2.  $\Psi_0$  and  $\Psi_1$  are the wave functions of ground and excited states respectively.  $\mu$  and  $m$  are electric dipole moment and magnetic dipole moment operators.

$$D_i = |\langle \Psi_0 | \mu | \Psi_1 \rangle|^2 \quad (1-1)$$

$$R_i = \text{Im}[\langle \Psi_0 | \mu | \Psi_1 \rangle \cdot \langle \Psi_1 | m | \Psi_0 \rangle] \quad (1-2)$$

By combining the experimental spectra with theoretical prediction, ECD and VCD can be used as a powerful tool in studying the absolute configuration and conformation of

chiral molecules. Furthermore, ECD and VCD can be used in conformational analysis of biological molecules, such as peptides, proteins and nucleic acids. In my study, VCD, combined with DFT calculation, is used to study the conformation of small chiral molecules. ECD and VCD are also used for conformational analysis of biomolecules.

### Optical Rotation

Optical rotation is a century old technique which measures the rotation of linearly polarized light after it passes through a chiral sample.<sup>11</sup> The sign of optical rotation is related to the absolute configuration of chiral molecules. Optical rotation plays an important role in the development of modern stereochemistry and is widely used in the organic labs. Although the measurement of optical rotation is very simple, the theoretical prediction of optical rotation is rather complex. The first *ab initio* prediction of optical rotation was published at 1997.<sup>12</sup> The density functional theory also was applied in prediction of optical rotation.<sup>13</sup> The quantum chemistry quantity related to optical rotation is the electric dipole-magnetic dipole polarizability tensor as shown in Equation 1-3.<sup>14</sup>  $\mu$  and  $m$  are electric dipole moment and magnetic dipole moment operators.  $\psi_s^0$  and  $\psi_n^0$  are the wave functions of ground and excited electronic state.  $\omega_{ns}$  relates to the excitations energy between  $n$  and  $s$ .  $\omega$  is the angular frequency of exciting radiation, which is usually the sodium D line.

$$G'_{\alpha\beta} = \frac{-4\pi}{h} \sum_{n \neq s} \frac{\omega}{\omega_{ns}^2 - \omega^2} \times \text{Im} \left\{ \langle \psi_s^0 | \hat{\mu}_\alpha | \psi_n^0 \rangle \langle \psi_s^0 | \hat{m}_\beta | \psi_n^0 \rangle \right\} \quad (1-3)$$

The specific rotation in units of  $\text{deg}\cdot\text{cm}^3\cdot\text{g}^{-1}\cdot\text{dm}^{-1}$  can be related to  $G'$  by Equations 1-4 and 1-5, where  $\bar{\nu}$  is wavenumber where the optical rotation is measured.  $n$  is refractive index and  $M$  is concentration in  $\text{g}\cdot\text{mol}^{-1}$ .

$$[\alpha] = 0.1343 \times 10^{-3} \beta \bar{\nu}^2 (n^2 + 2) / 3M \quad (1-4)$$

$$\beta = -\omega^{-1} (G'_{xx} + G'_{yy} + G'_{zz}) / 3 \quad (1-5)$$

In my study, optical rotation is used as a tool to research the conformation of small chiral molecules and biomolecules. The combination use of multiple chiroptical techniques will provide a powerful and convenient tool for stereochemistry research.

### Instruments

A Beckman HPLC system consisting of two 126 pumps, a 507 auto-sampler and a 166 UV detector, and controlled by Gold system, was used for all of the chromatography.

The ECD was measured on a JASCO J720 spectropolarimeter (Jasco, Easton, MD). The sample solutions (100  $\mu\text{L}$ ) were held in a circular quartz cell with a path length of 100- $\mu\text{m}$ .

The VCD was measured on a modified commercial Chiralir (BioTools, Wauconda IL) VCD instrument which has dual PEMs. The instrument has a ZnSe beam splitter (BS) and BaF<sub>2</sub> polarizer. The detector is a 2X2mm mercury cadmium telluride (HgCdTe) detector which needs to be kept at liquid nitrogen temperature. The PEMs are PEM-80 and PEM-90 (Hinds Instrument, Hillsboro, OR) without antireflection coating on the ZnSe optical element. Samples were held in variable pathlength cell with BaF<sub>2</sub> windows or fixed pathlength cell with BaF<sub>2</sub> windows.

The optical rotation was recorded on either Autopol III or Autopol IV polarimeter (Rudolph, Hackettstown, NJ). Samples were held in a 0.5dm cell with quartz windows.

More detailed experimental condition will be given out in the following chapters.

### Calculation

The theoretical prediction was carried out using Gaussian 98 or 03<sup>15</sup> software package.

More detailed calculation details will be given out in the following chapters.

### References

1. (a). Blaschke, G.; Kraft, H. P.; Fickentscher, K.; Kohler, F. *Arzneimittel-Forschung/Drug Research* **1979**, *29*, 1640. (b). Rouhi, A. M. *Chemical&Engineering News* **2003**, *81*, 45.
2. Beesley, T.E.; Scott, R.P.W. *Chiral Chromatography*; John Wiley & Sons: New York, 1998; pp221.
3. *IUPAC Compendium of Chemical Terminology*; 2nd Edition, 1997.
4. Cotton, A. M. *Ann Chim. Phys.* **1896**, *8*, 347.
5. Grosjean, M.; Legrand, M. *C. R. Acad. Sci. (Paris)* **1960**, *251*, 2150.
6. Purdie, N.; Swallows, K. A. *Anal. Chem.* **1989**, *61*, 77A.
7. (a). Holzwarth, G.; Hsu, E. C.; Mosher, H. S.; Faulkner, T. R.; Moscowitz, A. *Journal of the American Chemical Society* **1974**, *96*, 251. (b). Nafie, L. A.; Keiderling, T. A.; Stephens, P. J. *Journal of the American Chemical Society* **1976**, *98*, 2715.
8. Nafie, L. A.; Diem, M.; Vidrine, D. W. *Journal of the American Chemical Society* **1979**, *101*, 496.
9. Nafie, L. A. *Applied Spectroscopy* **2000**, *54*, 1634.
10. (a).Becke, A. D. *Journal of Chemical Physics* **1993**, *98*, 1372. (b). Becke, A. D. *Journal of Chemical Physics* **1993**, *98*, 5648.
11. Eliel, E. L.; Wilen, S. H.; Doyle, M. P. *Basic Organic Stereochemistry*; Wiley-

Interscience: New York, 2001.

12. Polavarapu, P. L. *Molecular Physics* **1997**, *91*, 551.

13. Stephens, P. J.; Devlin, F. J.; Cheeseman, J. R.; Frisch, M. J.; Rosini, C. *Organic Letters* **2002**, *4*, 4595.

14. Polavarapu, P. L.; Chakraborty, D. K. *Chemical Physics* **1999**, *240*, 1.

15. Frisch, M. J. T., G. W.; Schlegel, H. B.; Scuseria, G. E.; Robb, M. A.; Cheeseman, J. R.; Montgomery, Jr., J. A.; Vreven, T.; Kudin, K. N.; Burant, J. C.; Millam, J. M.; Iyengar, S. S.; Tomasi, J.; Barone, V.; Mennucci, B.; Cossi, M.; Scalmani, G.; Rega, N.; Petersson, G. A.; Nakatsuji, H.; Hada, M.; Ehara, M.; Toyota, K.; Fukuda, R.; Hasegawa, J.; Ishida, M.; Nakajima, T.; Honda, Y.; Kitao, O.; Nakai, H.; Klene, M.; Li, X.; Knox, J. E.; Hratchian, H. P.; Cross, J. B.; Bakken, V.; Adamo, C.; Jaramillo, J.; Gomperts, R.; Stratmann, R. E.; Yazyev, O.; Austin, A. J.; Cammi, R.; Pomelli, C.; Ochterski, J. W.; Ayala, P. Y.; Morokuma, K.; Voth, G. A.; Salvador, P.; Dannenberg, J. J.; Zakrzewski, V. G.; Dapprich, S.; Daniels, A. D.; Strain, M. C.; Farkas, O.; Malick, D. K.; Rabuck, A. D.; Raghavachari, K.; Foresman, J. B.; Ortiz, J. V.; Cui, Q.; Baboul, A. G.; Clifford, S.; Cioslowski, J.; Stefanov, B. B.; Liu, G.; Liashenko, A.; Piskorz, P.; Komaromi, I.; Martin, R. L.; Fox, D. J.; Keith, T.; Al-Laham, M. A.; Peng, C. Y.; Nanayakkara, A.; Challacombe, M.; Gill, P. M. W.; Johnson, B.; Chen, W.; Wong, M. W.; Gonzalez, C.; and Pople, J. A.; Gaussian, Inc.: Wallingford CT, 2004.



## CHAPTER II

### EVALUATION OF NEW L-PROLINE BASED CHIRAL STATIONARY PHASES FOR THE RESOLUTION OF ENANTIOMERS

#### **Introduction**

One of the most challenging goals relating to the use of enantio-selective HPLC for the resolution of racemic mixtures is the development of chiral stationary phases (CSPs) capable of separating the enantiomers of a wide variety of structurally different racemates. Through significant efforts by many research groups, a number of CSPs of efficiency and versatility have been developed, many of which are commercially available now.<sup>1</sup>

There are basically five types of chiral stationary phase in common use in LC<sup>2</sup>. The first type is the protein stationary phases.<sup>3</sup> These stationary phases were the first to be developed and usually take the form of natural proteins bonded to a silica matrix. These stationary phases are used with mobile phases with a high water content (mostly > 90%) and thus separations are largely by dispersive interactions. There are three commonly used commercial protein type stationary phases,  $\alpha_1$ -acid glycoprotein phase (CHIRAL-AGP), cellobiohydrolase (CHIRAL-CBH) and human serum albumin (CHIRAL-HSA). The second type of chiral stationary phase consisted of relatively small molecular weight chiral substances bonded to silica<sup>4</sup>. It is called brush type CSP. There are quite a large number of small chiral molecules that are used as chiral selectors for brush type stationary phase. These types of stationary phases can be operated either in the reversed phase mode or the normal mode. The most popular brush type stationary phase today is the Whelk-O1 CSP developed by Pirkle. The third type is cellulose and amylose

stationary phase <sup>5</sup>. Polymers of cellulose and amylose are derived to link appropriate interactive groups and then they are coated onto a silica support. Hexane-alcohol mixtures are usually employed as the mobile phase, so separations largely depend on polar interactions. There are more than 20 commercial columns available for cellulose and amylose phases. Among them, CHIRALPAK AD and CHIRALPAK OD are most widely used. The fourth type is the macrocyclic glycopeptides stationary phase introduced by Armstrong <sup>6</sup>. These are materials that contain a large number of chiral centers, together with molecular cavities in which solute molecules can enter and interact with neighboring groups. The macrocyclic glycopeptides are chemically bonded to silica gel. Three popular materials are Vancomycin and Teicoplanin and Avoparcin. The two best macrocyclic glycopeptides stationary phase are Chirobiotic V (Vancomycin) and Chirobiotic T (Teicoplanin). The fifth type is the cyclodextrin stationary phase.<sup>7</sup> The stationary phase is chemically bonded to a silica substrate. The cyclodextrin phases can be made from  $\alpha$ ,  $\beta$  or  $\gamma$ - cyclodextrins and offer a large number of chiral centers and contain a number of substantially deep inclusion centers that augment spatial selectivity.  $\alpha$ ,  $\beta$  and  $\gamma$ - cyclodextrins are the basis for the production of the CYCLOBOND I, CYCLOBOND II and CYCLOBOND III stationary phases, respectively.

Despite these advances in the development of CSPs, new CSPs with excellent versatility and enantio-discriminating abilities are still in great demands because more and more single-enantiomer chiral compounds are needed by chemical industry, especially drug industry. Chiral stationary phase method is still the best way to determine enantiomeric purity of chiral compounds. And it is also the fastest, most expedient method to obtain the pure enantiomers.

Brush type chiral stationary phase has some advantages over other types of CSPs. Firstly, there are quite a large number of small chiral molecules that are used as chiral selectors for this kind of stationary phase so it is very promising to design and develop new brush type stationary phases. And brush type stationary phases are covalently bonded to the silica, providing excellent column durability. Furthermore, brush type stationary phases are stable to use either in the reversed phase mode or the normal mode. They can stand most of the widely used solvents for HPLC. Another advantage is that for a targeted analyte, specific structure of CSP can be designed and optimized to achieve very high enantio-selectivity.

Our research is focused on the development of new brush type CSPs with high efficiency and versatility. L-proline structure is chosen as the key element in our design of new CSPs. Proline is a unique amino acid in many ways. Instead of having a primary amino group, as in other  $\alpha$ -amino acids, it contains a secondary amine. Because of the cyclic structure, rotation around the nitrogen- $\alpha$ -carbon bond is restricted. Also because of the cyclic structure, proline is not ideally suited for  $\alpha$ -helix or  $\beta$ -sheet conformation; instead, oligoproline and polyproline form unique helical conformations (polyproline I, or polyproline II, or both depending on preparation methods, states and solvents).<sup>8</sup>

Haurou et al prepared 4 CSPs containing benzyloxycarbonyl L-proline or *tert*-butoxycarbonyl L-proline as chiral selector<sup>9</sup>. The enantiomeric separation of a series of N-3,5-dinitrobenzyl amino acid esters was investigated using this CSPs. The influence of the amino acid, spacer and protective group of CSPs on the retention and selectivity was studied.

Pirkle et al also did some research on L-proline derived chiral stationary phases before<sup>10-14</sup>. They first designed two CSPs containing 3,5-dimethyl anilides of L-proline, which were used to separate the enantiomers of N-(3,5-dinitrobenzoyl)amino acid esters and amides and related analytes. They also investigated the effects of intercalative processes on chiral recognition with these two CSPs. Then they designed a CSP containing 3,5-dimethoxyl anilides of proline for use in the preparative chromatographic separation of enantiomers of two chiral selectors for commercial CSPs.

For the L-proline based CSPs in the previous study, there is only one residue of L-proline in the structure of chiral selector. In our study, more residues of L-prolines are adopted in the design of CSPs. Peptide structures are formed for the chiral selectors of CSPs with more residues of L-prolines. It turns out from our results that these peptide structures are one of the key factors to achieve good versatility and enantio-selectivity for these CSPs. In previous study, the chiral selectors were prepared in solution and then were coupled to the silica gel support. In our study, solid phase synthesis technique is adopted to prepare the CSPs. It is a simpler and more efficient method without the purification of compounds between steps in the synthesis. In previous study, separation of quite a narrow range of racemic compounds were investigated for the L-proline based CSPs. A wide range of analytes with diverse structures are chosen to test the versatility of L-proline based CSPs in our study.

In our research, 17 L-proline based CSPs, which have different support, linker, number of L-proline units and end group were designed, prepared and evaluated. 22 kinds of analytes were used to investigate the versatility and enantio-selectivity of these CSPs. The influence of these structural components on separation abilities of CSPs was

investigated. And effects of modification of L-proline residue and mobile phase system on the versatility and enantio-selectivity of CSPs were also investigated. The versatility and separation ability of the best CSP among them was compared with 3 commercial CSPs to study the possibility of developing this type of CSP into commercial CSPs.

## Experimental

### General supplies and equipment

Fmoc-L-proline-OH, N- $\alpha$ -Fmoc-O-*t*-butyl-trans-4-L-Hydroxyproline, and coupling reagents were purchased from NovaBiochem (San Diego, CA). All other chemicals and solvents were purchased from either Aldrich&Sigma (Milwaukee, WI), Fluka (Ronkonkoma, NY), or Fisher Scientific (Pittsburgh, PA). For three commercial chiral columns: CHIRALPAK OD-H(150×4.6 mm), CHIRALPAK AD-H(250×4.6 mm) were purchased from Daicel Chemical IND., LTD and Whelk-O2(250×4.6 mm) was purchased from Regis Technologies, Inc.(Morton Grove, IL).

For analytes, 1,2,3,4-Tetrahydro-4-(4-methoxyphenyl)-6-methyl-2-thioxo-5-pyrimidinecarboxylic acid ethyl ester, 1,2,3,4-Tetrahydro-4-(4-hydroxyphenyl)-6-methyl-2-thioxo-, 5-Pyrimidinecarboxylic acid ethyl ester, 5-Methyl-5-(2,5-dichloro)phenylhydantoin and 5-Methyl-5-phenyl hydantoin were synthesized by Dr. Yan Wang in our group. Temazepam was offered by Dr. David M. Hercules. Mephentoin was purchased from MicroSource Discovery Systems, Inc (Gaylordsville, CT). Other analytes were purchased from Aldrich&Sigma(Milwaukee, WI).

HPLC grade Kromasil silica gel (particle size 5  $\mu$ m, pore size 100 Å, and surface area 298 m<sup>2</sup>/g) was purchased from Akzo Nobel(EKA Chemicals, Bohus, Sweden). PRP-1

resin (particle size 7 $\mu$ m, pore size 100 Å, and surface area 396 m<sup>2</sup>/g) was purchased from Hamilton (Reno, NV, USA). A Beckman HPLC system consisting of two 126 pumps, a 507 auto-sampler and a 166 UV detector, and controlled by Gold system, was used for all of the chromatography. Elemental analysis was conducted by Atlantic Microlab, Inc. (Norcross, GA). UV spectra were obtained with a Shimadzu UV 201 spectrometer (cell volume 3 mL; cell pass-length 10 mm).

### **Preparation of CSPs**

#### Preparation of Piv-Pro-Pro-N(Me)-Ahx-PRP1 (CSP-1)

##### (1). Preparation of amino-PRP-1 resin

To 8.0g of PRP-1 resin (7 $\mu$ m, 100Å) in 160mL anhydrous DCM were added *N*-(chloromethyl)phthalimide (4.0g, 20mmol) and anhydrous iron(III) chloride (0.4g, 2.4mmol). After stirring at r.t. under argon for 10h, the resin was collected by filtration and washed with dioxane, 10%(V/V) concentrated hydrochloric acid in dioxane, water and methanol. The resulting resin was then refluxed with 20ml hydrazine in 80mL methanol and 80mL THF for 24h. The desired amino-PRP-1 resin was collected by filtration and washed with hot ethanol, hot methanol, DMF and DCM. The resin was dried under vacuum overnight, and the surface loading of amino group was determined to be 1.26mmol/g by Elem. Anal. (N:1.76).

##### (2). Synthesis of Fmoc-N(Me)-Ahx-OH

A solution of 100mmol (12.72g) of *N*-methylcaprolactam in 200ml of concentrated hydrochloric acid was stirred at r.t. for 1 h, and then heated to reflux for 24 h. The solution was washed with ethyl acetate, and after evaporation under vacuum, the residue

was crystallized in the mixture of ethanol and ether. 6-Methylamino hexanoic acid hydrochloride was isolated with 88% yield, as a white solid, m.p. 66~67°C. <sup>1</sup>H NMR(D<sub>2</sub>O): δ 1.31(m, 2H), 1.57(m, 4H), 2.31(t, J=7.3Hz, 2H), 2.60(s, 3H), 2.93(t, J=7.6Hz, 2H).

To a stirred solution of 6-Methylamino hexanoic acid hydrochloride(35mmol, 6.36g) and sodium hydroxide(70mmol) in 100ml of water was added gradually Fmoc-OSu(30 mmol, 10.12g) in 100ml of THF. After being stirred at r.t. for 8h, the reaction mixture was acidified to pH 2 with concentrated hydrochloric acid. The solution was extracted with ethyl acetate(3×100 mL), and the organic extract phase was washed with water and then dried over anhydrous sodium sulfate. After evaporation of the solvent the crude product was obtained. It was purified by flash column chromatography on silica gel (mobile phase 10% methanol in DCM) to give the desired compound as a colorless oil(9.04g, 82% yield), <sup>1</sup>H NMR(CD<sub>2</sub>Cl<sub>2</sub>): δ 1.1~1.7(m, 6H), 2.37(m, 2H), 2.8~3.3(m, 5H), 4.2~4.6(m, 3H), 7.2~7.9(m, 8H).

### (3). Preparation of the CSP of Piv-Pro-Pro-N(Me)-Ahx-PRP1

To a 50mL peptide synthesis vessel were added amino-PRP1 resin(2.00g, 2.52mmol of amino group), Fmoc-N(Me)-Ahx-OH(5equiv,4.63g), HOBt(3equiv., 1.16g), 20mL of DMF and 20mL of DCM. After shaking for 5min, DIC(5equiv., 1.59g) was added and then the mixture was agitated at r.t. for 8h. The resin was collected by filtration and washed with DMF, Methanol, and DCM(30mL×3). The unreacted free amine group on the silica gel was end-capped by reacting with acetic anhydride and pyridine in DCM(3:2.5:30, V/V/V). The surface Fmoc-N(Me)-Ahx concentration was determined to be 0.58mmol/g based on the Fmoc cleavage method. Then the Fmoc protecting group

was removed by treatment of the silica with 10mL of 20%(V/V) piperidine in DMF for 1h to get NH(Me)-Ahx-PRP1.

To 1.0g of NH(Me)-Ahx-PRP1 prepared above (loading: 0.58mmol/g) were added mixtures of Fmoc-Pro-OH (3equiv, 0.78g), HATU (3equiv, 0.88g), and DIPEA (3equiv, 0.40g) in 8mL of DMF. After agitating for 6h, the silica was filtered and washed with DMF, Methanol and DCM. The surface Pro concentration was determined to be 0.49mmol/g based on the Fmoc cleavage method. Then the Fmoc protecting group was removed by 20%(V/V) piperidine in DMF. The second module of Fmoc-Pro-OH was coupled following an identical reaction. The surface Pro concentration was determined to be 0.52 mmol/g. Then the Fmoc group was removed by 20%(V/V) piperidine in DMF. And the resin was end-capped by reacting with trimethylacetic anhydride (0.93g, 5mmol) and DIPEA (0.65g, 5mmol) in 10mL of DMF for 3h. The resulting chiral stationary phase was packed into a 50×4.6 mm HPLC column using a standard slurry packing method.

Other CSPs were prepared by following the similar solid phase synthesis procedures by Dr. Junmin Huang in our group.

### **Chromatographic Measurement**

22 kinds of racemic analytes (see table 2-1) were chosen to test the CSPs. Isocratic system of IPA/Hexane and DCM/Hexane/MeOH were used as the mobile phase.

Retention factor ( $k$ ) equals  $(t_r - t_0)/t_0$ , in which  $t_r$  is the retention time and  $t_0$  is the dead time. Dead time  $t_0$  was measured with 1,3,5-tri-*tert*-butylbenzene as the void volume marker. Separation factor ( $\alpha$ ) equals  $k_2/k_1$ , in which  $k_1$  and  $k_2$  are the retention factors of two enantiomers.



## Results and discussion

Generally the structures of the proline-based CSPs in our study are composed of four parts: support, linker, proline residue and end group. Each CSP differs in some parts from others. Two kinds of support: APS (aminopropyl silica gel) and a high performance cross-linked polystyrene support — PRP-1 resin, two linker molecules with a chain of 6 carbon atoms: -N(Me)-Ahx-(methylamino hexanoyl) and -NH-Ahx-(amino hexanoyl), 1,2, 4 and 6 residues of prolines, and 8 kinds of ending group: Fmoc(9-fluorenylmethoxycarbonyl), Boc(*tert*-butyloxycarbonyl), Cbz(benzyloxycarbonyl), Piv(pivaloyl), Aca(9-anthracenecarboxylyl), Tapa( (-)-2-(2,4,5,7-Tetranitro-9-fluorenylideneaminoxy)propionyl), Dmb(dimethylbenzyl) and Tpa(triphenyl acetyl) were studied in our research. CSPs containing *t*-butyl-trans-4-L-Hydroxyproline structure were also prepared and evaluated in the study.

According to the chiral interaction model, a minimum of three interaction sites between chiral selector and analyte is needed to achieve enantio-selective recognition. Most L-proline based CSPs in our study can have hydrogen bonding interaction,  $\pi$ - $\pi$  interaction and steric hindrance with analytes.

Resolution of 22 kinds of racemic analytes (their structures are shown in table 2-1.) was tested by these CSPs. These analytes include alcohol and their derivatives, axially and planar dissymmetric compounds, 4-aryldihydropyrimidine derivatives, 5-arylhydantoin derivatives and miscellaneous compounds. These analytes were chosen based on not only the pharmaceutical importance but also their structural diversity.

The influence of structural components(support, linker, number of L-proline units and end group), modification of L-proline structure, and mobile phase system on the

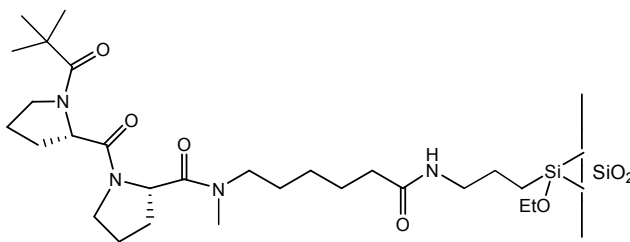
versatility and enantio-selectivity of CSPs was investigated. The versatility and enantio-selectivity of the most powerful CSP among the 17 was also compared with those of 3 commercial CSPs to investigate the possibility of developing proline-based CSP into a commercial one .

## 1. Influence of structural components on separation abilities of CSPs

### (1). Support

Two CSPs were used to study the effects of support on chiral discrimination. Their structures are shown in Figure 2-1. For CSP-1 and CSP-2, they both have the linker of -N(Me)-Ahx-, 2 residues of L-proline and Piv end group. The only difference is the support.

Piv-Pro-Pro-N(Me)-Ahx-APS: CSP-1



Piv-Pro-Pro-N(Me)-Ahx-PRP1: CSP-2

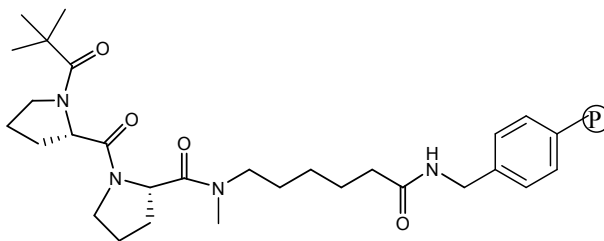


Figure 2-1 Structures of CSP-1 and CSP-2

The separation results for the 22 racemic analytes using these 2 CSPs are summarized on Table 2-1. The names and structures of analytes, separation factors, retention factors and mobile phase conditions are listed on this table.

By comparison of results of CSP-1 and CSP-2, aminopropyl silica gel seems to be a better support for these CSPs. 15 analytes were successfully separated by Piv-Pro-Pro-N(Me)-Ahx-APS(CSP-1) while only 6 analytes were resolved by Piv-Pro-Pro-N(Me)-Ahx-PRP1(CSP-2). This may be resulted from the fact that aminopropyl silica gel is hydrophilic and have a relatively rigid structure while PRP-1 resin is hydrophobic and its structure is more flexible. The hydrophilic and rigid support enhances chiral interaction between analytes and chiral selectors.

Table2-1 Comparison results for CSP-1 and CSP-2

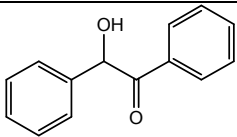
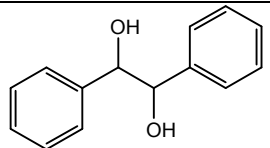
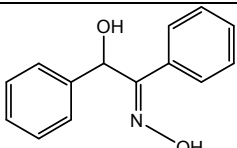
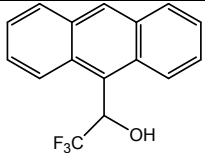
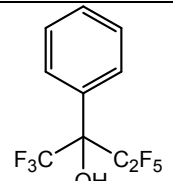
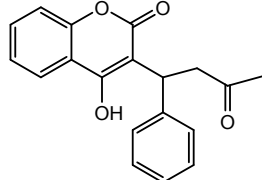
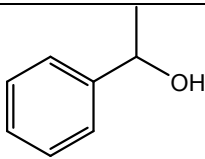
Analyte name	Analyte Structure	CSP-1	CSP-2
Benzoin		$\alpha^a$ : 1.12 $k_1^b$ :6.34 3%IPA in hexane <sup>c</sup>	$\alpha$ : 1.41 $k_1$ :6.40 3%IPA in hexane
Hydrobenzoin		$\alpha$ : 1.22 $k_1$ :17.00 4%IPA in hexane	$\alpha$ : 1 $k_1$ :21.40 4%IPA in hexane
Benzoin oxime		$\alpha$ : 1.12 $k_1$ :14.65 20%IPA in hexane	$\alpha$ :1 $k_1$ :13.04 20%IPA in hexane
2,2,2-Trifluoro-1-(9-anthryl) ethanol		$\alpha$ : 1.58 $k_1$ :22.40 10%IPA in hexane	$\alpha$ : 1.61 $k_1$ :17.40 10%IPA in hexane
a-(pentafluoroethyl)- a-(trifluoromethyl)- Benzenemethanol		$\alpha$ : 1.14 $k_1$ :8.89 3%IPA in hexane	$\alpha$ : 1.18 $k_1$ :6.80 3%IPA in hexane
Warfarin		$\alpha$ : 1.20 $k_1$ :12.41 10%IPA & 1% AcOH in hexane	$\alpha$ : 1 $k_1$ :11 10%IPA & 1% AcOH in hexane
Sec-Phenethyl alcohol		$\alpha$ : 1.08 $k_1$ :8.42 1%IPA in hexane	$\alpha$ : 1 $k_1$ :9.44 1%IPA in hexane

Table 2-1 continued.

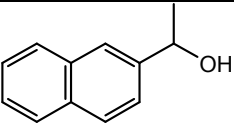
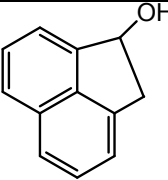
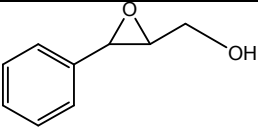
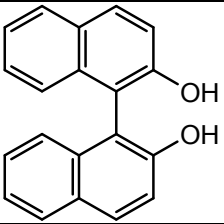
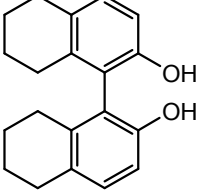
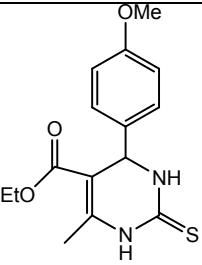
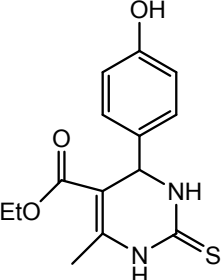
$\alpha$ -Methyl-2-Naphalenemethanol		$\alpha$ : 1 $k_1$ :17.31 1%IPA in hexane	$\alpha$ : 1 $k_1$ :21.54 1%IPA in hexane
1-Acenaphthenol		$\alpha$ : 1 $k_1$ :10.78 3%IPA in hexane	$\alpha$ : 1 $k_1$ :14 3%IPA in hexane
3-Phenyl-Glycidol		$\alpha$ : 1 $k_1$ :11.13 3%IPA in hexane	$\alpha$ : 1 $k_1$ :15.4 3%IPA in hexane
1,1'-Bi-2-naphthol		$\alpha$ : 1.34 $k_1$ :20.90 75%IPA in hexane	$\alpha$ : 1.19 $k_1$ :21 75%IPA in hexane
2,2'-Dihydroxy-5,5',6,6',7,7',8,8'-Octahydro-1,1'-binaphthyl		$\alpha$ : 1.08 $k_1$ :17.92 10%IPA in hexane	$\alpha$ : 1 $k_1$ :10.9 10%IPA in hexane
1,2,3,4-Tetrahydro-4-(4-methoxyphenyl)-6-methyl-2-thioxo-5-pyrimidinecarboxylic acid ethyl ester		$\alpha$ : 1.30 $k_1$ :11.34 15%IPA in hexane	$\alpha$ : 1.21 $k_1$ :24 15%IPA in hexane
1,2,3,4-Tetrahydro-4-(4-hydroxyphenyl)-6-methyl-2-thioxo-, 5-Pyrimidinecarboxylic acid ethyl ester		$\alpha$ : 1.49 $k_1$ :39.00 30%IPA in hexane	$\alpha$ : 1.46 $k_1$ :35.00 30%IPA in hexane

Table 2-1 continued.

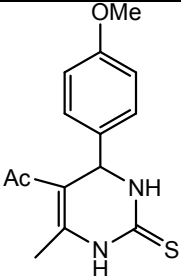
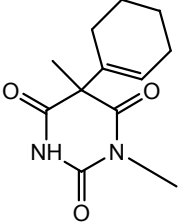
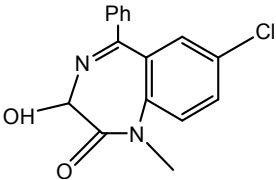
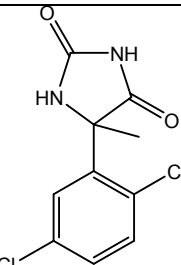
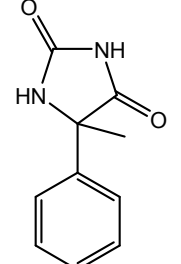
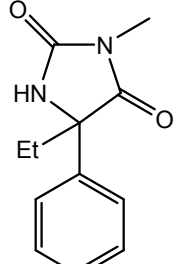
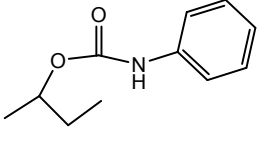
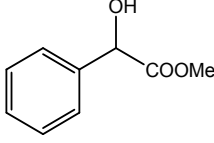
1-[1,2,3,4-Tetrahydro-4-(4-methoxyphenyl)-6-methyl-2-thioxo-5-pyrimidinyl]ethanone		$\alpha$ : 1.29 $k_1$ :26.27 15%IPA in hexane	$\alpha$ : 1 $k_1$ :27.00 15%IPA in hexane
Hexobarbital		$\alpha$ : 1 $k_1$ :11.51 1%IPA in hexane	$\alpha$ : 1 $k_1$ :13.80 1%IPA in hexane
Temazepam		$\alpha$ : 1 $k_1$ :17.73 2%IPA in hexane	$\alpha$ : 1 $k_1$ :16.20 2%IPA in hexane
5-Methyl-5-(2,5-dichloro)phenylhydantoin		$\alpha$ : 1.30 $k_1$ :10.00 15%IPA in hexane	$\alpha$ : 1 $k_1$ :9.4 15%IPA in hexane
5-Methyl-5-phenylhydantoin		$\alpha$ : 1.18 $k_1$ :17.91 8%IPA in hexane	$\alpha$ : 1 $k_1$ :17.40 8%IPA in hexane
Mephentoin		$\alpha$ : 1 $k_1$ :5.73 2%IPA in hexane	$\alpha$ : 1 $k_1$ :6.80 2%IPA in hexane

Table 2-1 continued.

<i>sec</i> -Butyl carbanilate		$\alpha$ : 1 $k_1$ :9.04 1%IPA in hexane	$\alpha$ : 1 $k_1$ :7.00 1%IPA in hexane
Methyl Mandelate		$\alpha$ : 1.23 $k_1$ :9.00 1%IPA in hexane	$\alpha$ : 1 $k_1$ :13.40 1%IPA in hexane

a. separation factor; b. retention factor of the first eluted enantiomer; c. IPA percentage in hexane of the mobile phase

(2). linker

4 CSPs are used to investigate the influence of linker structure on versatility and enantio-discrimination. Their structures are shown in Figure 2-2. For CSP-3 and CSP-4, they both have APS as the support, 1 residue of L-proline and Fmoc as end group. The only structural difference between CSP-3 and CSP-4 lies in the linker part: for CSP-3, NH-Ahx is used as the linker while N(Me)-Ahx is used as the linker for CSP-4. CSP-5 and CSP-6 with 2 residues of L-proline also only differ in the linker in their structures.

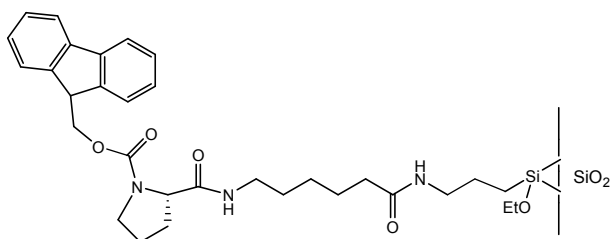
The separation results using these 4 CSPs are summarized on Table 2-2. By comparison of results of CSP-3 and CSP-4, and results of CSP-5 and CSP-6 respectively, it can be concluded that the *N*-methyl group in the linker(N(Me)-Ahx) plays a key role in the resolution of racemic analytes. Fmoc-Pro-N(Me)-Ahx-APS(CSP-4) resolved 6 analytes while Fmoc-Pro-NH-Ahx-APS(CSP-3) could only separate 1, and Fmoc-Pro-Pro-N(Me)-Ahx-APS(CSP-6) separated 16 analytes while Fmoc-Pro-Pro-NH-Ahx-APS(CSP-5) could only resolve 4 ones. The *N*-methylamino acid linker does not introduce a hydrogen-bonding donor NH group next to the Pro residue and a potential

source of nonspecific interaction due to hydrogen bonding is removed. The methyl group increases the steric hindrance near a chiral center which could amplify chiral recognition. The methyl group could also influence the rotation barrier of the amide bond that has partial double bond character.

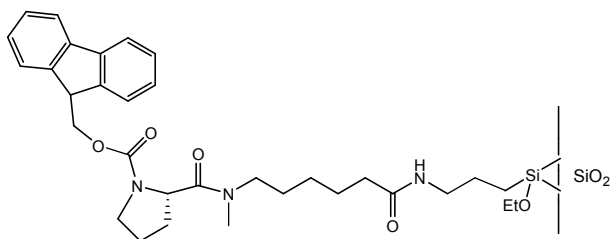
For Fmoc-Pro-N(Me)-Ahx-APS(CSP-4) and Fmoc-Pro-Pro-N(Me)-Ahx-APS(CSP-6), there is a big difference on their versatility and enantio-selectivity so the number of L-proline units also has great effects on the separation abilities of the CSPs.



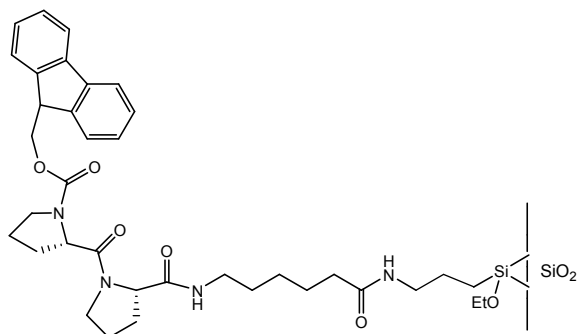
Fmoc-Pro-NH-Ahx-APS: CSP-3



Fmoc-Pro-NH-Ahx-APS: CSP-4



Fmoc-Pro-Pro-N(Me)-Ahx-APS: CSP-5



Fmoc-Pro-Pro-NH-Ahx-APS: CSP-6

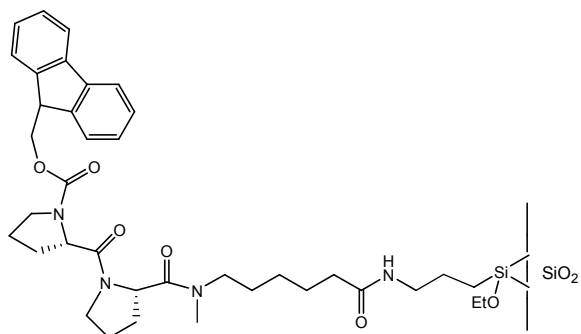


Figure 2-2 Structures of CSP-3 ~ CSP-6

Table 2-2 Comparison results for CSP-3 ~ CSP-6

Analyte name	CSP-3	CSP-4	CSP-5	CSP-6
Benzoin	$\alpha$ : 1 <sup>a</sup> k <sub>1</sub> :3.26 <sup>b</sup> 3%IPA <sup>c</sup>	$\alpha$ : 1 k <sub>1</sub> :5.78 3%IPA	$\alpha$ : 1 k <sub>1</sub> :3.93 3%IPA	$\alpha$ : 1.07 k <sub>1</sub> :8.22 3%IPA
Hydrobenzoin	$\alpha$ : 1 k <sub>1</sub> :9.33 4%IPA	$\alpha$ : 1 k <sub>1</sub> :17.71 4%IPA	$\alpha$ : 1 k <sub>1</sub> :27.45 4%IPA	$\alpha$ : 1.12 k <sub>1</sub> :21.15 4%IPA
Benzoin oxime	$\alpha$ : 1 k <sub>1</sub> :5.00 20%IPA	$\alpha$ : 1 k <sub>1</sub> :12.28 20%IPA	$\alpha$ : 1 k <sub>1</sub> :7.69 20%IPA	$\alpha$ : 1.09 k <sub>1</sub> :16.08 20%IPA
2,2,2-Trifluoro-1-(9-anthryl) ethanol	$\alpha$ : 1 k <sub>1</sub> :5.86 10%IPA	$\alpha$ : 1 k <sub>1</sub> :16.40 10%IPA	$\alpha$ : 1 k <sub>1</sub> :9.66 10%IPA	$\alpha$ : 1.28 k <sub>1</sub> :23.44 10%IPA
a-(pentafluoroethyl)-a-(trifluoromethyl)-Benzenemethanol	$\alpha$ : 1 k <sub>1</sub> :13.21 3%IPA	$\alpha$ : 1 k <sub>1</sub> :19.31 3%IPA	$\alpha$ : 1 k <sub>1</sub> :6.83 3%IPA	$\alpha$ : 1.06 k <sub>1</sub> :16.08 3%IPA
Warfarin	$\alpha$ : 1 k <sub>1</sub> :11.75 10%IPA & 1% AcOH	$\alpha$ : 1 k <sub>1</sub> :13.91 10%IPA & 1% AcOH	$\alpha$ : 1 k <sub>1</sub> :14.12 25%IPA	$\alpha$ : 1.11 k <sub>1</sub> :10.57 10%IPA & 1% AcOH
Sec-Phenethyl alcohol	$\alpha$ : 1 k <sub>1</sub> :5.35 1%IPA	$\alpha$ : 1 k <sub>1</sub> :6.67 1%IPA	$\alpha$ : 1 k <sub>1</sub> :5.79 1%IPA	$\alpha$ : 1.02 k <sub>1</sub> :11.3 1%IPA
$\alpha$ -Methyl-2-Naphalenemethanol	$\alpha$ : 1 k <sub>1</sub> :8.98 1%IPA	$\alpha$ : 1 k <sub>1</sub> :13.36 1%IPA	$\alpha$ : 1 k <sub>1</sub> :12.69 1%IPA	$\alpha$ : 1 k <sub>1</sub> :22.36 1%IPA
1-Acenaphthenol	$\alpha$ : 1 k <sub>1</sub> :5.74 2%IPA	$\alpha$ : 1 k <sub>1</sub> :7.83 3%IPA	$\alpha$ : 1 k <sub>1</sub> :7.45 3%IPA	$\alpha$ : 1 k <sub>1</sub> :13.36 3%IPA
3-Phenyl-Glycidol	$\alpha$ : 1 k <sub>1</sub> :5.73 3%IPA	$\alpha$ : 1 k <sub>1</sub> :5.23 3%IPA	$\alpha$ : 1 k <sub>1</sub> :7.31 3%IPA	$\alpha$ : 1 k <sub>1</sub> :5.64 3%IPA
1,1'-Bi-2-naphthol	$\alpha$ : 1 k <sub>1</sub> :3.23 75%IPA	$\alpha$ : 1.04 k <sub>1</sub> :11.48 75%IPA	$\alpha$ : 1.13 k <sub>1</sub> :7.39 75%IPA	$\alpha$ : 1.16 k <sub>1</sub> :32.80 75%IPA

Table 2-2 continued.

2,2'-Dihydroxy-5,5',6,6',7,7',8,8'-Octahydro-1,1'-binaphthyl	$\alpha$ : 1 $k_1$ :5.16 10%IPA	$\alpha$ : 1.14 $k_1$ :12.58 10%IPA	$\alpha$ : 1.10 $k_1$ :8.38 10%IPA	$\alpha$ : 1.17 $k_1$ :11.10 10%IPA
1,2,3,4-Tetrahydro-4-(4-methoxyphenyl)-6-methyl-2-thioxo-5-pyrimidinecarboxylic acid ethyl ester	$\alpha$ : 1.07 $k_1$ :9.28 10%IPA	$\alpha$ : 1.05 $k_1$ :14.81 15%IPA	$\alpha$ : 1 $k_1$ :9.00 15%IPA	$\alpha$ : 1.18 $k_1$ :18.68 15%IPA
1,2,3,4-Tetrahydro-4-(4-hydroxyphenyl)-6-methyl-2-thioxo-, 5-Pyrimidinecarboxylic acid ethyl ester	$\alpha$ : 1 $k_1$ :10.93 30%IPA	$\alpha$ : 1.12 $k_1$ :44.66 30%IPA	$\alpha$ : 1 $k_1$ :24.00 30%IPA	$\alpha$ : 1.20 $k_1$ :27.80 50%IPA
1-[1,2,3,4-Tetrahydro-4-(4-methoxyphenyl)-6-methyl-2-thioxo-5-pyrimidinyl]ethanone	$\alpha$ : 1 $k_1$ :10.63 10%IPA	$\alpha$ : 1 $k_1$ :27.03 15%IPA	$\alpha$ : 1 $k_1$ :21.76 15%IPA	$\alpha$ : 1.20 $k_1$ :40.60 15%IPA
Hexobarbital	$\alpha$ : 1 $k_1$ :13.86 1%IPA	$\alpha$ : 1 $k_1$ :28.86 1%IPA	$\alpha$ : 1 $k_1$ :13.5 1%IPA	$\alpha$ : 1 $k_1$ :22.28 1%IPA
Temazepam	$\alpha$ : 1 $k_1$ :23.23 2%IPA	$\alpha$ : 1.09 $k_1$ :22.03 2%IPA	$\alpha$ : 1 $k_1$ :22.71 2%IPA	$\alpha$ : 1 $k_1$ :25.54 2%IPA
5-Methyl-5-(2,5-dichloro)phenylhydantoin	$\alpha$ : 1 $k_1$ :9.96 15%IPA	$\alpha$ : 1 $k_1$ :11.21 15%IPA	$\alpha$ : 1 $k_1$ :7.34 15%IPA	$\alpha$ : 1.16 $k_1$ :14.6 15%IPA
5-Methyl-5-phenylhydantoin	$\alpha$ : 1 $k_1$ :8.65 8%IPA	$\alpha$ : 1 $k_1$ :16.24 8%IPA	$\alpha$ : 1 $k_1$ :12.79 8%IPA	$\alpha$ : 1.10 $k_1$ :25.00 8%IPA
Mephentoin	$\alpha$ : 1 $k_1$ :4.12 2%IPA	$\alpha$ : 1 $k_1$ :5.86 2%IPA	$\alpha$ : 1 $k_1$ :5.81 2%IPA	$\alpha$ : 1.14 $k_1$ :7.86 2%IPA
<i>sec</i> -Butyl carbanilate	$\alpha$ : 1 $k_1$ :4.18 1%IPA	$\alpha$ : 1 $k_1$ :3.62 1%IPA	$\alpha$ : 1.20 $k_1$ :4.00 1%IPA	$\alpha$ : 1 $k_1$ :7.30 1%IPA
Methyl Mandelate	$\alpha$ : 1 $k_1$ :5.72 1%IPA	$\alpha$ : 1.02 $k_1$ :7.97 1%IPA	$\alpha$ : 1.15 $k_1$ :6.41 1%IPA	$\alpha$ : 1.10 $k_1$ :10.8 1%IPA

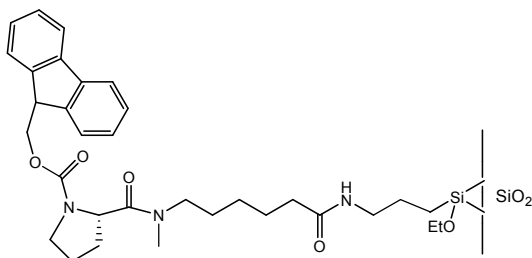
a. separation factor; b. retention factor of the first eluted enantiomer; c. IPA percentage in hexane of the mobile phase

### (3). Number of L-Proline units

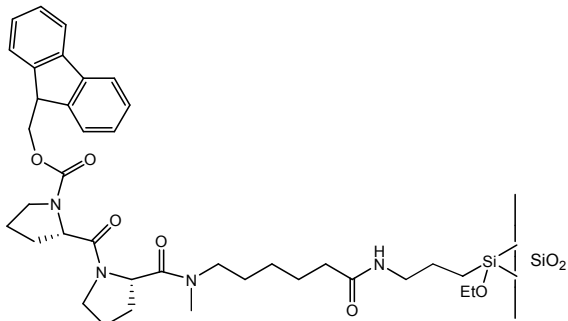
Four CSPs with 1, 2, 4 and 6 L-proline units in their structures were evaluated with the 22 analytes. The structures of these four CSPs are shown on Figure 2-3. And the separation results for these CSPs are summarized on Table 2-3.

From the results, as number of L-proline units increased from 1 to 2, then to 4, big difference was found in versatility and enantio-selectivity of these three CSPs. For versatility, CSP-4(Fmoc-Pro-N(Me)-Ahx-APS) resolved only 6 analytes, while CSP-6(Fmoc-Pro-Pro-N(Me)-Ahx-APS) separated 16 and CSP-7(Fmoc-Pro-Pro-Pro-Pro-N(Me)-Ahx-APS) separated 17 out of 22 analytes. For enantio-selectivity, lowest separation factors were found for CSP-4. For the 16 analytes resolved by both CSP-6 and CSP-7, bigger separation factors were achieved for CSP-7 in most cases.

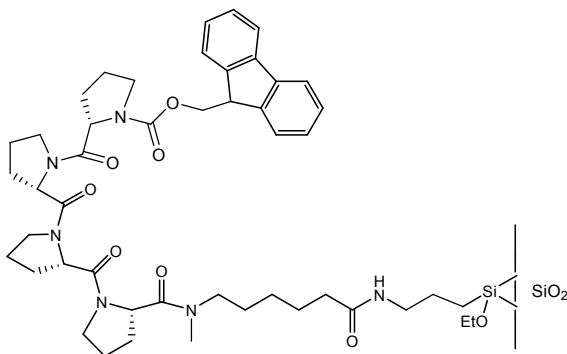
Fmoc-Pro-N(Me)-Ahx-APS: CSP-4



Fmoc-Pro-Pro-N(Me)-Ahx-APS: CSP-6



Fmoc-Pro-Pro-Pro-Pro-N(Me)-Ahx-APS: CSP-7



Fmoc-Pro-Pro-Pro-Pro-Pro-Pro-N(Me)-Ahx-APS: CSP-8

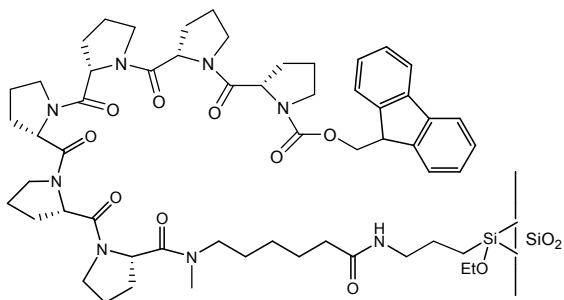


Figure 2-3 Structures of CSPs with different number of L-proline units

Table 2-3 Comparison results for CSPs with different number of L-proline units

Analyte name	CSP-4	CSP-6	CSP-7	CSP-8
Benzoin	$\alpha$ : 1 <sup>a</sup> $k_1$ :5.78 <sup>b</sup> 3%IPA <sup>c</sup>	$\alpha$ : 1.07 $k_1$ :8.22 3%IPA	$\alpha$ : 1.09 $k_1$ :6.35 3%IPA	$\alpha$ : 1.12 $k_1$ :16.0 5%IPA
Hydrobenzoin	$\alpha$ : 1 $k_1$ :17.71 4%IPA	$\alpha$ : 1.12 $k_1$ :21.15 4%IPA	$\alpha$ : 1.13 $k_1$ :17.98 4%IPA	$\alpha$ : 1.15 $k_1$ :25.79 8%IPA
Benzoin oxime	$\alpha$ : 1 $k_1$ :12.28 20%IPA	$\alpha$ : 1.09 $k_1$ :16.08 20%IPA	$\alpha$ : 1.13 $k_1$ :15.36 20%IPA	$\alpha$ : 1.20 $k_1$ :41.45 30%IPA
2,2,2-Trifluoro-1-(9-anthryl) ethanol	$\alpha$ : 1 $k_1$ :16.40 10%IPA	$\alpha$ : 1.28 $k_1$ :23.44 10%IPA	$\alpha$ : 1.56 $k_1$ :18.48 10%IPA	$\alpha$ : 1.78 $k_1$ :22.58 25%IPA
a-(pentafluoroethyl)-a-(trifluoromethyl)-Benzenemethanol	$\alpha$ : 1 $k_1$ :19.31 3%IPA	$\alpha$ : 1.06 $k_1$ :16.08 3%IPA	$\alpha$ : 1.10 $k_1$ :8.91 3%IPA	$\alpha$ : 1.10 $k_1$ :8.62 5%IPA
Warfarin	$\alpha$ : 1 $k_1$ :13.91 10%IPA & 1% AcOH	$\alpha$ : 1.11 $k_1$ :10.57 10%IPA & 1% AcOH	$\alpha$ : 1.08 $k_1$ :11.19 10%IPA & 1% AcOH	$\alpha$ : 1.18 $k_1$ :17.50 10%IPA & 1% AcOH
Sec-Phenethyl alcohol	$\alpha$ : 1 $k_1$ :6.67 1%IPA	$\alpha$ : 1.02 $k_1$ :11.3 1%IPA	$\alpha$ : 1.02 $k_1$ :8.07 1%IPA	$\alpha$ : 1.04 $k_1$ :19.42 1%IPA
$\alpha$ -Methyl-2-Naphalenemethanol	$\alpha$ : 1 $k_1$ :13.36 1%IPA	$\alpha$ : 1 $k_1$ :22.36 1%IPA	$\alpha$ : 1.04 $k_1$ :17.62 1%IPA	$\alpha$ : 1 $k_1$ :18.81 3%IPA
1-Acenaphthenol	$\alpha$ : 1 $k_1$ :7.83 3%IPA	$\alpha$ : 1 $k_1$ :13.36 3%IPA	$\alpha$ : 1 $k_1$ :10.28 3%IPA	$\alpha$ : 1 $k_1$ :28.06 3%IPA
3-Phenyl-Glycidol	$\alpha$ : 1 $k_1$ :5.23 3%IPA	$\alpha$ : 1 $k_1$ :5.64 3%IPA	$\alpha$ : 1 $k_1$ :6.77 3%IPA	$\alpha$ : 1 $k_1$ :10.38 5%IPA
1,1'-Bi-2-naphthol	$\alpha$ : 1.04 $k_1$ :11.48 75%IPA	$\alpha$ : 1.16 $k_1$ :32.80 75%IPA	$\alpha$ : 1.29 $k_1$ :23.83 75%IPA	$\alpha$ : 1.42 $k_1$ :9.94 90%IPA
2,2'-Dihydroxy-5,5',6,6',7,7',8,8'-Octahydro-1,1'-binaphthyl	$\alpha$ : 1.14 $k_1$ :12.58 10%IPA	$\alpha$ : 1.17 $k_1$ :11.10 10%IPA	$\alpha$ : 1.32 $k_1$ :10.95 10%IPA	$\alpha$ : 1.67 $k_1$ :19.75 25%IPA

Table 2-3 continued.

1,2,3,4-Tetrahydro-4-(4-methoxyphenyl)-6-methyl-2-thioxo-5-pyrimidinecarboxylic acid ethyl ester	$\alpha$ : 1.05 $k_1$ :14.81 15%IPA	$\alpha$ : 1.18 $k_1$ :18.68 15%IPA	$\alpha$ : 1.24 $k_1$ :12.60 15%IPA	$\alpha$ : 1.20 $k_1$ :23.53 15%IPA
1,2,3,4-Tetrahydro-4-(4-hydroxyphenyl)-6-methyl-2-thioxo-, 5-Pyrimidinecarboxylic acid ethyl ester	$\alpha$ : 1.12 $k_1$ :44.66 30%IPA	$\alpha$ : 1.20 $k_1$ :27.80 50%IPA	$\alpha$ : 1.41 $k_1$ :25.07 30%IPA	$\alpha$ : 1.32 $k_1$ :30.13 70%IPA
1-[1,2,3,4-Tetrahydro-4-(4-methoxyphenyl)-6-methyl-2-thioxo-5-pyrimidinyl]ethanone	$\alpha$ : 1 $k_1$ :27.03 15%IPA	$\alpha$ : 1.20 $k_1$ :40.60 15%IPA	$\alpha$ : 1.21 $k_1$ :25.72 15%IPA	$\alpha$ : 1.34 $k_1$ :33.90 25%IPA
Hexobarbital	$\alpha$ : 1 $k_1$ :28.86 1%IPA	$\alpha$ : 1 $k_1$ :22.28 1%IPA	$\alpha$ : 1 $k_1$ :16.98 1%IPA	$\alpha$ : 1 $k_1$ :11.26 3%IPA
Temazepam	$\alpha$ : 1.09 $k_1$ :22.03 2%IPA	$\alpha$ : 1 $k_1$ :25.54 2%IPA	$\alpha$ : 1 $k_1$ :20.24 2%IPA	$\alpha$ : 1 $k_1$ :25.52 5%IPA
5-Methyl-5-(2,5-dichloro)phenylhydantoin	$\alpha$ : 1 $k_1$ :11.21 15%IPA	$\alpha$ : 1.16 $k_1$ :14.6 15%IPA	$\alpha$ : 1.17 $k_1$ :8.55 15%IPA	$\alpha$ : 1.34 $k_1$ :11.64 25%IPA
5-Methyl-5-phenylhydantoin	$\alpha$ : 1 $k_1$ :16.24 8%IPA	$\alpha$ : 1.10 $k_1$ :25.00 8%IPA	$\alpha$ : 1.15 $k_1$ :15.6 8%IPA	$\alpha$ : 1.32 $k_1$ :10.7 20%IPA
Mephentoin	$\alpha$ : 1 $k_1$ :5.86 2%IPA	$\alpha$ : 1.14 $k_1$ :7.86 2%IPA	$\alpha$ : 1.14 $k_1$ :6.93 2%IPA	$\alpha$ : 1.27 $k_1$ :9.85 3%IPA
<i>sec</i> -Butyl carbanilate	$\alpha$ : 1 $k_1$ :3.62 1%IPA	$\alpha$ : 1 $k_1$ :7.30 1%IPA	$\alpha$ : 1 $k_1$ :7.64 1%IPA	$\alpha$ : 1 $k_1$ :15.34 3%IPA
Methyl Mandelate	$\alpha$ : 1.02 $k_1$ :7.97 1%IPA	$\alpha$ : 1.10 $k_1$ :10.8 1%IPA	$\alpha$ : 1.17 $k_1$ :8.31 1%IPA	$\alpha$ : 1 $k_1$ :17.49 3%IPA

a. separation factor; b. retention factor of the first eluted enantiomer; c. IPA percentage in hexane of the mobile phase

The number of L-proline units proved important. L-proline peptides are necessary to achieve better enantio-selectivity and versatility. With more L-proline units in the structure of CSPs, the rigidity of chiral selector is improved. And because of more carbonyl groups available in the structure, hydrogen bond interaction between analytes and chiral selectors is improved. And better chiral discrimination and versatility can be achieved.

However, as number of L-proline units increased from 1 to 2, then to 4, the retention factors did not change much for most analytes. It can be concluded that the achiral interaction is not improved much with increasing of number of L-proline units into 4.

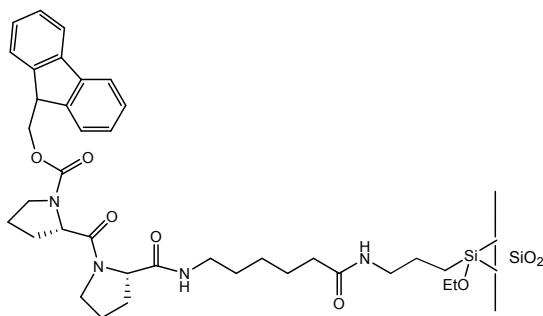
When number of L-proline units increased into 6, more polar mobile phases were needed to make sure that analytes could be eluted from the column efficiently and even with more polar mobile phase systems retention factors increased greatly. CSP-8(Fmoc-Pro-Pro-Pro-Pro-Pro-N(Me)-Ahx-APS) resolved 15 analytes. The versatility decreases a little but the separation factors of most analytes increase impressively compared with CSP-7. So when number of L-proline units becomes 6, there is improvement for both the chiral and achiral interaction between analytes and CSP.

#### (4) Modification of L-proline structure

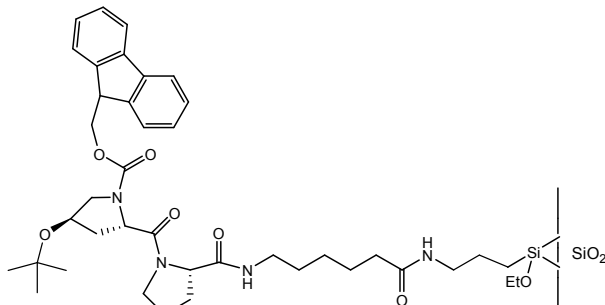
In our study, *t*-butyl-trans-4-L-Hydroxyproline was chosen to replace the L-proline structure for the CSPs. Two CSPs containing *t*-butyl-trans-4-L-Hydroxyproline structure were prepared and evaluated with 22 analytes. The separation results were compared with those of CSPs with only L-proline structures. The structures of the four CSPs are shown on Figure 2-4. The separation results are summarized on Table 2-4.



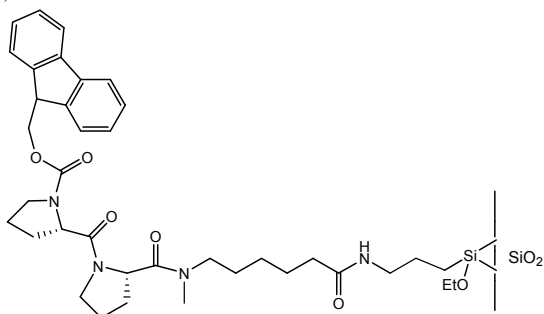
Fmoc-Pro-Pro-NH-Ahx-APS: CSP-5



Fmoc-(*t*Bu)Hyp-Pro-NH-Ahx-APS: CSP-9



Fmoc-Pro-Pro-N(Me)-Ahx-APS: CSP-6



Fmoc-(*t*Bu)Hyp-Pro-N(Me)-Ahx-APS: CSP-10

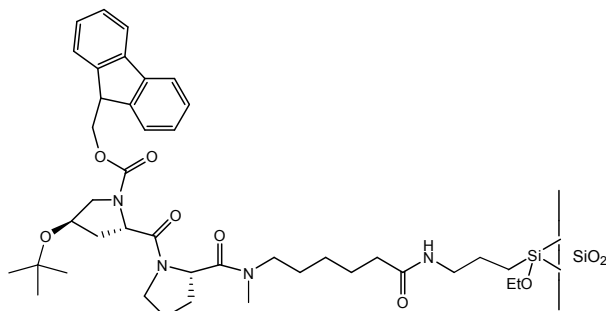


Figure 2-4 Structures of CSP-5, CSP-6, CSP-9 and CSP-10

Table 2-4. Comparison results of CSP-5, CSP-6, CSP-9 and CSP-10

Analyte name	CSP-5	CSP-9	CSP-6	CSP-10
Benzoin	$\alpha$ : 1 $k_1$ :3.93 3%IPA	$\alpha$ : 1.25 $k_1$ :3.21 3%IPA	$\alpha$ : 1.07 $k_1$ :8.22 3%IPA	$\alpha$ : 1.08 $k_1$ :6.42 3%IPA
Hydrobenzoin	$\alpha$ : 1 $k_1$ :27.45 4%IPA	$\alpha$ : 1 $k_1$ :13.04 4%IPA	$\alpha$ : 1.12 $k_1$ :21.15 4%IPA	$\alpha$ : 1.04 $k_1$ :17.95 4%IPA
Benzoin oxime	$\alpha$ : 1 $k_1$ :7.69 20%IPA	$\alpha$ : 1 $k_1$ :6.82 20%IPA	$\alpha$ : 1.09 $k_1$ :16.08 20%IPA	$\alpha$ : 1 $k_1$ :11.42 20%IPA
2,2,2-Trifluoro-1-(9-anthryl)ethanol	$\alpha$ : 1 $k_1$ :9.66 10%IPA	$\alpha$ : 1 $k_1$ :8.72 10%IPA	$\alpha$ : 1.28 $k_1$ :23.44 10%IPA	$\alpha$ : 1.34 $k_1$ :10.28 10%IPA
a-(pentafluoroethyl)-a-(trifluoromethyl)-Benzenemethanol	$\alpha$ : 1 $k_1$ :6.83 3%IPA	$\alpha$ : 1 $k_1$ :5.68 3%IPA	$\alpha$ : 1.06 $k_1$ :16.08 3%IPA	$\alpha$ : 1 $k_1$ :6.35 3%IPA
Warfarin	$\alpha$ : 1 $k_1$ :14.12 25%IPA	$\alpha$ : 1 $k_1$ :12.61 25%IPA	$\alpha$ : 1.11 $k_1$ :10.57 10%IPA & 1% AcOH	$\alpha$ : 1 $k_1$ :11.05 10%IPA & 1% AcOH
Sec-Phenethyl alcohol	$\alpha$ : 1 $k_1$ :5.79 1%IPA	$\alpha$ : 1 $k_1$ :5.79 1%IPA	$\alpha$ : 1.02 $k_1$ :11.3 1%IPA	$\alpha$ : 1 $k_1$ :7.82 1%IPA
$\alpha$ -Methyl-2-Naphalenemethanol	$\alpha$ : 1 $k_1$ :12.69 1%IPA	$\alpha$ : 1 $k_1$ :9.88 1%IPA	$\alpha$ : 1 $k_1$ :22.36 1%IPA	$\alpha$ : 1 $k_1$ :15.28 1%IPA
1-Acenaphthenol	$\alpha$ : 1 $k_1$ :7.45 3%IPA	$\alpha$ : 1 $k_1$ :6.04 3%IPA	$\alpha$ : 1 $k_1$ :13.36 3%IPA	$\alpha$ : 1 $k_1$ :8.30 3%IPA
3-Phenyl-Glycidol	$\alpha$ : 1 $k_1$ :7.31 3%IPA	$\alpha$ : 1 $k_1$ :7.63 3%IPA	$\alpha$ : 1 $k_1$ :5.64 3%IPA	$\alpha$ : 1 $k_1$ :8.70 3%IPA
1,1'-Bi-2-naphthol	$\alpha$ : 1.13 $k_1$ :7.39 75%IPA	$\alpha$ : 1 $k_1$ :4.68 75%IPA	$\alpha$ : 1.16 $k_1$ :32.80 75%IPA	$\alpha$ : 1 $k_1$ :45.07 25%IPA

Table 2-4 continued.

2,2'-Dihydroxy-5,5',6,6',7,7',8,8'-Octahydro-1,1'-binaphthyl	$\alpha$ : 1.10 $k_1$ :8.38 10%IPA	$\alpha$ : 1 $k_1$ :6.77 10%IPA	$\alpha$ : 1.17 $k_1$ :11.10 10%IPA	$\alpha$ : 1.05 $k_1$ :11.07 10%IPA
1,2,3,4-Tetrahydro-4-(4-methoxyphenyl)-6-methyl-2-thioxo-5-pyrimidinecarboxylic acid ethyl ester	$\alpha$ : 1 $k_1$ :9.00 15%IPA	$\alpha$ : 1 $k_1$ :5.22 15%IPA	$\alpha$ : 1.18 $k_1$ :18.68 15%IPA	$\alpha$ : 1.15 $k_1$ :13.30 15%IPA
1,2,3,4-Tetrahydro-4-(4-hydroxyphenyl)-6-methyl-2-thioxo-, 5-Pyrimidinecarboxylic acid ethyl ester	$\alpha$ : 1 $k_1$ :24.00 30%IPA	$\alpha$ : 1 $k_1$ :15.14 30%IPA	$\alpha$ : 1.20 $k_1$ :27.80 50%IPA	$\alpha$ : 1.21 $k_1$ :42.56 50%IPA
1-[1,2,3,4-Tetrahydro-4-(4-methoxyphenyl)-6-methyl-2-thioxo-5-pyrimidinyl]ethanone	$\alpha$ : 1 $k_1$ :21.76 15%IPA	$\alpha$ : 1 $k_1$ :14.79 15%IPA	$\alpha$ : 1.20 $k_1$ :40.60 15%IPA	$\alpha$ : 1 $k_1$ :29.70 15%IPA
Hexobarbital	$\alpha$ : 1 $k_1$ :13.5 1%IPA	$\alpha$ : 1 $k_1$ :10.95 1%IPA	$\alpha$ : 1 $k_1$ :22.28 1%IPA	$\alpha$ : 1 $k_1$ :12.02 1%IPA
Temazepam	$\alpha$ : 1 $k_1$ :22.71 2%IPA	$\alpha$ : 1.10 $k_1$ :22.16 2%IPA	$\alpha$ : 1 $k_1$ :25.54 2%IPA	$\alpha$ : 1.08 $k_1$ :20.56 2%IPA
5-Methyl-5-(2,5-dichloro)phenylhydantoin	$\alpha$ : 1 $k_1$ :7.34 15%IPA	$\alpha$ : 1 $k_1$ :5.47 15%IPA	$\alpha$ : 1.16 $k_1$ :14.6 15%IPA	$\alpha$ : 1.08 $k_1$ :8.87 15%IPA
5-Methyl-5-phenyl hydantoin	$\alpha$ : 1 $k_1$ :12.79 8%IPA	$\alpha$ : 1 $k_1$ :11.28 8%IPA	$\alpha$ : 1.10 $k_1$ :25.00 8%IPA	$\alpha$ : 1.09 $k_1$ :15.84 8%IPA
Mephentoin	$\alpha$ : 1 $k_1$ :5.81 2%IPA	$\alpha$ : 1 $k_1$ :4.44 2%IPA	$\alpha$ : 1.14 $k_1$ :7.86 2%IPA	$\alpha$ : 1.36 $k_1$ :4.44 2%IPA
<i>sec</i> -Butyl carbanilate	$\alpha$ : 1.20 $k_1$ :4.00 1%IPA	$\alpha$ : 1 $k_1$ :4.02 1%IPA	$\alpha$ : 1 $k_1$ :7.30 1%IPA	$\alpha$ : 1 $k_1$ :4.86 1%IPA
Methyl Mandelate	$\alpha$ : 1.15 $k_1$ :6.41 1%IPA	$\alpha$ : 1 $k_1$ :7.53 1%IPA	$\alpha$ : 1.10 $k_1$ :10.8 1%IPA	$\alpha$ : 1 $k_1$ :9.81 1%IPA

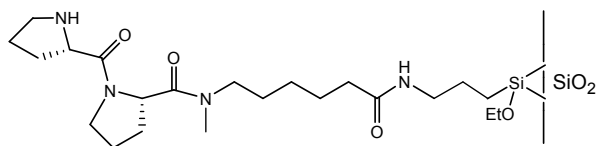
a. separation factor; b. retention factor of the first eluted enantiomer; c. IPA percentage in hexane of the mobile phase

By comparison of results of CSP-5 and CSP-9, and results of CSP-6 and CSP-10, it is quite clear that modification of one residue of L-proline into *t*-butyl-trans-4-L-Hydroxyproline in the CSP structure has negative effects on the versatility of CSPs: Fmoc-Pro-Pro-NH-Ahx-APS(CSP-5) resolved 4 analytes while Fmoc-(*t*Bu)Hyp-Pro-NH-Ahx-APS(CSP-9) could resolve 2, and Fmoc-Pro-Pro-N(Me)-Ahx-APS(CSP-6) separated 16 analytes while Fmoc-(*t*Bu)Hyp-Pro-N(Me)-Ahx-APS(CSP-10) could only separate 10 ones. So addition of the steric group of *t*-Bu-O- to L-proline in the CSP structure does not improve the chiral interaction between analytes and CSPs.

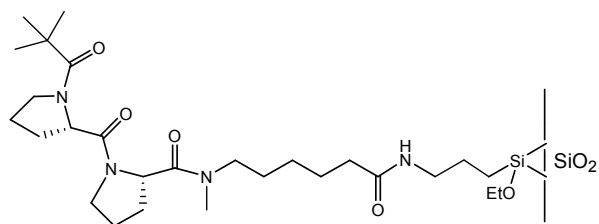
#### (5.) End group

9 CSPs with different end groups or with no end group were chosen to investigate the influence of end group in the structure of CSP on the enantio-selectivity towards the 22 analytes. The structure of these 9 CSPs are shown on Figure2-5.

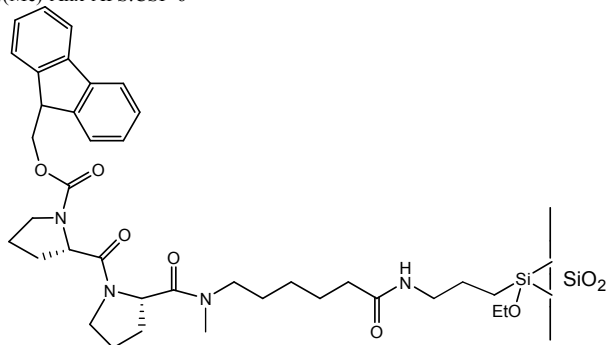
Pro-Pro-N(Me)-Ahx-APS: CSP-11



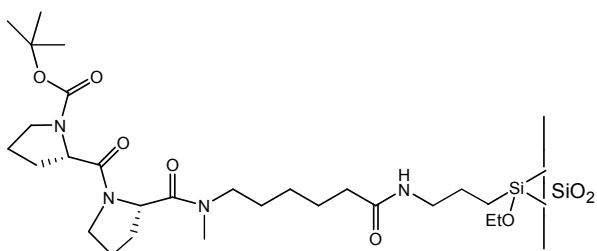
Piv-Pro-Pro-N(Me)-Ahx-APS: CSP-1



Fmoc-Pro-Pro-N(Me)-Ahx-APS: CSP-6



Boc-Pro-Pro-N(Me)-Ahx-APS: CSP-12



Cbz-Pro-Pro-N(Me)-Ahx-APS: CSP-13

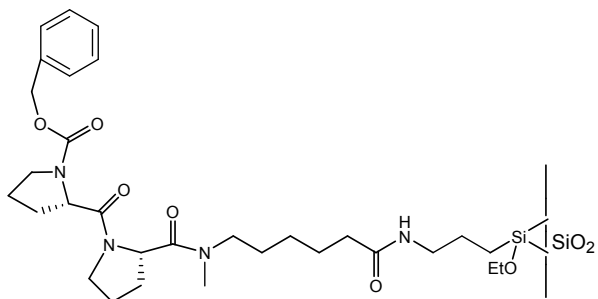
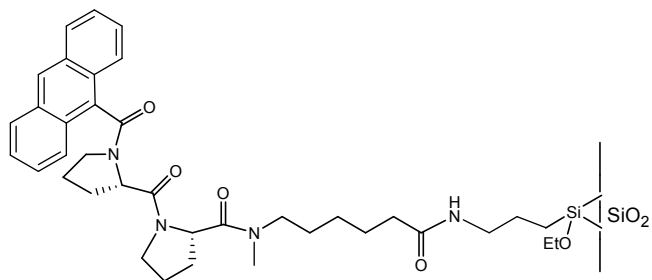
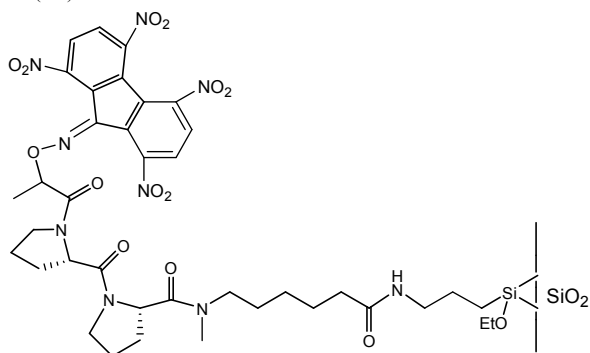


Figure 2-5, continued.

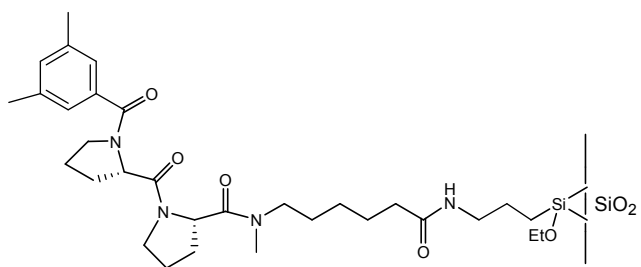
Aca-Pro-Pro-N(Me)-Ahx-APS: CSP-14



Tpa-Pro-Pro-N(Me)-Ahx-APS: CSP-15



Dmb-Pro-Pro-N(Me)-Ahx-APS: CSP-16



Tpa-Pro-Pro-N(Me)-Ahx-APS: CSP-17

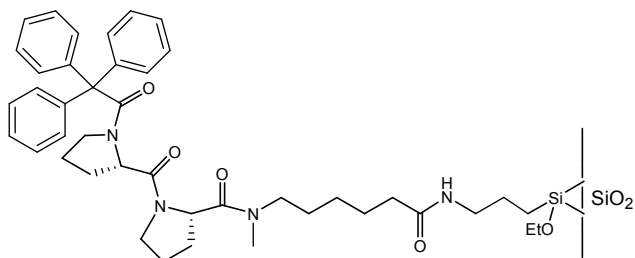


Figure 2-5 Structures of CSPs with different end groups

The comparison results are summarized on Table 2-5. All these 9 CSPs have APS as the support, -N(Me)-Ahx- group as the linker and two L-proline units in their structures. The only difference is that they have different end groups or no end group.

For CSP-11(Pro-Pro-N(Me)-Ahx-APS) without any end group in its structure, it has worst versatility among the 9 CSPs: only 4 analytes were resolved. So end group is a key factor to achieve good versatility for CSPs.

Among these 9 CSPs, CSP-6 with Fmoc end group has the best versatility. CSP-6 resolved 16 analytes out of 22 while CSP-1 with Piv group separated 15, CSP-16 with Dmb group separated 14, CSP-12 with Boc and CSP-13 with Cbz both resolved 13, CSP-14 with Aca group and CSP-17 with Tpa group showed separation for 12, and CSP-15 with Tapa only resolved 8 analytes.

For the enantio-selectivity, CSP-1 with Piv group achieved highest separation factors for most analytes among these 9 CSPs. By comparing CSP-1 and CSP-12, obviously CSP-1 has better versatility and enantio-selectivity. The only difference between the structures of these two CSPs is that Boc end group in CSP-12 has oxycarbonyl group connected with *t*-butyl group while Piv in CSP-1 has carbonyl group connected with *t*-butyl. Piv increases the rigidity of CSP structure. Rigid structure is helpful to achieve better versatility and separation results.

But versatility and enantio-selectivity are also determined by other factors besides rigidity of the structure of CSP. CSP-14 and CSP-17 have rigid structures but they did not achieve good versatility and separation results. The Fmoc end group in CSP-6 is not very rigid but CSP-6 has the best versatility and good enantio-discrimination.

Among these 9 CSPs, CSP-1 does not have aromatic group in its structure but it has best enantio-selectivity and good versatility while CSP-14, CSP-15 and CSP-17 possess strong aromatic groups but do not achieve good separation results and versatility. So it can be concluded that  $\pi$ - $\pi$  interaction is not a key factor to achieve good versatility and enantio-selectivity for the proline-based CSPs in our study. Hydrogen bonding interaction and steric hindrance are factors which have greater influence on chiral recognition ability of these proline-based CSPs.

The separation results of CSP-1 with Piv end group are very promising. CSP-1 achieved great enantio-selectivity towards most of the analytes. Although versatility of CSP-1 is not as good as CSP-6 with Fmoc group, CSP-1 has great potential to separate a wider range of analytes and have better durability because Piv group has a more stable structure compared with Fmoc group. Fmoc group is unstable in basic mobile phases or in the presence of basic analytes.



Table 2-5. Comparison results of CSPs with different end groups

Analyte name	CSP-11	CSP-1	CSP-6	CSP-12	CSP-13	CSP-14	CSP-15	CSP-16	CSP-17
Benzoin	$\alpha$ : 1 $k_1$ :5.84 3%IPA	$\alpha$ : 1.12 $k_1$ :6.34 3%IPA	$\alpha$ : 1.07 $k_1$ :8.22 3%IPA	$\alpha$ : 1.07 $k_1$ :4.45 3%IPA	$\alpha$ : 1.08 $k_1$ :6.63 3%IPA	$\alpha$ : 1 $k_1$ :7.71 3%IPA	$\alpha$ : 1 $k_1$ :19.02 3%IPA	$\alpha$ : 1.10 $k_1$ :7.76 3%IPA	$\alpha$ : 1.07 $k_1$ :6.00 3%IPA
Hydrobenzoin	$\alpha$ : 1.07 $k_1$ :16.71 4%IPA	$\alpha$ : 1.22 $k_1$ :17.00 4%IPA	$\alpha$ : 1.12 $k_1$ :21.15 4%IPA	$\alpha$ : 1.11 $k_1$ :10.7 1 4%IPA	$\alpha$ : 1.11 $k_1$ :13.33 4%IPA	$\alpha$ : 1.10 $k_1$ :16.81 4%IPA	$\alpha$ : 1.14 $k_1$ :26.41 4%IPA	$\alpha$ : 1.13 $k_1$ :18.09 4%IPA	$\alpha$ : 1.16 $k_1$ :15.17 4%IPA
Benzoin oxime	$\alpha$ : 1 $k_1$ :11.44 20%IPA	$\alpha$ : 1.12 $k_1$ :14.65 20%IPA	$\alpha$ : 1.09 $k_1$ :16.08 20%IPA	$\alpha$ : 1 $k_1$ :10.0 9 20%IPA	$\alpha$ : 1 $k_1$ :12.23 20%IPA	$\alpha$ : 1 $k_1$ :13.44 20%IPA	$\alpha$ : 1 $k_1$ :16.03 20%IPA	$\alpha$ : 1.10 $k_1$ :15.00 20%IPA	$\alpha$ : 1.08 $k_1$ :11.71 20%IPA
2,2,2-Trifluoro-1-(9-anthryl) ethanol	$\alpha$ : 1 $k_1$ :17.23 10%IPA	$\alpha$ : 1.58 $k_1$ :22.4 10%IPA	$\alpha$ : 1.28 $k_1$ :23.44 10%IPA	$\alpha$ : 1.28 $k_1$ :15.0 8 10%IPA	$\alpha$ : 1.33 $k_1$ :15.82 10%IPA	$\alpha$ : 1.16 $k_1$ :20.02 10%IPA	$\alpha$ : 1.28 $k_1$ :31.59 40%IPA	$\alpha$ : 1.30 $k_1$ :20.47 10%IPA	$\alpha$ : 1.40 $k_1$ :16.03 10%IPA
a-(pentafluoroethyl)-a-(trifluoromethyl)-Benzenemethanol	$\alpha$ : 1 $k_1$ :9.72 3%IPA	$\alpha$ : 1.14 $k_1$ :8.89 3%IPA	$\alpha$ : 1.06 $k_1$ :16.08 3%IPA	$\alpha$ : 1.11 $k_1$ :7.55 3%IPA	$\alpha$ : 1.10 $k_1$ :5.76 3%IPA	$\alpha$ : 1.06 $k_1$ :6.18 3%IPA	$\alpha$ : 1.10 $k_1$ :8.13 1%IPA	$\alpha$ : 1.09 $k_1$ :13.80 3%IPA	$\alpha$ : 1.09 $k_1$ :5.75 3%IPA

Table 2-5 continued.

Warfarin	$\alpha$ : 1 $k_1$ :41.10 90%IPA	$\alpha$ : 1.20 $k_1$ :12.41 10%IPA & 1% AcOH	$\alpha$ : 1.11 $k_1$ :10.57 10%IPA & 1% AcOH	$\alpha$ : 1 $k_1$ :19.5 3 25%IP A	$\alpha$ : 1.16 $k_1$ :11.55 10%IPA & 1% AcOH	$\alpha$ : 1.12 $k_1$ :14.34 10%IPA & 1% AcOH	$\alpha$ : 1 $k_1$ :28.61 10%IPA & 1% AcOH	$\alpha$ : 1.16 $k_1$ :13.41 25%IPA	$\alpha$ : 1.14 $k_1$ :12.68 10%IPA & 1% AcOH
<i>Sec</i> -Phenethyl alcohol	$\alpha$ : 1 $k_1$ :6.47 1%IPA	$\alpha$ : 1.08 $k_1$ :8.42 1%IPA	$\alpha$ : 1.02 $k_1$ :11.3 1%IPA	$\alpha$ : 1.03 $k_1$ :6.30 1%IPA	$\alpha$ : 1 $k_1$ :6.02 1%IPA	$\alpha$ : 1 $k_1$ :6.84 1%IPA	$\alpha$ : 1 $k_1$ :9.37 1%IPA	$\alpha$ : 1 $k_1$ :19.34 1%IPA	$\alpha$ : 1 $k_1$ :1.90 1%IPA
$\alpha$ -Methyl-2-Naphalenemethanol	$\alpha$ : 1 $k_1$ :15.30 1%IPA	$\alpha$ : 1 $k_1$ :17.31 1%IPA	$\alpha$ : 1 $k_1$ :22.36 1%IPA	$\alpha$ : 1 $k_1$ :13.0 7 1%IPA	$\alpha$ : 1.02 $k_1$ :12.96 1%IPA	$\alpha$ : 1.10 $k_1$ :14.89 1%IPA	$\alpha$ : 1 $k_1$ :17.15 5%IPA	$\alpha$ : 1.04 $k_1$ :7.65 1%IPA	$\alpha$ : 1 $k_1$ :1.19 1%IPA
1-Acenaphthenol	$\alpha$ : 1 $k_1$ :8.12 3%IPA	$\alpha$ : 1 $k_1$ :10.78 3%IPA	$\alpha$ : 1 $k_1$ :13.36 3%IPA	$\alpha$ : 1 $k_1$ :7.34 3%IPA	$\alpha$ : 1 $k_1$ :8.45 3%IPA	$\alpha$ : 1 $k_1$ :11.04 3%IPA	$\alpha$ : 1 $k_1$ :21.41 7%IPA	$\alpha$ : 1 $k_1$ :13.90 3%IPA	$\alpha$ : 1 $k_1$ :8.95 3%IPA
3-Phenyl-Glycidol	$\alpha$ : 1 $k_1$ :9.54 3%IPA	$\alpha$ : 1 $k_1$ :11.13 3%IPA	$\alpha$ : 1 $k_1$ :5.64 3%IPA	$\alpha$ : 1 $k_1$ :10.7 5 3%IPA	$\alpha$ : 1 $k_1$ :9.12 3%IPA	$\alpha$ : 1 $k_1$ :11.29 3%IPA	$\alpha$ : 1 $k_1$ :20.85 3%IPA	$\alpha$ : 1 $k_1$ :15.49 3%IPA	$\alpha$ : 1 $k_1$ :9.78 3%IPA
1,1'-Bi-2-naphthol	$\alpha$ : 1.05 $k_1$ :13.31 75%IPA	$\alpha$ : 1.34 $k_1$ :20.90 75%IPA	$\alpha$ : 1.16 $k_1$ :32.80 75%IPA	$\alpha$ : 1.17 $k_1$ :13.2 1 75%IP A	$\alpha$ : 1.17 $k_1$ :17.07 75%IPA	$\alpha$ : 1.35 $k_1$ :15.73 75%IPA	$\alpha$ : 1 $k_1$ :28.63 75%IPA	$\alpha$ : 1.18 $k_1$ :21.89 75%IPA	$\alpha$ : 1.30 $k_1$ :19.51 75%IPA

Table 2-5 continued.

2,2'-Dihydroxy-5,5',6,6',7,7',8,8'-Octahydro-1,1'-binaphthyl	$\alpha$ : 1 $k_1$ :13.03 10%IPA	$\alpha$ : 1.08 $k_1$ :17.92 10%IPA	$\alpha$ : 1.17 $k_1$ :11.10 10%IPA	$\alpha$ : 1.06 $k_1$ :8.80 10%IPA	$\alpha$ : 1.14 $k_1$ :12.16 10%IPA	$\alpha$ : 1.33 $k_1$ :12.33 10%IPA	$\alpha$ : 1.34 $k_1$ :7.83 10%IPA	$\alpha$ : 1.24 $k_1$ :13.54 10%IPA	$\alpha$ : 1 $k_1$ :12.73 10%IPA
1,2,3,4-Tetrahydro-4-(4-methoxyphenyl)-6-methyl-2-thioxo-5-pyrimidinecarboxylic acid ethyl ester	$\alpha$ : 1 $k_1$ :11.52 10%IPA	$\alpha$ : 1.30 $k_1$ :11.34 15%IPA	$\alpha$ : 1.18 $k_1$ :18.68 15%IPA	$\alpha$ : 1.19 $k_1$ :7.91 15%IPA	$\alpha$ : 1.15 $k_1$ :12.93 15%IPA	$\alpha$ : 1.22 $k_1$ :13.36 15%IPA	$\alpha$ : 1.48 $k_1$ :23.07 15%IPA	$\alpha$ : 1.19 $k_1$ :14.24 15%IPA	$\alpha$ : 1.26 $k_1$ :9.61 15%IPA
1,2,3,4-Tetrahydro-4-(4-hydroxyphenyl)-6-methyl-2-thioxo-, 5-Pyrimidinecarboxylic acid ethyl ester	$\alpha$ : 1.07 $k_1$ :36.72 70%IPA	$\alpha$ : 1.49 $k_1$ :39.00 30%IPA	$\alpha$ : 1.20 $k_1$ :27.80 50%IPA	$\alpha$ : 1.40 $k_1$ :23.11 30%IPA	$\alpha$ : 1.36 $k_1$ :31.14 30%IPA	$\alpha$ : 1.37 $k_1$ :27.18 30%IPA	$\alpha$ : 1.26 $k_1$ :28.56 40%IPA	$\alpha$ : 1.40 $k_1$ :24.64 40%IPA	$\alpha$ : 1.36 $k_1$ :16.80 30%IPA
1-[1,2,3,4-Tetrahydro-4-(4-methoxyphenyl)-6-methyl-2-thioxo-5-pyrimidinyl]ethanone	$\alpha$ : 1 $k_1$ :26.54 10%IPA	$\alpha$ : 1.29 $k_1$ :26.27 15%IPA	$\alpha$ : 1.20 $k_1$ :40.60 15%IPA	$\alpha$ : 1.24 $k_1$ :19.00 15%IPA	$\alpha$ : 1.11 $k_1$ :32.93 15%IPA	$\alpha$ : 1.34 $k_1$ :31.72 15%IPA	$\alpha$ : 1 $k_1$ :50.85 15%IPA	$\alpha$ : 1.34 $k_1$ :34.45 15%IPA	$\alpha$ : 1.23 $k_1$ :17.30 15%IPA
Hexobarbital	$\alpha$ : 1 $k_1$ :29.92 1%IPA	$\alpha$ : 1 $k_1$ :11.51 1%IPA	$\alpha$ : 1 $k_1$ :11.88 1%IPA	$\alpha$ : 1.22 $k_1$ :7.21 1%IPA	$\alpha$ : 1.10 $k_1$ :13.11 1%IPA	$\alpha$ : 1 $k_1$ :15.02 1%IPA	$\alpha$ : 1 $k_1$ :9.74 2%IPA	$\alpha$ : 1 $k_1$ :14.94 1%IPA	$\alpha$ : 1 $k_1$ :15.27 1%IPA

Table 2-5 continued.

Temazepam	$\alpha$ : 1 $k_1$ :20.77 2%IPA	$\alpha$ : 1 $k_1$ :17.73 2%IPA	$\alpha$ : 1 $k_1$ :25.54 2%IPA	$\alpha$ : 1 $k_1$ :12.52 2%IPA	$\alpha$ : 1 $k_1$ :17.34 2%IPA	$\alpha$ : 1 $k_1$ :27.75 2%IPA	$\alpha$ : 1 $k_1$ :25.44 10%IPA	$\alpha$ : 1 $k_1$ :20.24 2%IPA	$\alpha$ : 1 $k_1$ :27.30 2%IPA
5-Methyl- 5-(2,5-dichloro) phenylhydantoin	$\alpha$ : 1 $k_1$ :9.35 10%IPA	$\alpha$ : 1.30 $k_1$ :10.00 15%IPA	$\alpha$ : 1.16 $k_1$ :14.6 15%IPA	$\alpha$ : 1 $k_1$ :12.39 15%IPA	$\alpha$ : 1 $k_1$ :15.78 15%IPA	$\alpha$ : 1 $k_1$ :8.27 15%IPA	$\alpha$ : 1 $k_1$ :7.52 15%IPA	$\alpha$ : 1.22 $k_1$ :9.91 15%IPA	$\alpha$ : 1.16 $k_1$ :7.30 15%IPA
5-Methyl-5-phenyl hydantoin	$\alpha$ : 1 $k_1$ :18.12 8%IPA	$\alpha$ : 1.18 $k_1$ :17.91 8%IPA	$\alpha$ : 1.10 $k_1$ :10.44 8%IPA	$\alpha$ : 1.08 $k_1$ :12.93 8%IPA	$\alpha$ : 1.16 $k_1$ :14.71 8%IPA	$\alpha$ : 1 $k_1$ :13.54 8%IPA	$\alpha$ : 1.16 $k_1$ :13.44 8%IPA	$\alpha$ : 1.10 $k_1$ :19.00 8%IPA	$\alpha$ : 1 $k_1$ :14.25 8%IPA
Mephentoin	$\alpha$ : 1 $k_1$ :7.42 2%IPA	$\alpha$ : 1 $k_1$ :5.73 2%IPA	$\alpha$ : 1.14 $k_1$ :7.86 2%IPA	$\alpha$ : 1 $k_1$ :5.43 2%IPA	$\alpha$ : 1 $k_1$ :5.43 2%IPA	$\alpha$ : 1 $k_1$ :6.27 2%IPA	$\alpha$ : 1.10 $k_1$ :9.74 2%IPA	$\alpha$ : 1 $k_1$ :8.09 2%IPA	$\alpha$ : 1.07 $k_1$ :9.00 2%IPA
<i>sec</i> -Butyl carbanilate	$\alpha$ : 1.47 $k_1$ :4.09 1%IPA	$\alpha$ : 1 $k_1$ :9.04 1%IPA	$\alpha$ : 1 $k_1$ :7.30 1%IPA	$\alpha$ : 1.04 $k_1$ :5.91 1%IPA	$\alpha$ : 1 $k_1$ :5.91 1%IPA	$\alpha$ : 1 $k_1$ :7.74 1%IPA	$\alpha$ : 1 $k_1$ :11.89 1%IPA	$\alpha$ : 1 $k_1$ :9.64 1%IPA	$\alpha$ : 1 $k_1$ :9.61 1%IPA
Methyl Mandelate	$\alpha$ : 1 $k_1$ :9.24 1%IPA	$\alpha$ : 1.23 $k_1$ :9.00 1%IPA	$\alpha$ : 1.10 $k_1$ :10.8 1%IPA	$\alpha$ : 1 $k_1$ :6.50 1%IPA	$\alpha$ : 1 $k_1$ :8.46 1%IPA	$\alpha$ : 1.10 $k_1$ :6.27 1%IPA	$\alpha$ : 1 $k_1$ :19.37 1%IPA	$\alpha$ : 1 $k_1$ :19.00 1%IPA	$\alpha$ : 1 $k_1$ :17.64 1%IPA

a.

separation factor; b. retention factor of the first eluted enantiomer; c. IPA percentage in hexane of the mobile phase

## 2 Mobile phase

Two kinds of mobile phase system: IPA/Hexane and DCM/Hexane/MeOH were chosen to investigate the influence of mobile phase conditions on the separation of analytes of CSPs. Two CSPs: CSP-7(Fmoc-Pro-Pro-Pro-Pro-N(Me)-Ahx-APS)and CSP-2(PIV-Pro-Pro-N(Me)-Ahx-PRP-1) were tested using these two mobile phase systems. The comparison results are summarized on Table 2-6.

For CSP-7 with APS as the support, better versatility was achieved in IPA/hexane mobile phase system: 17 analytes were separated in IPA/hexane while 15 were resolved in the other system. For CSP-2 with PRP-1 as the support, better versatility was got in DCM/Hexane/MeOH system: 6 analytes were resolved in IPA/hexane while 8 were separated in DCM/Hexane/MeOH.

By comparison of chromatograms, peak shape in chromatograms of DCM/Hexane/MeOH system are better for most analytes. The peaks seem to be sharper and narrower in DCM/Hexane/MeOH system for the two CSPs.

Table 2-6. Comparison results of CSP-7 and CSP-2 in two types of mobile phase systems

Analyte name	CSP-7		CSP-2	
	IPA/Hex	DCM/Hex/MeOH	IPA/Hex	DCM/Hex/MeOH
Benzoin	$\alpha$ : 1.09 <sup>a</sup> $k_1$ :6.35 <sup>b</sup> 3%IPA <sup>c</sup>	$\alpha$ : 1.07 $k_1$ :11.61 5%DCM in Hexane	$\alpha$ : 1.41 $k_1$ :6.40 3%IPA	$\alpha$ : 1 $k_1$ :5.04 10%DCM in Hexane
Hydrobenzoin	$\alpha$ : 1.13 $k_1$ :17.98 4%IPA	$\alpha$ : 1.12 $k_1$ :12.93 40%DCM in Hexane	$\alpha$ : 1 $k_1$ :21.40 4%IPA	$\alpha$ : 1.16 $k_1$ :5.06 40%DCM in Hexane
Benzoin oxime	$\alpha$ : 1.13 $k_1$ :15.36 20%IPA	$\alpha$ : 1.08 $k_1$ :15.85 100%DCM	$\alpha$ :1 $k_1$ :13.04 20%IPA	$\alpha$ :1 $k_1$ :4.92 100%DCM
2,2,2-Trifluoro-1-(9-anthryl) ethanol	$\alpha$ : 1.56 $k_1$ :18.48 10%IPA	$\alpha$ : 1.20 $k_1$ :9.54 100%DCM	$\alpha$ : 1.61 $k_1$ :17.40 10%IPA	$\alpha$ : 1.50 $k_1$ :3.35 100%DCM
a-(pentafluoroethyl)-a-(trifluoromethyl)-Benzenemethanol	$\alpha$ : 1.10 $k_1$ :8.91 3%IPA	$\alpha$ : 1.06 $k_1$ :28.23 30%DCM in Hexane	$\alpha$ : 1.18 $k_1$ :6.80 3%IPA	$\alpha$ : 1.15 $k_1$ :7.96 5%DCM in Hexane
Warfarin	$\alpha$ : 1.08 $k_1$ :11.19 10%IPA & 1% AcOH	$\alpha$ : 1.08 $k_1$ :8.30 40%DCM in Hexane& 1%AcOH	$\alpha$ : 1 $k_1$ :11 10%IPA & 1% AcOH	$\alpha$ : 1 $k_1$ :7.18 50%DCM in Hexane
Sec-Phenethyl alcohol	$\alpha$ : 1.02 $k_1$ :8.07 1%IPA	$\alpha$ : 1.02 $k_1$ :13.08 10%DCM in Hexane	$\alpha$ : 1 $k_1$ :9.44 1%IPA	$\alpha$ : 1 $k_1$ :5.82 10%DCM in Hexane
$\alpha$ -Methyl-2-Naphalenemethanol	$\alpha$ : 1.04 $k_1$ :17.62 1%IPA	$\alpha$ : 1 $k_1$ :23.66 10%DCM in Hexane	$\alpha$ : 1 $k_1$ :21.54 1%IPA	$\alpha$ : 1 $k_1$ :12.92 10%DCM in Hexane
1-Acenaphthenol	$\alpha$ : 1 $k_1$ :28.46 3%IPA	$\alpha$ : 1 $k_1$ :7.31 30%DCM in Hexane	$\alpha$ : 1 $k_1$ :14 3%IPA	$\alpha$ : 1 $k_1$ :3.29 10%DCM in Hexane

Table 2-6, continued.

3-Phenyl-Glycidol	$\alpha$ : 1 $k_1$ :6.77 3%IPA	$\alpha$ : 1 $k_1$ :7.39 30%DCM in Hexane	$\alpha$ : 1 $k_1$ :15.4 3%IPA	$\alpha$ : 1 $k_1$ :3.80 10%DCM in Hexane
1,1'-Bi-2-naphthol	$\alpha$ : 1.29 $k_1$ :23.83 75%IPA	$\alpha$ : 1.06 $k_1$ :12.21 1%MeOH in Hexane	$\alpha$ : 1.19 $k_1$ :21 75%IPA	$\alpha$ : 1.20 $k_1$ :7.51 30%DCM in Hexane
2,2'-Dihydroxy-5,5',6,6',7,7',8,8'-Octahydro-1,1'-binaphthyl	$\alpha$ : 1.32 $k_1$ :10.95 10%IPA	$\alpha$ : 1 $k_1$ :12.08 50%DCM in Hexane	$\alpha$ : 1 $k_1$ :10.9 10%IPA	$\alpha$ : 1 $k_1$ :10.67 50%DCM in Hexane
1,2,3,4-Tetrahydro-4-(4-methoxyphenyl)-6-methyl-2-thioxo-5-pyrimidinecarboxylic acid ethyl ester	$\alpha$ : 1.24 $k_1$ :12.60 15%IPA	$\alpha$ : 1.18 $k_1$ :6.26 60%DCM in Hexane	$\alpha$ : 1.21 $k_1$ :24 15%IPA	$\alpha$ : 1.26 $k_1$ :22.53 50%DCM in Hexane
1,2,3,4-Tetrahydro-4-(4-hydroxyphenyl)-6-methyl-2-thioxo-, 5-Pyrimidinecarboxylic acid ethyl ester	$\alpha$ : 1.41 $k_1$ :25.07 30%IPA	$\alpha$ : 1.19 $k_1$ :12.72 3%MeOH in Hexane	$\alpha$ : 1.46 $k_1$ :35.00 30%IPA	$\alpha$ : 1.40 $k_1$ :3.82 3%MeOH in Hexane
1-[1,2,3,4-Tetrahydro-4-(4-methoxyphenyl)-6-methyl-2-thioxo-5-pyrimidinyl]ethanone	$\alpha$ : 1.21 $k_1$ :25.72 15%IPA	$\alpha$ : 1.22 $k_1$ :12.20 60%DCM in Hexane	$\alpha$ : 1 $k_1$ :27.00 15%IPA	$\alpha$ : 1.31 $k_1$ :8.47 50%DCM in Hexane
Hexobarbital	$\alpha$ : 1 $k_1$ :5.96 1%IPA	$\alpha$ : 1 $k_1$ :8.08 30%DCM in Hexane	$\alpha$ : 1 $k_1$ :13.80 1%IPA	$\alpha$ : 1 $k_1$ :1.14 10%DCM in Hexane
Temazepam	$\alpha$ : 1 $k_1$ :20.24 2%IPA	$\alpha$ : 1 $k_1$ :4.62 10%DCM in Hexane	$\alpha$ : 1 $k_1$ :16.20 2%IPA	$\alpha$ : 1 $k_1$ :4.24 30%DCM in Hexane
5-Methyl-5-(2,5-dichloro)phenylhydantoin	$\alpha$ : 1.17 $k_1$ :8.55 15%IPA	$\alpha$ : 1.12 $k_1$ :13.56 100%DCM	$\alpha$ : 1 $k_1$ :9.4 15%IPA	$\alpha$ : 1.25 $k_1$ :5.72 100%DCM
5-Methyl-5-phenyl hydantoin	$\alpha$ : 1.15 $k_1$ :15.6 8%IPA\	$\alpha$ : 1.11 $k_1$ :18.51 100%DCM	$\alpha$ : 1 $k_1$ :17.40 8%IPA	$\alpha$ : 1 $k_1$ :8.80 100%DCM

Table 2-6 continued.

Mephentoin	$\alpha$ : 1.14 $k_1$ :6.93 2%IPA	$\alpha$ : 1.17 $k_1$ :17.10 20%DCM in Hexane	$\alpha$ : 1 $k_1$ :6.80 2%IPA	$\alpha$ : 1 $k_1$ :10.18 20%DCM in Hexane
<i>sec</i> -Butyl carbanilate	$\alpha$ : 1 $k_1$ :7.64 1%IPA	$\alpha$ : 1.12 $k_1$ :4.16 10%DCM in Hexane	$\alpha$ : 1 $k_1$ :7.00 1%IPA	$\alpha$ : 1 $k_1$ :8.27 10%DCM in Hexane
Methyl Mandelate	$\alpha$ : 1.17 $k_1$ :8.31 1%IPA	$\alpha$ : 1 $k_1$ :8.18 10%DCM in Hexane	$\alpha$ : 1 $k_1$ :13.40 1%IPA	$\alpha$ : 1 $k_1$ :6.84 10%DCM in Hexane

a. separation factor; b. retention factor of the first eluted enantiomer; c. IPA percentage in hexane of the mobile phase.

### 3. Comparison of CSP-7 with commercial CSPs

The CSP with best separation results and versatility in the study: CSP-7(Fmoc-Pro-Pro-Pro-N(Me)-Ahx-APS) was compared with three commercial CSPs: CHIRALPAK OD-H, CHIRALPAK AD-H and Whelk-O2. These three commercial CSPs are the most widely used in pharmaceutical industries and research labs. The comparison results are shown on Table 2-7.

Among the 4 CSPs, CSP-7 resolved 17 analytes while CHIRALPAK OD-H separated 18, CHIRALPAK AD-H resolved 17 and Whelk-O2 resolved 15 out of 22 analytes. So the versatility of CSP-6 is comparable with these commercial CSPs. Considering the fact that column size of CSP-7 is 50×4.6 mm and columns sizes of commercial CSPs are 150×4.6 mm or 250×4.6 mm, these results are very encouraging.

For enantio-selectivity, CSP-7 got comparable separation factors for most analytes with the three commercial CSPs. For some analytes, CSP-7 even achieved better



separations: it resolved TFAE with  $\alpha$  of 1.56 , 1,1'-Bi-2-naphthol with  $\alpha$  of 1.29, 2,2'-Dihydroxy-5,5',6,6',7,7',8,8'-Octahydro-1,1'-binaphthyl with  $\alpha$  of 1.32 and 1,2,3,4-Tetrahydro-4- (4-hydroxyphenyl)- 6-methyl-2-thioxo-, 5-Pyrimidinecarboxylic acid ethyl ester with  $\alpha$  of 1.41. CSP-7 shows great potential to be developed into a commercial CSP. The chromatograms of TFAE separated by these 4 CSPs are shown on Figure 2-6.

For CSP-7, the retention factors are bigger for most analytes compared with commercial CSPs. And peak shapes of analytes in chromatograms are broader for CSP-7. So preparation process needs to be improved to increase the column efficiency and decrease the retention factor.

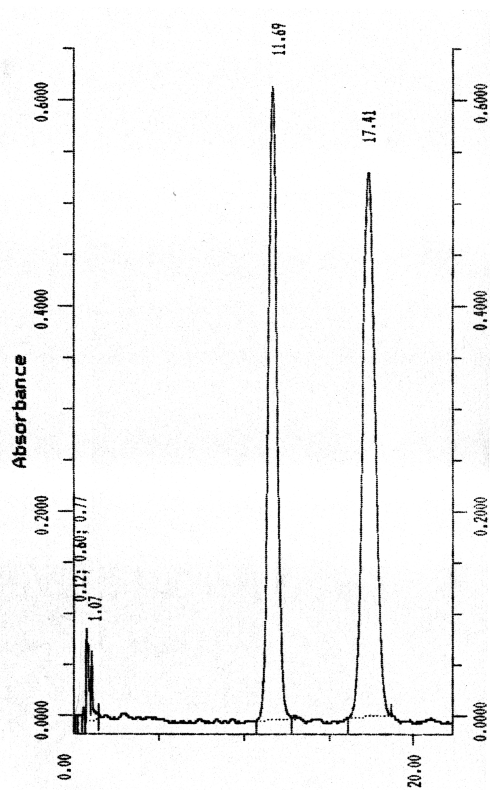
Table 2-7. Comparison results of CSP-7 and three commercial CSPs

Analyte name	CSP-7	CHIRALPAK OD-H	CHIRALPAK AD-H	Whelk-O2
Benzoin	$\alpha$ : 1.09 <sup>a</sup> $k_1$ :6.35 <sup>b</sup> 3%IPA <sup>c</sup>	$\alpha$ : 1.61 $k_1$ :4.68 15%IPA	$\alpha$ : 1.32 $k_1$ :3.46 15%IPA	$\alpha$ : 2.12 $k_1$ :1.83 5%IPA
Hydrobenzoin	$\alpha$ : 1.13 $k_1$ :17.98 4%IPA	$\alpha$ : 1 $k_1$ :7.35 4%IPA	$\alpha$ : 1.08 $k_1$ :5.15 8%IPA	$\alpha$ :1.33 $k_1$ :4.18 4%IPA
Benzoin oxime	$\alpha$ : 1.13 $k_1$ :15.36 20%IPA	$\alpha$ : 1.13 $k_1$ :2.82 10%IPA	$\alpha$ : 1.24 $k_1$ :4.55 15%IPA	$\alpha$ : 1.31 $k_1$ :1.40 10%IPA
2,2,2-Trifluoro-1-(9-anthryl) ethanol(TFAE)	$\alpha$ : 1.56 $k_1$ :18.48 10%IPA	$\alpha$ : 1.13 $k_1$ :1.26 15%IPA	$\alpha$ : 1.47 $k_1$ :1.99 10%IPA	$\alpha$ : 1.13 $k_1$ :0.62 10%IPA
a-(pentafluoroethyl)-a-(trifluoromethyl)-Benzenemethanol	$\alpha$ : 1.10 $k_1$ :8.91 3%IPA	$\alpha$ : 1.16 $k_1$ :0.90 1%IPA	$\alpha$ : 1.11 $k_1$ :0.79 3%IPA	$\alpha$ : 1 $k_1$ :0.70 3%IPA
Warfarin	$\alpha$ : 1.08 $k_1$ :11.19 10%IPA & 1% AcOH	$\alpha$ : 2.49 $k_1$ :6.40 15%IPA	$\alpha$ :3.94 $k_1$ :5.02 20%IPA	$\alpha$ : 1.97 $k_1$ :10.06 20%IPA
Sec-Phenethyl alcohol	$\alpha$ : 1.02 $k_1$ :8.07 1%IPA	$\alpha$ : 1.37 $k_1$ :8.30 1%IPA	$\alpha$ : 1 $k_1$ :4.12 2%IPA	$\alpha$ : 1.03 $k_1$ :3.64 2%IPA
$\alpha$ -Methyl-2-Naphalenemethanol	$\alpha$ : 1.04 $k_1$ :17.62 1%IPA	$\alpha$ : 1 $k_1$ :6.25 3%IPA	$\alpha$ : 1.05 $k_1$ :1.98 10%IPA	$\alpha$ : 1.02 $k_1$ :4.39 3%IPA
1-Acenaphthenol	$\alpha$ : 1 $k_1$ :28.46 3%IPA	$\alpha$ : 1.16 $k_1$ :5.46 3%IPA	$\alpha$ : 1.08 $k_1$ :6.58 3%IPA	$\alpha$ : 1.28 $k_1$ :4.96 3%IPA
3-Phenyl-Glycidol	$\alpha$ : 1 $k_1$ :6.77 3%IPA	$\alpha$ : 1.15 $k_1$ :16.87 10%IPA	$\alpha$ : 1 $k_1$ :8.01 8%IPA	$\alpha$ : 1.37 $k_1$ :8.74 10%IPA
1,1'-Bi-2-naphthol	$\alpha$ : 1.29 $k_1$ :23.83 75%IPA	$\alpha$ : 1.16 $k_1$ :4.49 8%IPA	$\alpha$ : 1.13 $k_1$ :3.58 25%IPA	$\alpha$ : 1 $k_1$ :1.26 5%IPA

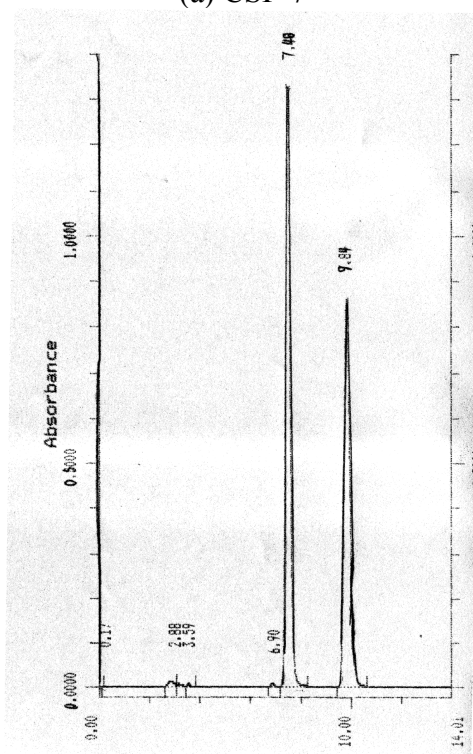
Table 2-7 continued.

2,2'-Dihydroxy-5,5',6,6',7,7',8,8'- Octahydro-1,1'-binaphthyl	$\alpha$ : 1.32 $k_1$ :10.95 10%IPA	$\alpha$ : 1.32 $k_1$ :3.98 5%IPA	$\alpha$ :1 $k_1$ :8.53 10%IPA	$\alpha$ : 1 $k_1$ :4.47 5%IPA
1,2,3,4-Tetrahydro-4- (4-methoxyphenyl)- 6-methyl-2-thioxo- 5-pyrimidinecarboxylic acid ethyl ester	$\alpha$ : 1.24 $k_1$ :12.60 15%IPA	$\alpha$ : 1.15 $k_1$ :2.13 15%IPA	$\alpha$ :1.40 $k_1$ :3.44 15%IPA	$\alpha$ : 1.16 $k_1$ :2.27 15%IPA
1,2,3,4-Tetrahydro-4- (4-hydroxyphenyl)- 6-methyl-2-thioxo-, 5- Pyrimidinecarboxylic acid ethyl ester	$\alpha$ : 1.41 $k_1$ :25.07 30%IPA	$\alpha$ : 1.30 $k_1$ :2.87 15%IPA	$\alpha$ :1.36 $k_1$ :4.62 15%IPA	$\alpha$ : 1 $k_1$ :2.23 15%IPA
1-[1,2,3,4-Tetrahydro-4- (4-methoxyphenyl)- 6-methyl-2-thioxo- 5-pyrimidinyl]ethanone	$\alpha$ : 1.21 $k_1$ :25.72 15%IPA	$\alpha$ : 1.18 $k_1$ :2.62 15%IPA	$\alpha$ :1.70 $k_1$ :3.62 15%IPA	$\alpha$ : 1 $k_1$ :1.83 15%IPA
Hexobarbital	$\alpha$ : 1 $k_1$ :5.96 1%IPA	$\alpha$ : 1.12 $k_1$ :6.26 5%IPA	$\alpha$ :1.46 $k_1$ :2.42 8%IPA	$\alpha$ : 1 $k_1$ :1.95 5%IPA
Temazepam	$\alpha$ : 1 $k_1$ :20.24 2%IPA	$\alpha$ : 1 $k_1$ :3.39 25%IPA	$\alpha$ :1 $k_1$ :4.12 25%IPA	$\alpha$ : 1.19 $k_1$ :3.40 25%IPA
5-Methyl- 5-(2,5-dichloro) phenylhydantoin	$\alpha$ : 1.17 $k_1$ :8.55 15%IPA	$\alpha$ : 1.08 $k_1$ :4.29 8%IPA	$\alpha$ :1 $k_1$ :4.80 8%IPA	$\alpha$ : 1.11 $k_1$ :1.96 10%IPA
5-Methyl-5-phenyl hydantoin	$\alpha$ : 1.15 $k_1$ :15.6 8%IPA	$\alpha$ : 1.09 $k_1$ :4.06 8%IPA	$\alpha$ :1 $k_1$ :3.24 8%IPA	$\alpha$ : 1.46 $k_1$ :1.67 10%IPA
Mephentoin	$\alpha$ : 1.14 $k_1$ :6.93 2%IPA	$\alpha$ : 1.10 $k_1$ :5.20 4%IPA	$\alpha$ :1.37 $k_1$ :3.56 4%IPA	$\alpha$ : 1 $k_1$ :3.35 4%IPA
<i>sec</i> -Butyl carbanilate	$\alpha$ : 1 $k_1$ :7.64 1%IPA	$\alpha$ : 1 $k_1$ :6.18 2%IPA	$\alpha$ :1.04 $k_1$ :3.35 2%IPA	$\alpha$ : 1.05 $k_1$ :3.36 1%IPA
Methyl Mandelate	$\alpha$ : 1.17 $k_1$ :8.31 1%IPA	$\alpha$ : 1.25 $k_1$ :2.82 3%IPA	$\alpha$ :1.08 $k_1$ :1.85 10%IPA	$\alpha$ : 1.07 $k_1$ :1.12 10%IPA

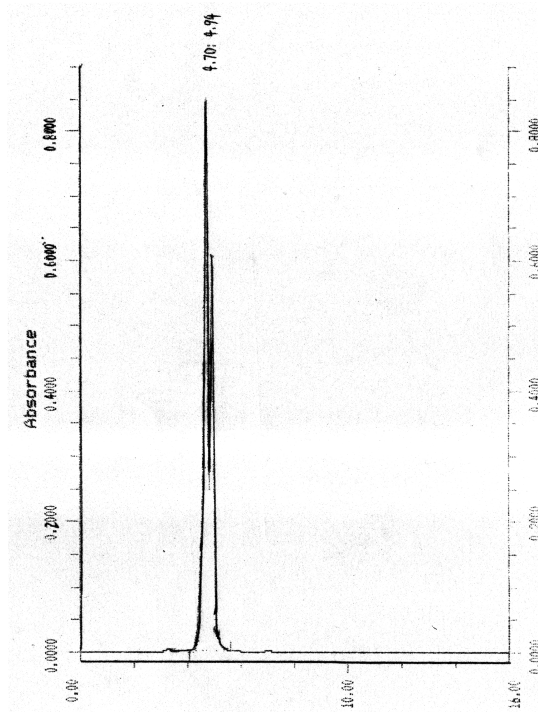
a. separation factor; b. retention factor of the first eluted enantiomer; c. IPA percentage in hexane of the mobile phase



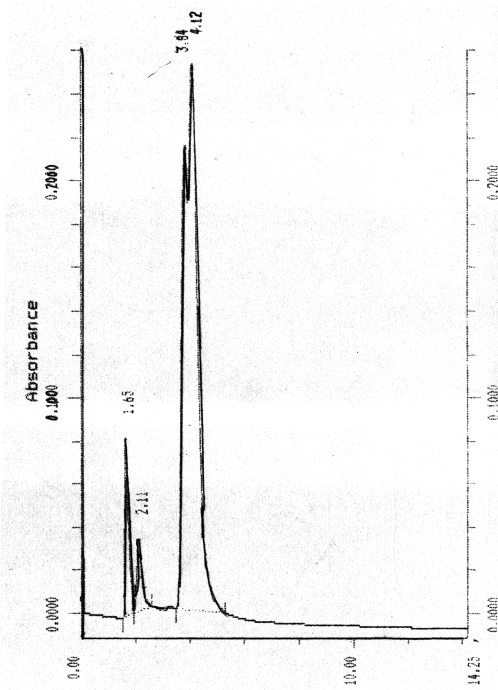
(a) CSP-7



(b) CHIRALPAK AD-H



(c) CHIRALPAK OD-H



(d) Whelk-O2

Figure 2-6. Chromatograms of TFAE separated by CSP-7 and three commercial CSPs

## Conclusion

17 new L-proline based CSPs were designed, prepared and evaluated. The influence of structural components of these CSPs, including support, linker, number of L-proline units, modification of L-proline unit and end group, and mobile phase system on the enantioselectivity and versatility of CSPs was investigated.

To achieve better versatility and enantioselectivity, APS support is much better than PRP-1 in IPA/Hexane mobile phase and -N(Me)-Ahx- linker capable of accepting hydrogen bond is more adaptable than -NH-Ahx- linker capable of donating hydrogen bond.

The increase of number of L-proline units in the structure of CSP can improve the enantioselectivity and versatility but the achiral retention of analytes is also increased and versatility decreased slightly if the number of L-proline units reaches 6.

Modification of L-proline into *t*-butyl-trans-4-L-Hydroxyproline structure has negative effects on the separation abilities of CSPs.

End groups in the structure have great influence on the enantio-discrimination and versatility of CSPs. CSP with Piv group has great enantioselectivity towards the 22 analytes and CSP with Fmoc group shows good versatility. Piv and Fmoc groups seem to be good choices for end group.

The mobile phase also has effects on the separation abilities of CSPs. CSP-7 with APS as the support got better versatility in IPA/Hexane system while CSP-2 with PRP-1 as the support had better versatility in DCM/Hexane/MeOH system.

Separation ability of the best CSP among the 17 ones — CSP-7(Fmoc-Pro-Pro-Pro-Pro-N(Me)-Ahx-APS) were also compared with those of three popular commercial CSPs. The enantio-selectivity and versatility of this CSP is comparable with commercial ones.

### References

1. Iuliano, A.; Attolino, E.; Salvadori, P.; *Eur. J.Org. Chem.* **2001**, 13523.
2. Beesley, T. E.; Scott, R. P. W. *Chiral Chromatography*; John Wiley & Sons: New York, 1998; pp221.
3. Hermansson, J. *Journal of Chromatography* **1983**, 269, 71-80.
4. Pirkle, W. H.; House, D.W. *J. Org. Chem.* **1979**, 44, 1957.
5. Okamoto, Y. *Chem. Lett.* **1998**, 1237.
6. Armstrong, D.W.; Tang, Y.; Chen, S.; Zhou, Y.; Bagwill, C.; Chen, J.R. *Anal. Chem.* **1994**, 66, 1473.
7. Armstrong, D. W.; Ward, T. J.; Armstrong, R. D.; Beesley, T. E. *Science* **1986**, 232, 1132-1135.
8. Creighton, T. E. *Proteins. Structures and Molecular Properties*, 2nd ed; W. H. Freeman and Company: New York, 1993.
9. Haurou, C. D.; Declercq, G.; Ramiandrasoa, P. *J. Chromatog.* **1991**, 547, 31.
10. Pirkle, W.H.; Koscho, M.E. *J. Chromatogr. A* **1999**, 840, 151.
11. Pirkle, W.H.; Murray, P.G. *J. Chromatogr.* **1993**, 641, 11.
12. Pirkle, W.H.; Murray, P.G. *J. Chromatogr. A* **1996**, 719, 299.
13. Pirkle, W.H.; Murray, P.G.; Rausch, D.J.; McKenna, S.T. *J.Org. Chem.* **1996**, 61, 4769.
14. Pirkle, W.H.; Murray, P.G.; Wilson, S.R. *J. Org. Chem.* **1996**, 61, 4775.

## CHAPTER III

### SPECTROSCOPIC RATIONALIZATION OF THE SEPARATION ABILITIES OF DECAPROLINE CHIRAL SELECTOR IN DICHLOROMETHANE-ISOPROPANOL SOLVENT MIXTURE

#### Introduction

A series of chiral columns, with proline oligomers as chiral selectors, have been developed recently<sup>1-3</sup>. These columns have relatively broad chiral selectivity and their separation performance is comparable to some popular commercial columns. To understand the separation mechanism of these oligoproline-based chiral columns, it is necessary to understand the conformations of proline oligomers in the mobile phase. Because of the cyclic structure of proline, the oligomers of proline form unique helical conformations, namely polyproline I (PPI)<sup>4</sup> and polyproline II (PPII)<sup>5</sup>, which are distinctly different from standard  $\alpha$ -helix and  $\beta$ -sheet structures<sup>6</sup>. The PPI helix is a right handed helix with an axial translation of 1.90Å composed of 3.3 residues per turn, and its all peptide bonds are in cis configuration with backbone dihedral angles of  $\varphi=-75^\circ$ ,  $\psi=+160^\circ$ ,  $\omega=0^\circ$ .<sup>4</sup> The PPII helix is a left-handed helix with an axial translation of 3.20Å composed of 3.0 residues per turn, and its all peptide bonds are in trans configuration with  $\varphi=-75^\circ$ ,  $\psi=+145^\circ$ ,  $\omega=180^\circ$ .<sup>5</sup>

The conformations of some proline oligopeptides have been previously studied using different spectroscopic techniques<sup>7-12</sup>. Most of the literature work dealt with the conformation of proline oligopeptides in aqueous solutions although some papers also



reported the conformation of proline oligomers in pure organic solvents, such as chloroform<sup>10</sup>, methanol<sup>8b</sup> and 1-propanol<sup>8b</sup>.

Using infrared (IR) absorption spectral measurements on KBr disks, Isemura and coworkers<sup>7a</sup> did not see differences for the peptide carbonyl absorption bands of PPI and PPII conformations. However, Strassmair and coworkers<sup>7b</sup> studied poly-O-acetyl-L-hydroxyproline in solution and found that for PPI conformation in dichloromethane (DCM), the position of peptide carbonyl absorption band remains almost unchanged when alcohol (benzyl alcohol or *n*-butanol) is added to DCM. But for PPII conformation, the peptide carbonyl absorption band continuously shifted to lower frequencies as the percent alcohol added is increased. Based on this observation they have concluded<sup>7b</sup> that the peptide carbonyl groups bind to alcohol solvent molecules much stronger in PPII conformation than in PPI conformation. Swenson and Formanek have reported<sup>7c</sup> that the peptide carbonyl absorption band of PPII in D<sub>2</sub>O appears at 1624 cm<sup>-1</sup> and this band shifts to a higher frequency at elevated temperature. They suggested that conformational change resulting from rotation around C<sub>α</sub>-C(=O) could be one explanation for the observed spectral changes. Dukor and Keiderling reported<sup>9b</sup> that the peptide carbonyl absorption band for PPII in D<sub>2</sub>O solution appears at 1623 cm<sup>-1</sup> and that for PPI appears at 1635 cm<sup>-1</sup>.

Using electronic circular dichroism (ECD)<sup>8</sup> spectral measurements in H<sub>2</sub>O, Okabayashi and coworkers indicated that proline oligopeptides, containing three or more proline units adopt PPII conformation which gives a weak positive ECD in the 221-225 nm range and a strong negative ECD in the 200-210 nm range. Kakinoki and coworkers have indicated<sup>8b</sup> that proline oligopeptides adopt PPII conformation in water and

trifluoroethanol solvents. They reported that PPII conformation is characterized by an ECD spectrum with a strong negative band at 202-206nm and a weak positive band at 225-229nm and that PPI is characterized by an ECD spectrum with a medium intensity negative band at 198-200nm, a strong positive band at 214-215nm, and a weak negative band at 231-232nm. For the oligopeptide containing 13 proline residues, they also noted a transition from PPII to PPI conformation in pure aliphatic alcohols, such as methanol and propanol.

Dukor and Keiderling used vibrational circular dichroism (VCD) measurements on unblocked proline oligomers, (Pro)<sub>n</sub>, with n=3-7, in D<sub>2</sub>O and indicated<sup>9a</sup> that PPII structure is favored. The PPII structure is characterized by a negative VCD couplet, with positive VCD on the higher frequency side and negative VCD on the lower frequency side of the absorption band center at 1623 cm<sup>-1</sup>. Conversion between PPII and PPI conformations has also been studied<sup>9b</sup> in D<sub>2</sub>O for poly-L-proline using VCD. The VCD of PPI conformation was found to be similar to that of PPII, namely a negative VCD couplet, but the absorption maximum of PPI at 1635 cm<sup>-1</sup> and its associated VCD is shifted to higher frequency compared to that of PPII at 1623 cm<sup>-1</sup>.

From NMR studies, Blout and coworkers have concluded<sup>10a</sup> that for t-butyloxycarbonyl-(L-Pro)<sub>n</sub> benzyl esters in chloroform, a random distribution of cis and trans peptide bonds appears for n=2-4, but a PPII conformation is favored when n = 5 and 6. But Zhang and Madalengoitia<sup>10b</sup> concluded that for these oligomers PPII conformation is favored in CDCl<sub>3</sub> solvent, without any limit for critical chain length. Walton et al<sup>11</sup> presented Raman spectra for three proline oligomers (trimer, tetramer and pentamer) with

*tert*-amyloxycarbonyl blocking group and found that all these three oligomers have PPII structures in aqueous solution.

Optical rotation was one of the earliest techniques applied to study the conformation of proline polypeptides<sup>4a,12</sup>. Kurtz et al<sup>12a</sup> found that, in acetic acid or water, PPI exhibits a specific rotation  $[\alpha]_D = +50^\circ$  while PPII exhibits a very different specific rotation  $[\alpha]_D = -540^\circ$  and that PPI mutarotates in water to PPII over a period of several days.

Recently, a liquid chromatographic column with decaproline oligomer as the chiral selector has been developed<sup>1</sup> and this column has demonstrated even better separation abilities than the proline-based columns described in CHAPTER II. The decaproline oligomer (see Figure 3-1), with *t*-butoxy carbonyl (Boc) group replaced by trimethyl acetyl (TMA) group, was connected to the support of 3-methylaminopropyl silica gel (see Figure 3-2), and was used as the stationary phase. This column could resolve more than 40, out of 53, analytes chosen randomly for testing. In normal-phase HPLC experiments, the commonly used solvent mixtures for the mobile phase are isopropanol(IPA)/DCM and IPA/hexane. In this manuscript we investigate the conformation of decaproline oligomer with Boc end group (Figure 3-1), in the IPA/DCM solvent mixtures using multiple spectroscopic techniques, namely optical rotation, ECD, IR and VCD. The conformational information obtained for the decaproline oligomer is then related to the separation results of the chiral column.

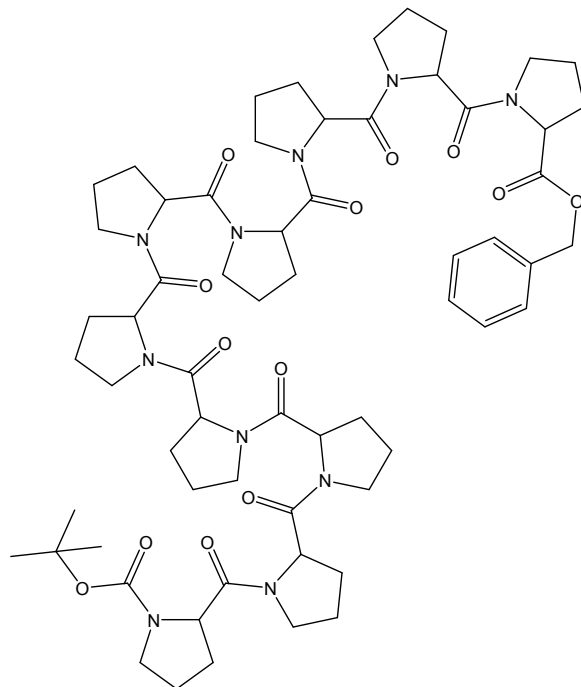


Figure 3-1. Structure of the decaproline oligomer (Boc-(Pro)<sub>10</sub>-OBn).

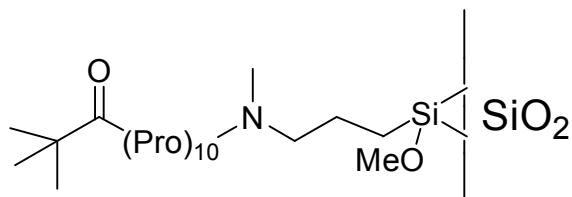


Figure 3-2. The chemical structure of the CSP with the decaproline oligomer as chiral selector.

## Experimental

*N*-Boc O-benzyl protected decaproline oligomer (Boc-(Pro)<sub>10</sub>-OBn) was synthesized according to the reported method<sup>10a</sup>. The solvents, IPA and DCM were purchased from Aldrich.

For IR, VCD and ECD measurements, six sample solutions of the same concentration (3.5 mg/mL), but with varying proportions of IPA and DCM were prepared from a stock solution with 35 mg Boc-(Pro)<sub>10</sub>-OBn dissolved in 1 mL of DCM. For 0% IPA solution, 200  $\mu$ L of the stock solution was added to 800  $\mu$ L of DCM; for 20% IPA solution, 200  $\mu$ L of the stock solution was added to 600  $\mu$ L of DCM and 200  $\mu$ L of IPA; for 40% IPA solution, 200  $\mu$ L of the stock solution was added to 400  $\mu$ L of DCM and 400  $\mu$ L of IPA; for 60% IPA solution, 200  $\mu$ L of the stock solution was added to 200  $\mu$ L of DCM and 600  $\mu$ L of IPA; for 80% IPA solution, 200  $\mu$ L of the stock solution was added to 800  $\mu$ L of IPA. For 100% IPA solution, 3.5 mg decaproline oligomer was dissolved in 1 mL of IPA. For optical rotation measurements also six sample solutions were prepared using the same procedure as that mentioned above, except that the concentration of each sample solution was 1.0 mg/mL and 2 mL solution was prepared for each sample.

An Autopol IV polarimeter with a resolution of 0.001° (reproducibility of 0.002°) was used for optical rotation measurements. Sodium D line was used to measure the optical rotation at the wavelength of 589 nm. Each of the sample solutions (1.5 mL) was transferred to a 1.0 dm cell and optical rotation was measured three different times (by removing the cell from and reinserting the cell into the sample compartment) to check for consistency. The averages of these measurements were used to calculate specific rotation.

All ECD measurements were made on a JASCO J720 spectropolarimeter at room temperature, using a resolution of 1 nm, and sensitivity of 100 mdeg. All spectra reported in this study were averages of 3 individual scans. The spectra were recorded at a scan speed of 100 nm/min and a time constant of 0.125 s. The sample solutions (100  $\mu$ L) were held in a circular quartz cell with a path length of 100  $\mu$ m. The corresponding solvent spectrum was subtracted from the ECD spectrum of the decaproline oligomer. For ease in comparison of spectra, all ECD spectra presented are normalized so that their positive bands have the same intensity.

All IR absorption and VCD spectra were recorded on a commercial Chiralir spectrometer (Bomem-Biotools, Canada). The absorption spectra were recorded at 4  $\text{cm}^{-1}$  resolution with 225 scans, while VCD spectra were recorded at 8  $\text{cm}^{-1}$  resolution with a spectral collection time of 3h. The sample solutions were held in a demountable cell with  $\text{BaF}_2$  windows and 500  $\mu$ m spacer. The absorption and VCD spectra of solvents were subtracted from the corresponding spectra of the decaproline oligomer.

The HPLC experiments for the separation of 2,2,2-Trifluoro-1-[10-(2,2,2-trifluoro-1-hydroxy-ethyl-anthracen-9-yl)]-ethanol (DiTFAE) by the decaproline column in IPA/DCM mobile phase were conducted with the following conditions: UV detection at 254 nm; flow rate at 1 mL/min; mobile phase: IPA/DCM; dead time  $t_0$  was measured with 1,3,5-tri-*t*-butylbenzene.

## Results and discussion

The optical rotation, ECD, IR and VCD spectral measurements were obtained by varying the composition of IPA/DCM solvent mixture from 0% IPA (pure DCM) to 100% IPA.

### 1. Optical rotation

The specific rotations of the decaproline oligomer in IPA/DCM solvent mixture (0% IPA ~100% IPA) are shown in Figure 3-3.

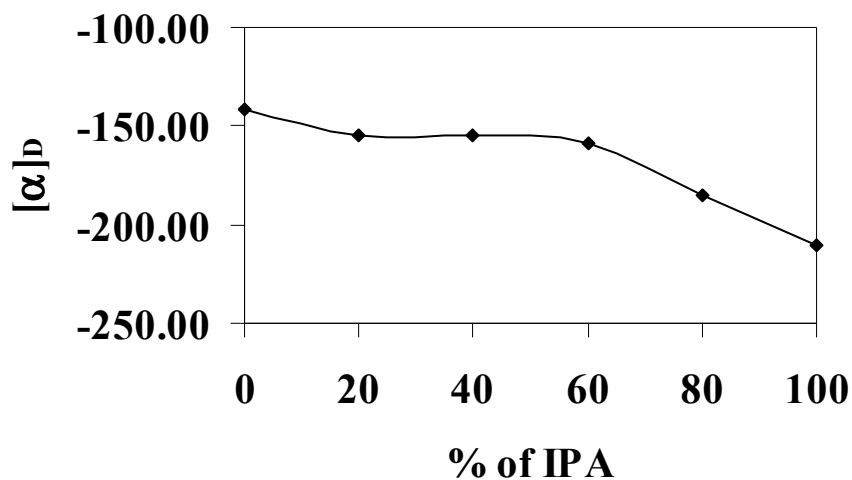


Figure 3-3. Specific rotation,  $[\alpha]_D$ , of the decaproline oligomer in IPA/DCM solvent mixtures.

As the composition of the solvent is changed from 0% IPA to 20% IPA, the magnitude of specific rotation,  $[\alpha]_D$  of the decaproline oligomer increases slightly. As the percentage of IPA in solvent system increases from 20% to 40%, then to 60%, the specific rotation of this oligomer remains the same. When the solvent system is changed

from 60% IPA to 80% IPA and then to 100% IPA, the magnitude of specific rotation of this oligomer increases again. In the entire range of IPA/DCM solvent mixture, from 0% to 100% IPA, the sign of  $[\alpha]_D$  remained negative and the specific rotation changed from  $-140^\circ$  in 0% IPA to  $-210^\circ$  in 100% IPA.

In the literature studies on  $[\alpha]_D$  of PPI and PPII conformations, PPI is characterized<sup>4a,12</sup> by a slightly positive  $[\alpha]_D$  in water or acetic acid solvents. PPII is characterized<sup>4a,12</sup> by a large negative  $[\alpha]_D$  in water or acetic acid solvents. But  $[\alpha]_D$  of PPI or PPII conformation in pure DCM, pure IPA or IPA/DCM mixture was not reported before. From the observed behavior of  $[\alpha]_D$  of this decaprolin oligomer, there are two possibilities for the conformation of this oligomer in IPA/DCM solvent system. Since PPII conformation was characterized by negative  $[\alpha]_D$ , it is possible that the decaprolin oligomer in IPA/DCM mixture may also have a PPII conformation. Then the change in magnitude of optical rotation with solvent composition may have to be attributed to solvent related effects. The second possibility is that both PPII and PPI conformations may be present in IPA/DCM mixture for this oligomer, with population of one conformer decreasing and that of second conformer increasing as the percentage of IPA in the solvent mixture increases. Additional evidence is needed to establish one of these two possibilities.

## **2. Electronic circular dichroism spectra**

The literature studies have used ECD to distinguish PPI and PPII conformations. PPI is generally characterized by an ECD spectrum with a medium intensity negative band at 198-200 nm, a strong positive band at 214-215 nm, and a weak negative band at 231-232



nm.<sup>8b</sup> PPII is generally characterized by a ECD spectrum with a strong negative band at 202-206nm and a weak positive band at 225-229nm.<sup>8b</sup>

The present ECD spectra of the decaproline oligomer in varying IPA/DCM solvent mixtures are shown at Figure 3-4. All these spectra exhibit the same pattern of ECD bands: a strong negative band at lower wavelength and a weak positive band at higher wavelength. As the percentage of IPA in the solvent system increases from 0% to 100%, the position of the positive band remains unchanged at 226 nm. The position of the negative band shifts from 209 nm gradually to 205 nm when the percentage of IPA increases from 0% to 60%. Beyond this point, as the percentage of IPA increases from 60% to 100%, the position of the negative band remains almost unchanged at 205 nm. The ECD patterns observed here are those assigned to PPII conformation, and we did not see strong positive ECD at 215 nm that is characteristic of PPI conformation. Thus it appears that the decaproline oligomer is in PPII conformation in IPA/DCM solvent system (0% IPA ~ 100% IPA).

The blue shift of the negative ECD band, as the percent of IPA increased from 0 to 60%, is considered to be caused by hydrogen bonding of C=O groups of the decaproline oligomer with IPA molecules. Previously<sup>8b</sup> the blue shift of negative ECD band, with a decrease in the number of residues, was attributed to the decreased stability of standard PPII helix. Then it is possible that some changes in dihedral angle around  $C_{\alpha}$ -C(=O) occur as the percent of IPA is increased in the solvent mixture. Overall the shift of the negative band is very small (from 209 nm to 205 nm). Infrared and VCD spectra are expected to be more sensitive to hydrogen bonding influence and therefore we have undertaken these studies.

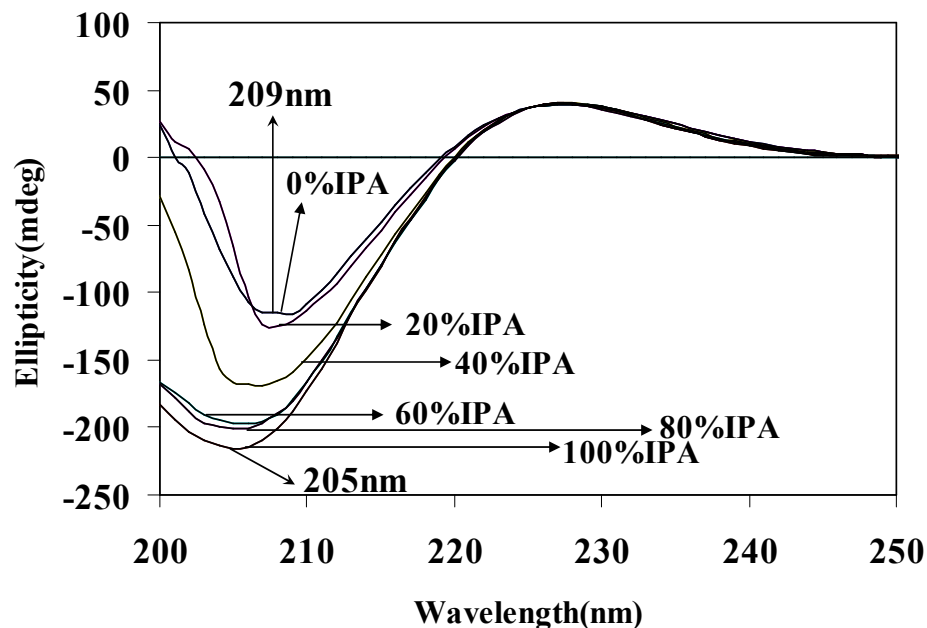


Figure 3-4. ECD spectra of the decaproline oligomer in IPA/DCM solvent mixtures.

### 3. Infrared absorption spectra

The decaproline oligomer (Figure 3-1) contains three different types of carbonyl groups: the peptide carbonyl groups, the Boc carbonyl groups and the carbonyl group connected to the benzyloxy protecting group. In the preparation of chiral stationary phase, the decaproline oligomer is connected to a linker molecule by removing the benzyloxy group and forming another amide bond. As a result, vibrational bands originating from the peptide carbonyl groups and Boc carbonyl groups are of interest here.

In presenting the infrared absorption bands of the peptide C=O groups (Figure 3-5), the bands are normalized to  $A_{\max} = 1.0$  for the ease in comparison of spectra. As the solvent composition changes from 0% IPA to 60% IPA, there is a significant shift in band

position (Figure 3-6) for the carbonyl absorption band. As the composition of IPA increases further only a small frequency shift is found.

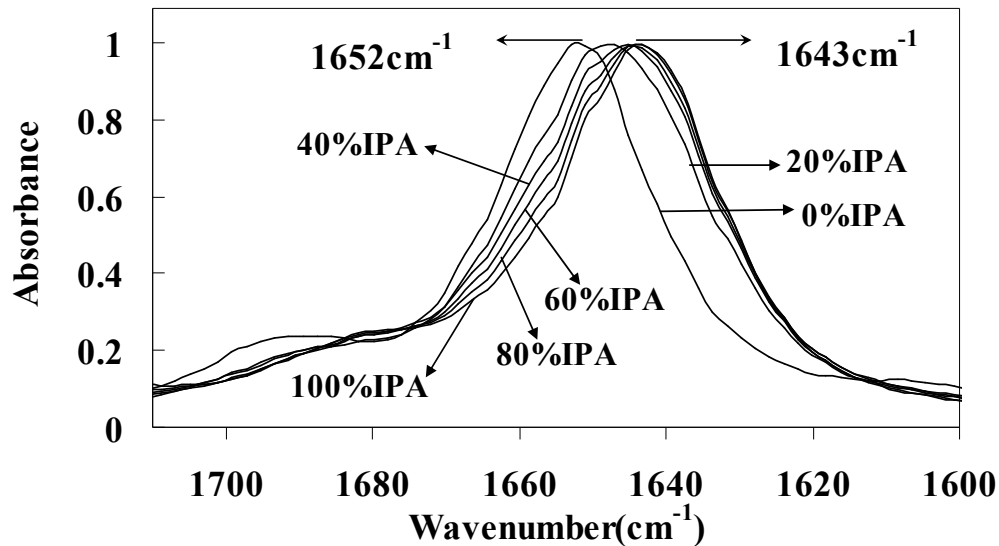


Figure 3-5. Infrared absorption spectra of the peptide C=O groups of decaproline oligomer in IPA/DCM solvent system.

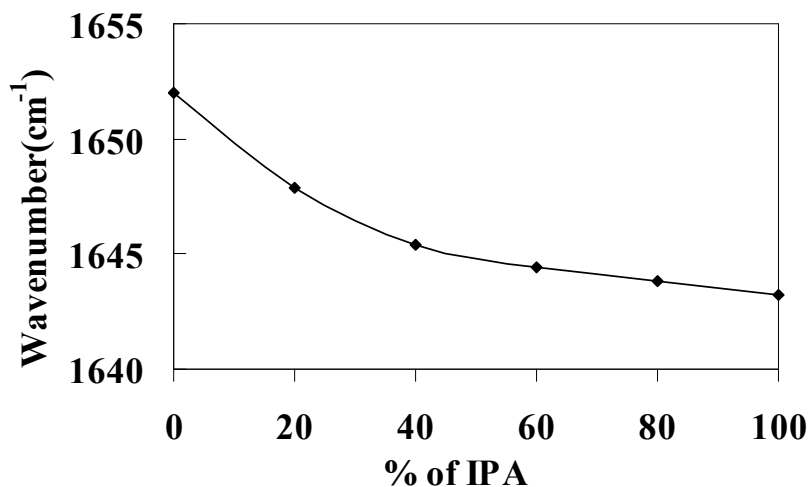


Figure 3-6. Frequencies of peptide carbonyl band of the decaproline oligomer in IPA/DCM solvent system.

Strassmair et al reported<sup>7b</sup> that for poly-O-acetyl-L-hydroxyproline in PPI conformation, the position of carbonyl absorption band remained almost unchanged in DCM when alcohol (benzyl alcohol or *n*-butanol) was added to DCM, but in PPII conformation, there was a significant shift of carbonyl absorption band to lower frequencies when alcohol was added. For the decaprolin oligomer here in IPA/DCM system, a clear shift to lower frequencies (compared with that in pure DCM) is observed for the peptide carbonyl absorption band as the content of IPA increases. This offers further evidence that the decaprolin oligomer is in PPII conformation in IPA/DCM system. The IPA molecules can form hydrogen bonding to the peptide C=O groups, influence the dihedral angle around C<sub>α</sub>-C(=O), and cause the peptide C=O band to shift to lower frequency. The DCM molecules on the other hand do not participate in hydrogen bonding. In pure DCM solvent (0% IPA), the peptide C=O groups of decaprolin oligomer can be regarded as free CO groups. When the percentage of IPA in the solvent increases from 60% to 100%, the shift of the peptide C=O band becomes small indicating that the hydrogen bonding with the solvent, and concomitant changes in the dihedral angle around C<sub>α</sub>-C(=O), are near saturation when the content of IPA in the solvent mixture reaches 60%.

The infrared absorption bands of the Boc carbonyl group are shown in Figure 3-7. As the solvent composition changes from 0% IPA to 60% IPA, there is a large shift in the band position (from 1689 cm<sup>-1</sup> to 1678 cm<sup>-1</sup>). Also the intensity of this band decreases. As the percentage of IPA in the solvent increases from 60% to 100%, the position of the band remains unchanged at 1678 cm<sup>-1</sup> and the intensity of the band increases.

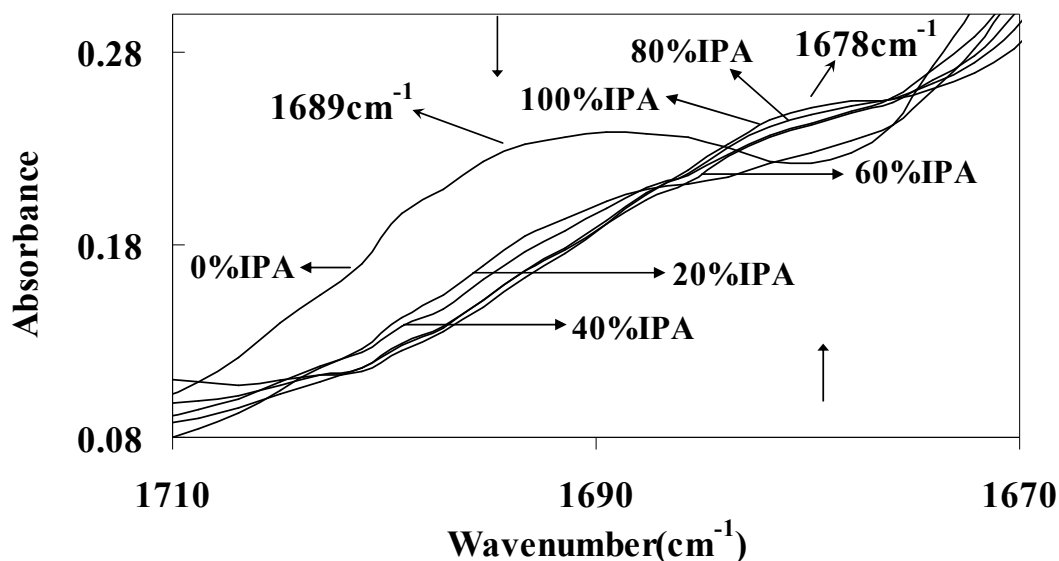


Figure 3-7. IR spectra of the C=Os of Boc groups of the decaproline oligomer in IPA/DCM solvent system.

#### 4. Vibrational circular dichroism spectra

Among the three kinds of carbonyl groups in the decaproline oligomer, only the peptide carbonyl groups exhibit measurable VCD at the concentration and pathlength used. There is not enough absorption to measure VCD for the other two kinds of carbonyl groups and therefore much higher concentration or pathlength is needed to measure the corresponding VCD. The solubility limits and interfering absorption from solvent mixture, prevent VCD measurements for the other two kinds of C=O groups.

The VCD associated with the peptide carbonyl groups in different IPA/DCM solvent mixtures are shown in Figure 3-8. All these VCD spectra exhibit a negative couplet, with positive VCD band at the higher frequency and negative VCD band at the lower frequency, which is a characteristic of the PPII conformation. As the percentage of IPA in the solvent system increases from 0% to 60%, the position of the positive band shifts from 1660  $\text{cm}^{-1}$  to 1654  $\text{cm}^{-1}$  and that of the negative band shifts from 1643  $\text{cm}^{-1}$  to 1635

$\text{cm}^{-1}$ , gradually. As the percentage of IPA increases further from 60% to 100%, the position of the negative band remains almost unchanged at  $1635 \text{ cm}^{-1}$ , but that of positive band continues to decrease to  $1652 \text{ cm}^{-1}$ . The negative VCD couplet, which is a characteristic of the PPII conformation, remained in the entire range of solvent mixtures (0%-100% IPA). As mentioned earlier, ECD spectra also indicated decaproline oligomer is in PPII conformation in the entire range of solvent mixtures (0%-100% IPA).

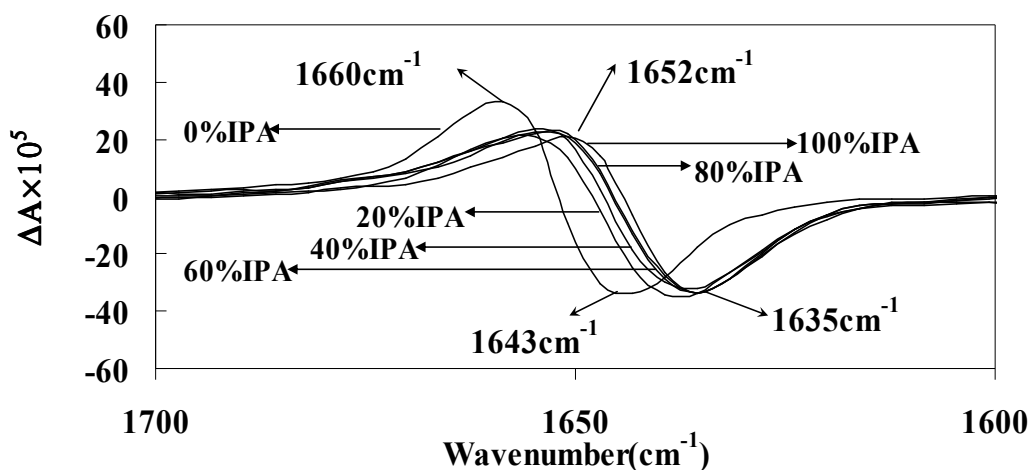


Figure 3-8. VCD spectra of the peptide C=O groups of the decaproline oligomer in IPA/DCM solvent system.

### 5. Rationalization of separation abilities of the decaproline chiral selector

The representations of PPI and PPII structures constructed from six proline residues are shown in Figure 3-9. It is obvious that PPI is a more crowded structure with stronger steric effects. The C=O groups in PPII are much more exposed to the solvent than those in PPI structure. For these proline-based chiral columns, the key factors to achieve good separation towards a wide range of analytes include a rigid structure and chiral

interaction sites. Both PPII and PPI conformations are rigid structures. Interactions between chiral selector and analytes include hydrogen bonding,  $\pi$ - $\pi$  interaction and steric effects. For the decaprolone oligomer, there are no aromatic rings, so  $\pi$ - $\pi$  interactions are not available. Then the interactions between the oligomer and analytes are mainly hydrogen bonding and steric effects. The C=O groups in PPI structure are much less exposed to solvent so the hydrogen bonding with solvent molecules or analytes is not significant. For PPII structure, the C=O groups in PPII structure are much more exposed, so the hydrogen bonding with solvent molecules or analytes is much easier. It appears that hydrogen bonding is a more important factor for the decaprolone column to achieve broad separation abilities. Differences in the ability of forming hydrogen bonds with solvent molecules for PPI and PPII structures can be used to explain why there is a large shift of infrared absorption band of PPII structure when alcohol is added to DCM while there is almost no change<sup>7b</sup> in the position of infrared absorption band of PPI structure with the addition of alcohol into DCM.

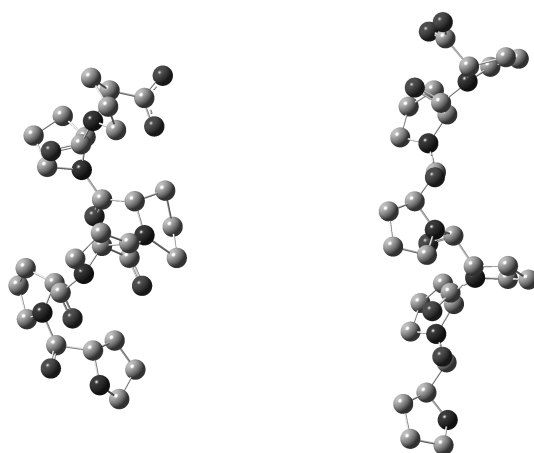


Figure 3-9. Representations of PPI (left) and PPII (right) structures constructed from six proline residues.

2,2,2-Trifluoro-1-[10-(2,2,2-trifluoro-1-hydroxy-ethyl-anthracen-9-yl)]-ethanol (DiTFAE) is a useful compound for the evaluation of chiral columns<sup>1</sup>. Its structure is shown in Figure 3-10. The separation of racemic DiTFAE by the decaprolone column was studied in IPA/DCM solvent system (20% IPA ~ 100% IPA). The separation of DiTFAE by the decaprolone column was not done in pure DCM system (0% IPA) because it takes very long time (more than 3 hr) to wash out the two enantiomers of DiTFAE from this column in pure DCM and their chromatographic peaks are so flat that they can not be used for data analysis. The separation results are shown in Figure 3-11, where the changes of retention factor ( $k$ ) and separation factor ( $\alpha$ ) of DiTFAE with the change of percentage of IPA in the solvent are presented. Retention factor ( $k$ ) equals  $(t_r - t_0)/t_0$ , in which  $t_r$  is the retention time and  $t_0$  is the dead time. Separation factor ( $\alpha$ ) equals  $k_2/k_1$ , in which  $k_1$  and  $k_2$  are the retention factors of two enantiomers. In this case  $k_1$  is the retention factor of (*R*)-enantiomer of DiTFAE and  $k_2$  is the retention factor of (*S*)-enantiomer of DiTFAE. As the percentage of IPA increases in solvent mixture, the retention factors of the two enantiomers, and also the separation factor, decrease first and then increase when the percentage of IPA reach 60%. This has a good correlation with the changes in optical rotation, ECD, IR and VCD properties, where the composition of 60% IPA is also seen as the turning point for hydrogen bonding interactions with the solvent, and associated changes in the dihedral angle around  $C_\alpha-C(=O)$ .



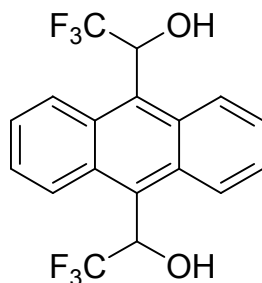


Figure 3-10. Structure of 2,2,2-Trifluoro-1-[10-(2,2,2-trifluoro-1-hydroxy-ethyl)-anthracen-9-yl]-ethanol (DiTFAE).

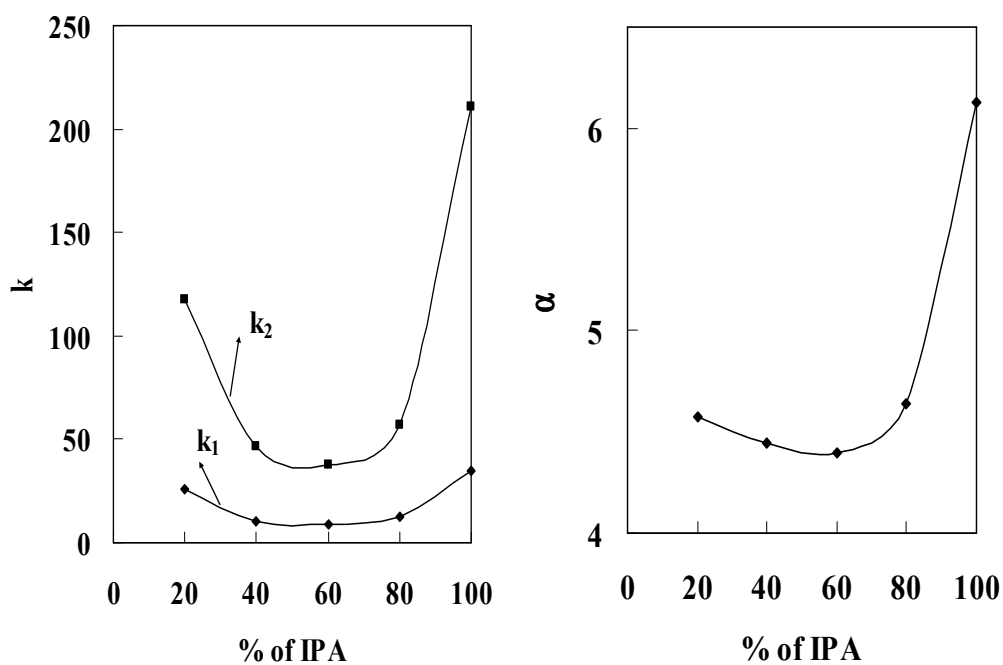


Figure 3-11. Retention factors (left panel) and separation factor (right panel) of DiTFAE achieved in the decaproline column in IPA/DCM solvent system.  $k_1$  is the retention factor of *R* enantiomer of DiTFAE and  $k_2$  is the retention factor of *S* enantiomer of DiTFAE.

The present spectroscopic results provide an explanation for the observed changes in retention time and separation factor in the decaproline column. It appears that the competition between solvent and analyte molecules for interaction with decaproline CSP column is changing with the percent composition of IPA. The hydrogen bonding

interactions between decaprolone and IPA are less significant at lower composition of IPA (<20%), and are saturated at higher composition (>60%) of IPA. At lower composition of IPA, the analyte molecules have direct interactions with the column. In the 0-20% IPA range, as the percent IPA increases IPA molecules compete successfully with analyte molecules for interaction with decaprolone CSP, leading to a decrease in the separation factor and retention times for the analyte. In this process, there may have been some amount of distortion of dihedral angles around  $C_{\alpha}$ -C(=O) in the decaprolone structure from the standard PPII helix. When the percent IPA comes to 60%, the hydrogen bonding interactions between IPA and decaprolone come to a saturation point. From this point onwards, the analyte molecules interact directly with IPA bound decaprolone column leading to an increase in the separation factor and retention times for the analyte. Thus it appears that decaprolone column saturated with hydrogen bonding with IPA is more effective in separations than the one with limited amount of IPA.

### **Conclusions**

The conformation of the decaprolone oligomer, the chiral selector of a newly developed chiral column, was investigated in IPA/DCM solvent system using multiple spectroscopic techniques including optical rotation, ECD, IR and VCD. Based on these studies, this oligomer is suggested to be in the PPII conformation in IPA/DCM solvent system (0% IPA ~ 100% IPA). The C=O groups in the decaprolone oligomer become saturated with hydrogen bonding to IPA molecules when the content of IPA in the solvent mixture reaches 60%. Based on separation results of racemic DiTFAE by the decaprolone column, the 60% IPA is also seen to be the turning point for the change of

retention factors and separation factor of DiTFAE with the change of content of IPA in the solvent mixture.

### References

1. Huang, J. M.; Chen, H.; Li, T. Y. *J Chromatogr A* **2006**, *1113*, 109-115.
2. Huang, J. M.; Chen, H.; Zhang, P.; Li, T. Y. *J Chromatogr A* **2006**, *1109*, 307-311.
3. Huang, J. M.; Zhang, P.; Chen, H.; Li, T. Y. *Anal Chem* **2005**, *77*, 3301-3308.
4. (a).Traub, W.; Shmueli, U. *In aspects of protein structure*; Academic Press: New York, 1963; pp81; (b). Traub, W.; Shmueli, U. *Nature* **1963**, *198*, 1165-1166.
5. (a). Sasisekharan, V. *Acta Cryst.* **1959**, *12*, 897-903; (b). Cowan, P.M.; McGavin, S. *Nature* **1955**, *176*, 501-503.
6. Creighton, T. E. *Proteins. Structures and molecular properties*; 2<sup>nd</sup> ed, W. H. Freeman Company: New York, 1993.
7. (a). Isemura, T.; Okabayas.H; Sakakiba.S *Biopolymers* **1968**, *6*, 307-321; (b). Strassma.H; Engel, J.; Knof, S. *Biopolymers* **1971**, *10*, 1759-1776; (c).Swenson, C. A.; Formanek, R. *J Phys Chem-Us* **1967**, *71*, 4073-4077.
8. (a).Okabayas.H; Isemura, T.; Sakakiba.S *Biopolymers* **1968**, *6*, 323-330; (b).Kakinoki, S.; Hirano, Y.; Oka, M. *Polym Bull* **2005**, *53*, 109-115.
9. (a).Dukor, R. K.; Keiderling, T. A.; Gut, V. *Int J Pept Prot Res* **1991**, *38*, 198-203; (b).Dukor, R. K.; Keiderling, T. A. *Biospectroscopy* **1996**, *2*, 83-100.
10. (a).Deber, C. M.; Bovey, F. A.; Carver, J. P.; Blout, E. R. *J Am Chem Soc* **1970**, *92*, 6191-6198; (b). (1) Zhang, R.; Madalengoitia, J. S. *Tetrahedron Lett* **1996**, *37*, 6235-6238.
11. Rippon, W. B.; Koenig, J. L.; Walton, A. G. *J Am Chem Soc* **1970**, *92*, 7455-7459.
12. (a). Kurtz, J.; Berger, A.; Katchalski, E. *Nature*, **1956**, *178*, 1066-7; (b). Steinberg, I. Z.; Berger, A.; Katchalski, E. *Biochim. Biophys. Acta* **1958**, *28*, 647-648; (c). Steinberg, I.Z.; Harrington, W. F.; Berger, A.; Sela, M.; Katchalski, E. *Journal of the American Chemical Society* **1960**, *82*, 5263-5279.

## CHAPTER IV

### VIBRATIONAL ABSORPTION, VIBRATIONAL CIRCULAR DICHROISM AND SPECIFIC ROTATION STUDY ON DIALKYL TARTRATES AND THEIR CYCLODEXTRIN COMPLEXES

#### **Introduction**

Vibrational circular dichroism (VCD) technique has been successfully used for determining the absolute configuration and predominant conformations of chiral molecules in the solution phase.<sup>1</sup> The utility of VCD for structural elucidation is facilitated by two advances: (a) improvements in VCD instrumentation have made it possible to obtain the VCD spectra with enhanced signal-to-noise ratio and (b) ab initio applications using density functional theory (DFT)<sup>2</sup> have become state-of-the-art in recent years. The DFT theory, which provides vibrational frequencies and intensities that are comparable to the post-SCF calculations employing electron correlation, has also been extended to the VCD intensity calculations<sup>3</sup> and implemented in standard software<sup>4</sup>.

Recently VCD technique was also applied to the study of cyclodextrin complexes.<sup>5</sup> VCD is becoming a useful tool to investigate the host/guest interactions in the complexes.

Specific rotation is an age-old technique that has experienced a renaissance in the past few years, following the first prediction<sup>6</sup> of specific rotation using ab initio methods. Recent implementation of DFT for predicting specific rotation has led to accurate predictions of specific rotation.<sup>7</sup> The specific rotations measured in the gas phase are ideal for comparison with predictions on isolated molecules; however, such measurements require special instrumentation and are not routine. Because the

condensed-phase experimental specific rotations (often reported for neat liquids or in some convenient solvent at some convenient concentration) can be influenced by solute-solute interactions, a quantitative comparison of predicted and condensed-phase experimental specific rotations may not be reliable. This drawback can be alleviated with the measurement of intrinsic rotation (specific rotation in the limit of zero concentration)<sup>8</sup>, which is devoid of solute-solute interactions. The combined use of experimental intrinsic rotations and predicted specific rotations is another approach to study the conformations of chiral molecules in solutions.

Tartaric acid and its derivatives play an important role in organic and pharmaceutical chemistry<sup>9</sup>. Dialkyl tartrates are a category of tartaric acid derivatives which have wide applications in both academic laboratories and chemical industries. They can be used as good asymmetric synthesis catalysts and they are also chiral intermediates for several pharmaceuticals and agrochemicals<sup>10</sup>.

Dialkyl tartrates have been studied by VA and VCD techniques before. Keiderling et al<sup>11</sup> found bisignate VCD associated with the O-H stretching vibrations of dimethyl (*R,R*)-tartrate in CCl<sub>4</sub> solution. They carried out further VCD measurements in the O-H stretching region by varying the temperature and found out the restricted conformational mobility of this molecule in dilute CCl<sub>4</sub> solution. They also did the VCD measurements in the C=O stretching region and found bisignate VCD for the C=O stretching vibrations in CCl<sub>4</sub>.

Our group also did some research on VA and VCD spectra of dialkyl tartrates<sup>12</sup>. VCD spectra of dimethyl tartrate, diethyl tartrate and diisopropyl tartrate were measured in the 1600-900 cm<sup>-1</sup> region in different solvents (CCl<sub>4</sub>, DMSO and CS<sub>2</sub>) and different

concentrations. It was found that VCD associated with the C-O stretching vibrations in the region of 1250-1000  $\text{cm}^{-1}$  is identical for all these molecules in all three solvents. But in the 1600-1250  $\text{cm}^{-1}$  region absorption and VCD spectra are quite different in  $\text{CCl}_4$  and DMSO solvents. Absorption spectra were also studied in the C=O stretching region (1850-1600  $\text{cm}^{-1}$ ). It is found that in DMSO solvent the spectra show two absorption bands as opposed to one in  $\text{CCl}_4$ . Intermolecular hydrogen bonding in DMSO was thought to cause the difference. But there was no further investigation of this issue.

In this article we report further investigations of VA and VCD spectra in the mid-infrared region in different solvents ( $\text{CCl}_4$ ,  $\text{DMSO-d}_6$  and  $\text{D}_2\text{O}$ ) for three dialkyl tartrates. VA and VCD spectra in  $\text{CCl}_4$  and  $\text{CS}_2$  were found to be quite similar<sup>12</sup>.  $\text{DMSO-d}_6$  and  $\text{D}_2\text{O}$  are used instead of DMSO and  $\text{H}_2\text{O}$  to avoid solvent absorption interference in the Mid-infrared region. Intrinsic rotations of dialkyl tartrates were not reported before. We measured the intrinsic rotations of dimethyl D-tartrate (with the configuration of *S,S*) in different solvents ( $\text{CCl}_4$ , DMSO and  $\text{H}_2\text{O}$ ). The DFT calculations for dimethyl (*S,S*)-tartrate, a representative compound among these tartrates, were performed in isolated state and in different solvents to study the conformational change of this molecule in different solvents.

Dialkyl tartrate-cyclodextrin complexes were also prepared for the first time. VA and VCD spectra in the mid-IR region, intrinsic rotations, and binding constants of these complexes were also measured to investigate the intercation between guest and host molecules in these complexes.

## Experimental

Dimethyl D-tartrate, dimethyl L-tartrate, diethyl D-tartrate, diethyl L-tartrate diisopropyl D-tartrate, and diisopropyl L-tartrate were all purchased from Aldrich Chemicals;  $\alpha$  and  $\beta$ -cyclodextrins were purchased from Sigma Chemicals.

### Preparation of dialkyl tartrate-cyclodextrin complexes

These complexes were prepared using coprecipitation method<sup>13</sup>. Take diethyl D-tartrate  $\beta$ -CD complex as an example. The mixture of  $\beta$ -CD (1mmole) and diethyl D-tartrate (10mmol) was dissolved in hot H<sub>2</sub>O (5mL) at 90°C. Then the solution was allowed to cool down slowly and crystals were obtained after filtration.  $\alpha$ -CD complex of diethyl L-tartrate and  $\beta$ -CD complexes of diethyl D-tartrate, diethyl L-tartrate, diisopropyl D-tartrate, and diisopropyl L-tartrate were prepared using the same procedure. And these complexes were characterized by <sup>1</sup>H NMR:

for diethyl L-tartrate  $\alpha$ -CD complex complex:

<sup>1</sup>H NMR  $\delta$  (D<sub>2</sub>O): 1.2 (t, 6H), 3.4-3.5 (m, 6H), 3.7-3.8 (m, 6H), 3.8-3.9 (m, 6H), 4.2 (m, 4H) and 5.0(s, 6H).

for diethyl D-tartrate  $\beta$ - CD complex complex:

<sup>1</sup>H NMR  $\delta$  (D<sub>2</sub>O): 1.2 (t, 6H), 3.4-3.5 (m, 7H), 3.7-3.8 (m, 7H), 3.8-3.9 (m, 7H), 4.2 (m, 4H) and 5.0(s, 7H).

for diethyl L-tartrate  $\beta$ - CD complex complex:

<sup>1</sup>H NMR  $\delta$  (D<sub>2</sub>O): 1.2 (t, 6H), 3.4-3.5 (m, 7H), 3.7-3.8 (m, 7H), 3.8-3.9 (m, 7H), 4.2 (m, 4H) and 5.0(s, 7H).

for diisopropyl D-tartrate  $\beta$ - CD complex complex:

$^1\text{H}$  NMR  $\delta$  ( $\text{D}_2\text{O}$ ): 1.2 (d, 12H), 3.4-3.5 (m, 7H), 3.7-3.8 (m, 7H), 3.8-3.9 (m, 7H), 4.5 (m, 2H) and 5.0(s, 7H).

for diisopropyl L-tartrate  $\beta$ - CD complex complex:

$^1\text{H}$  NMR  $\delta$  ( $\text{D}_2\text{O}$ ): 1.2 (d, 12H), 3.4-3.5 (m, 7H), 3.7-3.8 (m, 7H), 3.8-3.9 (m, 7H), 4.5 (m, 2H) and 5.0(s, 7H).

### **Determination of binding constants of dialkyl tartrate-cyclodextrin complexes**

The binding constants of diethyl L-tartrate complexes of  $\alpha$ -CD and  $\beta$ -CD were determined in both  $\text{H}_2\text{O}$  and DMSO solvents by isothermal titration calorimetry(ITC)<sup>14</sup>.

An isothermal calorimeter (Microcal Inc., MA), was used in all microcalorimetric experiments. For microcalorimetric experiments in  $\text{H}_2\text{O}$ , 20 injections of 5 $\mu\text{L}$  of diethyl L-tartrate in  $\text{H}_2\text{O}$  (100mM) were added at an interval of 5 min into the  $\alpha$ -CD or  $\beta$ -CD solution in  $\text{H}_2\text{O}$  (2mM) in the reaction cell (cell volume = 1.4mL) while stirring at 300 rpm at 298K. The duration time of each injection is 20 sec. For microcalorimetric experiments in DMSO, 20 injections of 10 $\mu\text{L}$  of diethyl L-tartrate in DMSO were added at an interval of 5 min into the  $\alpha$ -CD or  $\beta$ -CD solution in DMSO (20mM) in the cell with the stirring speed at 550 rpm at 298K. The concentrations of diethyl L-tartrate were 150mM for the titration with  $\beta$ -CD and 450mM for the titration with  $\alpha$ -CD respectively. For each injection the duration time is 7.1 sec.

Dilution effects were determined by identical injections of the diethyl L-tartrate solutions into the pure solvents and were subtracted from the raw titration to produce the final binding curve. The ORIGIN software (Microcal), used for the calculation of  $K$ ,  $\Delta\text{H}$  and  $\Delta\text{S}$  from the titration curve, gave the relevant standard deviations based on the scatter of the data points in a single titration curve.



## VA and VCD measurements

The VA and VCD spectra were recorded on a commercial Fourier transform VCD spectrometer, Chiralir (Bomem-BioTools, Canada) with a ZnSe beam splitter, BaF<sub>2</sub> polarizer, optical filter (transmitting below 2000 cm<sup>-1</sup>) and a 2 × 2 mm HgCdTe detector. One difference from the standard Chiralir instrument is that the photo elastic modulator used was a PEM-80 model (Hinds Instruments) without AR coating on the ZnSe optical element. The VCD spectra were recorded, using the supplied Chiralir software, with 3 h data collection time at 4 cm<sup>-1</sup> resolution. The transmission properties of optical filter and BaF<sub>2</sub> substrates used in the instrument restrict the range of measurements to 2000-900 cm<sup>-1</sup>.

In the CCl<sub>4</sub> solvent spectra were measured for diethyl D-tartrate and diethyl L-tartrate at the concentration of 0.017 M at path length of 600 μm in a variable path length cell with BaF<sub>2</sub> windows. In the DMSO-d<sub>6</sub> solvent spectra were measured for dimethyl D-tartrate, diethyl D-tartrate, diisopropyl D-tartrate and diisopropyl L-tartrate. Their concentrations were 0.046, 0.040, 0.035 and 0.035M, respectively. Spectra were also measured for β-CD complexes of diethyl D-tartrate, diethyl L-tartrate diisopropyl D-tartrate and diisopropyl L-tartrate at the concentrations of 0.040M in the DMSO-d<sub>6</sub>. The samples were held in a demountable path length cell (200 μm) with BaF<sub>2</sub> windows. In the D<sub>2</sub>O solvent spectra were measured for dimethyl D-tartrate, diethyl D-tartrate and α-CD complex of diethyl L-tartrate at the concentration of 0.048, 0.041M and 0.044M respectively in a demountable path length cell (100μm) with BaF<sub>2</sub> windows. In the presented VA and VCD spectra, the solvent absorption and VCD spectra were subtracted out respectively.

### **Optical rotation measurement**

For optical rotation measurement, an Autopol IV polarimeter with a resolution of  $0.001^\circ$  (reproducibility of  $0.002^\circ$ ) and analytical balances with accuracy of  $0.00001$  g were used. Optical rotations were measured at the wavelength of 589 nm. Optical rotations of dimethyl D-tartrate were measured in  $\text{CCl}_4$  at the concentration range of 0.0028-0.0010M, in DMSO at 0.0570-0.013M and in  $\text{H}_2\text{O}$  at 0.0590-0.0037M respectively. Optical rotations of diethyl D-tartrate, diethyl L-tartrate, diisopropyl D-tartrate, diisopropyl L-tartrate,  $\alpha$ -CD and  $\beta$ -CD were also measured in  $\text{H}_2\text{O}$  with the concentration ranges of 0.0439-0.0027M, 0.0614-0.0038M, 0.0521-0.0016M, 0.0408-0.0026M, 0.0083-0.0003M and 0.0077-0.0002M respectively. Optical rotations of  $\alpha$ -CD complex of diethyl L-tartrate were measured in  $\text{H}_2\text{O}$  at the concentration range of 0.0031-0.0001M. And optical rotations of  $\beta$ -CD complexes of diethyl L-tartrate, diethyl D-tartrate, diisopropyl L-tartrate and diisopropyl D-tartrate were also measured in  $\text{H}_2\text{O}$  with the concentration ranges of 0.0058-0.0002M, 0.0058-0.0002M, 0.0031-0.00008M and 0.0031-0.00008M respectively. Optical rotations of dimethyl D-tartrate were also measured at other wavelengths besides 589nm. Optical rotations of dimethyl D-tartrate were measured at 0.0014M in  $\text{CCl}_4$  and at 0.0064M in DMSO respectively at the wavelengths of 633, 589, 546, 436, 405, and 365nm. For experiments to measure the intrinsic rotations for dimethyl D-tartrate in DMSO, optical rotations were also measured at the wavelength of 365nm at the concentration range of 0.027-0.008M.

Each time the solution was transferred to a 1.0 dm cell and optical rotation was measured three different times to check for consistency. The averages of these

measurements were used to calculate specific rotation. This procedure ensured that no unusual data scatter was present in the measurements.

Based on experimental results for dialkyl tartrates, cyclodextrins and the complexes, plots of  $c$ (concentration) Vs.  $\alpha$ (observed rotation) and  $c$ (concentration) Vs.  $[\alpha]$ (specific rotation) are made and equation fittings are performed for each case. Normal least-squares fitting is appropriate for  $\alpha$  vs.  $c$  data, weighted least-squares fitting is needed for fitting the  $[\alpha]$  vs.  $c$  data. Intrinsic rotation ( $[\alpha]_{c=0}$  or  $\{\alpha\}$ ) can be obtained from these equations. For example, if the measured specific rotation as a function of concentration follows the equation  $[\alpha] = A_1c + B_1$ , then the observed rotation  $\alpha$  must follow the quadratic equation, as  $\alpha = A_2c^2 + B_2c$ . Then  $\{\alpha\}$  equals  $B_1$ . It is to be noted that the linear relation,  $[\alpha] = A_1c + B_1$ , may not apply in all situations; in some cases  $[\alpha]$  may be constant, or follow quadratic, cubic, or some other complicated relation.

### **DFT calculations**

The DFT geometry optimization, vibrational frequencies, absorption, and VCD intensities, specific-rotation calculations for isolated dimethyl (*S,S*)-tartrate were calculated using Gaussian 98 or 03 program<sup>4</sup>. The calculations used DFT with B3LYP functional (6-31G\* and aug-cc-pVDZ basis sets). The DFT geometry optimization, VCD and specific-rotation calculations for dimethyl (*S,S*)-tartrate in CCl<sub>4</sub> were calculated using Gaussian 03 program<sup>4</sup>. The solvent influence was investigated with a polarizable continuum model (PCM) that was incorporated in Gaussian 03 program. The DFT geometry optimization, vibrational frequencies, absorption, and VCD intensities, specific-rotation calculations for clusters of dimethyl (*S,S*)-tartrate with DMSO molecules

were also calculated using the DFT method with B3LYP functional(6-31G\* basis set) in Gaussian 98 or 03 program.

The theoretical absorption and VCD spectra were simulated with Lorentzian band shapes and  $5\text{ cm}^{-1}$  full width at half-height. Since the predicted band positions with 6-31G\* basis set are higher than the experimental values, the predicted frequencies have been scaled with 0.96.

## **Results and discussion**

### **1. VA and VCD study of dialkyl tartrate**

Because of solvent inference, VCD spectra of dialkyl tartrate can only be obtained in the regions of  $2000\text{-}1600\text{ cm}^{-1}$  and  $1500\text{-}900\text{ cm}^{-1}$  in  $\text{CCl}_4$ , in the region of  $2000\text{-}1100\text{ cm}^{-1}$  in  $\text{DMSO-d}_6$  and in the region of  $2000\text{-}1250\text{ cm}^{-1}$  in  $\text{D}_2\text{O}$ . The vibrational absorption and VCD spectra of dialkyl tartrates, measured in  $\text{CCl}_4$ ,  $\text{DMSO-d}_6$  and  $\text{D}_2\text{O}$  solvents in the mid-infrared region, are shown in Figures 4-1 ~ 4-3. The VCD spectra of both enantiomers of diethyl tartrate were shown in Figure 4-1. The absorption and VCD spectra of dimethyl L-tartrate in the mid-infrared region in  $\text{CCl}_4$  have been reported by Buffeteau et al<sup>17</sup> before. The absorption and VCD spectra in the mid-infrared region in the same solvent system remain almost unaffected for these esters as the alkyl group in their structures changes from methyl to ethyl and isopropyl. Difference is found for only absorption spectra in the region of  $1500\text{-}1400\text{ cm}^{-1}$  as the alkyl group changes. For a given tartrate, the absorption and VCD signs are affected significantly when the solvent is changed from  $\text{CCl}_4$  to  $\text{DMSO-d}_6$  and  $\text{D}_2\text{O}$ . Several VCD bands are seen in the mid-infrared region in both  $\text{CCl}_4$  and  $\text{DMSO-d}_6$  solvent while no VCD bands are found in

D<sub>2</sub>O. In the C=O stretching region (1850-1600 cm<sup>-1</sup>), one absorption band and bisignate VCD signs (negative-positive for D enantiomer) are found in CCl<sub>4</sub> and two absorption bands and three VCD bands (negative-positive-negative triplet for D enantiomers) are seen in DMSO-d<sub>6</sub> while one broader absorption band and no VCD signals are found in D<sub>2</sub>O. In the 1500-900 cm<sup>-1</sup> region, three positive couplets (positive at lower frequency and negative at higher frequency for D enantiomer) are observed at the 1400-1240 cm<sup>-1</sup>, 1240-1150 cm<sup>-1</sup> and 1150-1050 cm<sup>-1</sup> regions respectively in the VCD spectra in CCl<sub>4</sub> while a pattern of a negative couplet (negative at higher frequency and positive at lower frequency for D enantiomers) is seen in the 1250-1100 cm<sup>-1</sup> region in DMSO-d<sub>6</sub>. No VCD signals are observed in D<sub>2</sub>O.

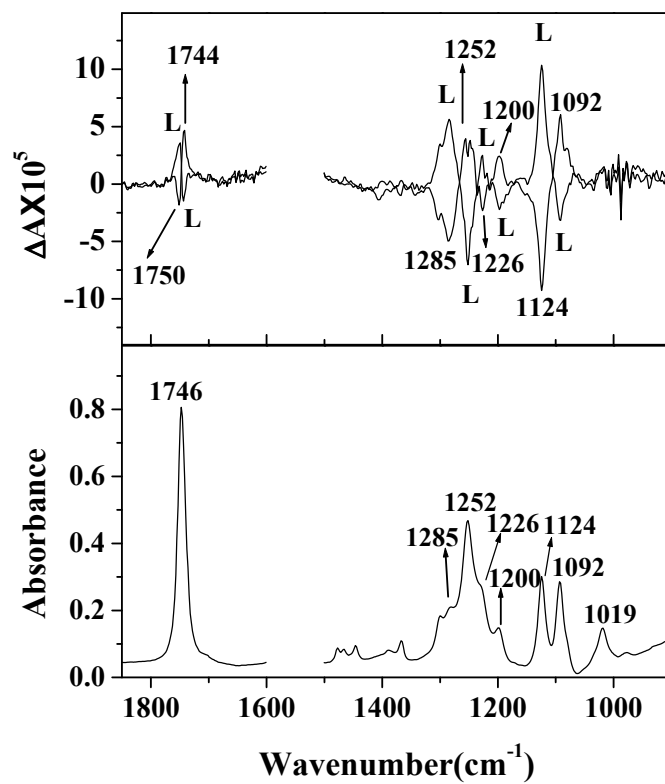


Figure 4-1. Vibrational absorption(bottom) and VCD(top) spectra in the Mid IR region in CCl<sub>4</sub> solution of both enantiomers of diethyl tartrate(0.017M), L enantiomer is labeled with L.

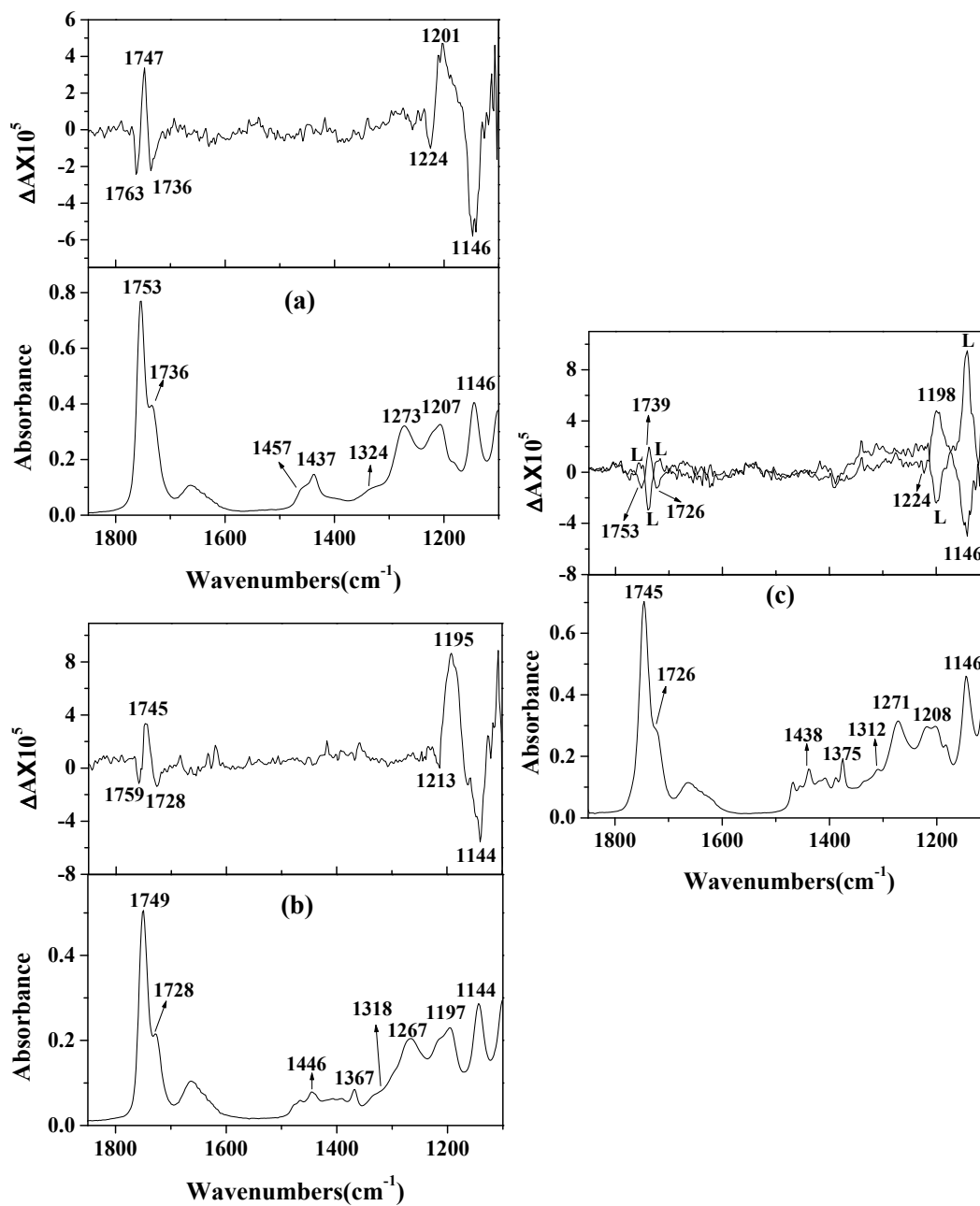


Figure 4-2. Vibrational absorption(bottom) and VCD(top) spectra in the Mid IR region in DMSO-d<sub>6</sub> solution of: (a) dimethyl D-tartrate(0.046M), (b) diethyl D-tartrate(0.040M), (c)both enantiomers of diisopropyl tartrate(0.035M), L enantiomer is labeled with L.

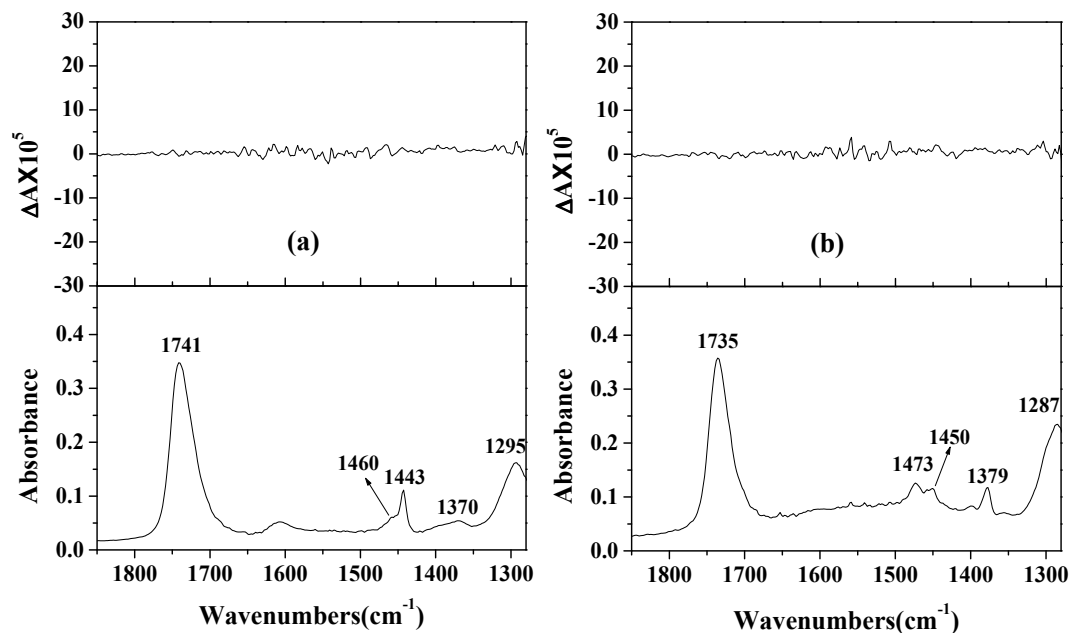


Figure 4-3. Vibrational absorption(bottom) and VCD(top) spectra in the C=O stretching region in  $\text{D}_2\text{O}$  solution of: (a) dimethyl D-tartrate(0.048M), (b) diethyl D-tartrate(0.041M).

## 2. Optical rotation study of dialkyl tartrates

The intrinsic rotations of dimethyl D-tartrate were measured in three solvents:  $\text{CCl}_4$ , DMSO and  $\text{H}_2\text{O}$ . The specific rotation,  $[\alpha]_{\text{D}}$ , and observed rotation,  $\alpha_{\text{D}}$ , as a function of concentration in different solvents are displayed in Figure 4-4. The intrinsic rotations,  $\{\alpha\}_{\text{D}}$  are derived from these data. The  $\{\alpha\}_{\text{D}}$  for dimethyl D-tartrate is 43.0 in  $\text{CCl}_4$ . In DMSO, the intrinsic rotation is -3.1 while this value changes to -20.3 in  $\text{H}_2\text{O}$  solvent. So the intrinsic rotation of dimethyl D-tartrate is significantly affected when the solvent is changed from  $\text{CCl}_4$  to DMSO and  $\text{H}_2\text{O}$ .



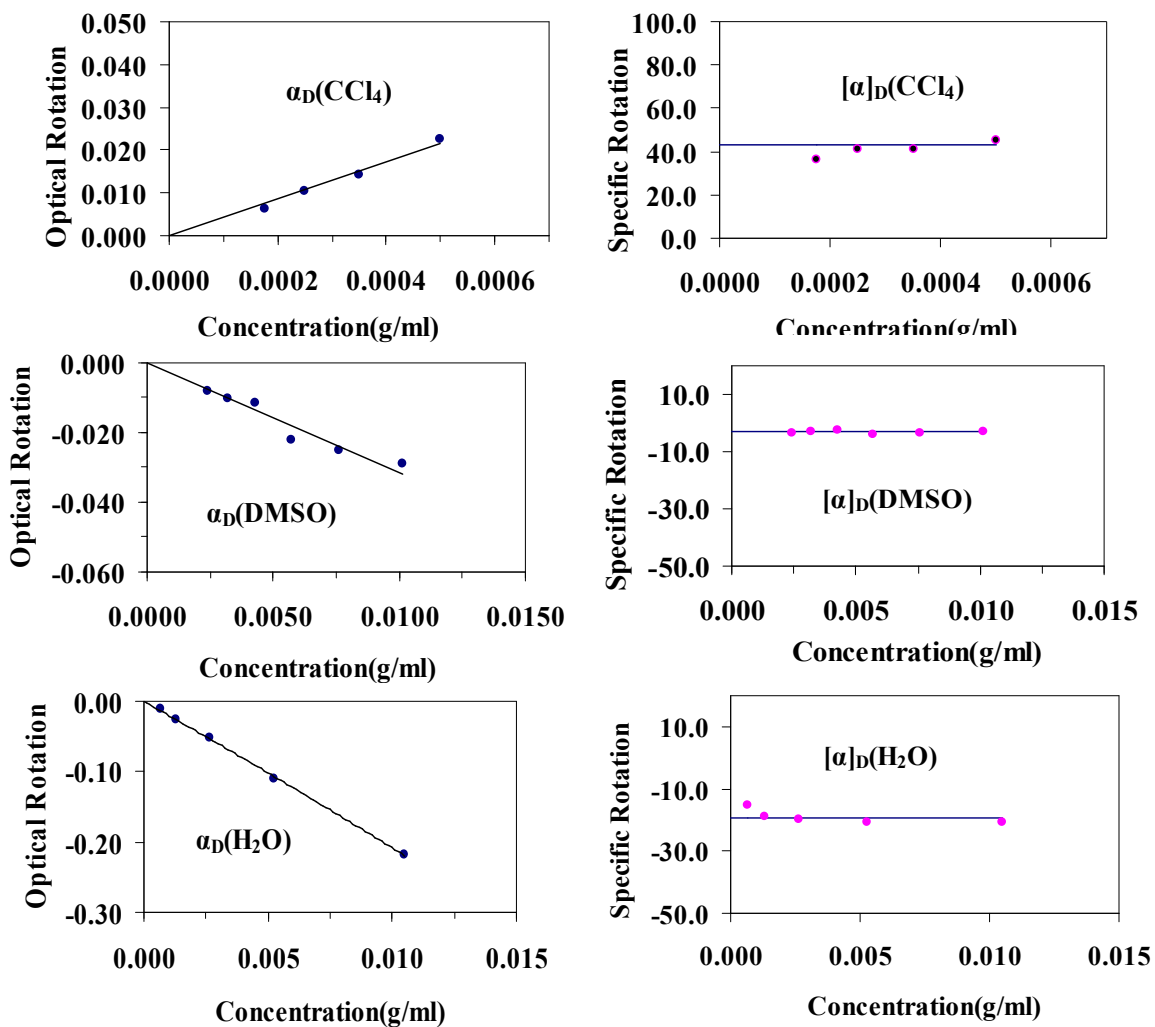


Figure 4-4. Optical rotation ( $\alpha_D$ ) and specific rotation ( $[\alpha]_D$ ) of dimethyl D-tartrate, as a function of concentration in CCl<sub>4</sub>, DMSO and H<sub>2</sub>O solutions. In CCl<sub>4</sub>, a plot of  $\alpha_D$  versus concentration was fit to  $\alpha_D = 43.02c$ ; a plot of  $[\alpha]_D$  versus concentration was fit to  $[\alpha]_D = 43.0$ . In DMSO, a plot of  $\alpha_D$  versus concentration was fit to  $\alpha_D = -3.13c$  and a plot of  $[\alpha]_D$  versus concentration was fit to  $[\alpha]_D = -3.1$ . In H<sub>2</sub>O, a plot of  $\alpha_D$  versus concentration was fit to  $\alpha_D = -20.75c$  and a plot of  $[\alpha]_D$  versus concentration was fit to  $[\alpha]_D = -20.8$ . Fitting of the specific rotation versus concentration required the weighted least-squares method.

### 3. DFT calculations

Different absorption and VCD spectra and different optical rotations in different solvents are usually caused by conformational change of molecules in different solvents. DFT calculations were performed to study the conformation of dialkyl tartrate molecules in different solvents. Based on previous VCD and NMR studies, T conformer (shown on Figure 4-5) is the favored structure for dialkyl tartrate.<sup>12,15</sup> Rychlewska et al analyzed the conformation of isolated dimethyl (*R,R*)-tartrate by ab-initio quantum calculations and proposed five lowest energy conformers. Among them, two T conformers (T(ss) and T(as)) are the lowest energy forms.<sup>16</sup>

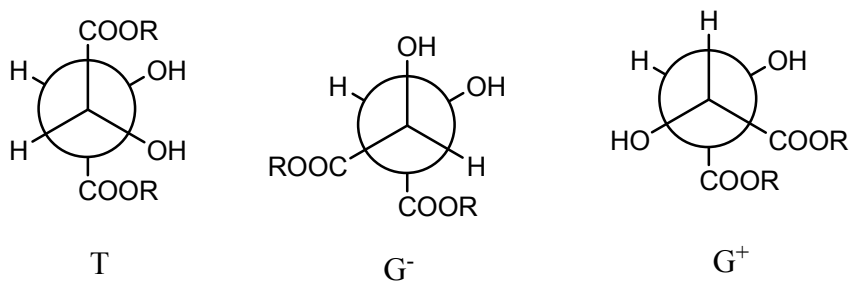


Figure 4-5. The three principle conformations of dialkyl (*R,R*)-tartrate around the C\*-C\* bond.

Recently Buffeteau et al<sup>17</sup> reported predicted VA and VCD spectra of using DFT theory for several conformers of dimethyl L-tartrate in isolated state and in CCl<sub>4</sub>. B3LYP/6-31G\* basis set was used for calculation. It was found that experimental spectra in CCl<sub>4</sub> corresponds well with predicted spectra for the conformer of T(ss).

In our study, DFT calculations were done first for isolated dimethyl (*S,S*)-tartrate. 22 conformers of the isolated molecules were considered and B3LYP/6-31G\* and B3LYP/

aug-cc-pVDZ basis sets were both used for calculations. VA and VCD spectra in the mid-infrared region and specific rotation for isolated dimethyl (*S,S*)-tartrate were both predicted.

22 geometries for isolated dimethyl (*S,S*)-tartrate molecule were optimized with the B3LYP/6-31G\* basis set in Gaussian 98 program. These geometries and their electronic energies are listed in Table 4-1. The five most stable conformations (see Figure 4-6) are found and they were further examined at aug-cc-pVDZ basis set. Four among these five conformers correspond well with most stable ones in Rychlewska's study. The most stable conformer is trans-COOCH<sub>3</sub>-1 with two internal hydrogen bonds between the hydrogen atoms of OH groups and their nearest C=O groups. Trans-COOCH<sub>3</sub>-1 corresponds to T(ss) in Rychlewska's study. The only exception is the second lowest energy conformer: trans-COOCH<sub>3</sub>-2. Trans-COOCH<sub>3</sub>-2 has one internal hydrogen bond between the hydrogen atom of OH group and its nearest C=O and the hydrogen atom of second OH group is approximately in between the oxygen atom of first OH group and the nearest ester oxygen atom. In Rychlewska's study, the second lowest one is T(as) with two internal hydrogen bonds: one between the hydrogen atom of OH group and its nearest ester oxygen and the other between the hydrogen atom of the other OH group and its nearest C=O. Actually in our study, the geometry of T(as) was considered and it was converted into the geometry of trans-COOCH<sub>3</sub>-2 in the optimization calculation. Trans-COOCH<sub>3</sub>-2 matches well with the second lowest energy conformer in Buffeteau's study.<sup>17</sup>

Table 4-1. Geometries and electronic energies of the 22 conformers at B3LYP/6-31G\* level

Conformer	intramolecular hydrogen bonding	energy(hartrees)
trans-COOCH <sub>3</sub> -1	Both: OH.....C=O attached to the same chiral carbon	-685.995246
trans-COOCH <sub>3</sub> -2	1 OH.....C=O attached to the same chiral carbon; 1 OH: between the oxygen atom of first OH group and the nearest ester oxygen atom	-685.993571
trans-COOCH <sub>3</sub> -3	Both: OH.....C=O attached to the adjacent chiral carbons	-685.986590
trans-COOCH <sub>3</sub> -4	Both: OH.....ester oxygen attached to the same chiral carbon	-685.960518
trans-COOCH <sub>3</sub> -5	Both: OH.....ester oxygen attached to the adjacent chiral carbons	-685.975453
trans-COOCH <sub>3</sub> -6	1 OH.....C=O attached to the adjacent chiral carbons; 1 OH.....OH	-685.988945
trans-COOCH <sub>3</sub> -7	1 OH.....ester oxygen attached to the same chiral carbons; 1 OH: between the oxygen atom of first OH group and the nearest ester oxygen atom	-685.988838
trans-COOCH <sub>3</sub> -8	1 OH.....ester oxygen attached to the adjacent chiral carbons; 1 OH.....OH	-685.984855
trans-COOCH <sub>3</sub> -9	1 OH.....C=O attached to the same chiral carbons; 1 OH.....ester oxygen attached to the same chiral carbons;	-685.993571 (converted to trans-COOCH <sub>3</sub> -2)
trans-OH-1	Both: OH.....C=O attached to the same chiral carbon	-685.992120
trans-OH-2	Both: OH.....C=O attached to the adjacent chiral carbons	-685.993837
trans-OH-3	1 OH.....C=O attached to the same chiral carbons; 1 OH.....ester oxygen attached to the adjacent chiral carbons;	-685.992194
trans-OH-4	Both: OH.....ester oxygen attached to the same chiral carbon	-685.993837 (converted to trans-OH-2)
trans-OH-5	Both: OH.....ester oxygen attached to the adjacent chiral carbons	-685.992126 (converted to trans-OH-1)
trans-OH-6	1 OH.....C=O attached to the same chiral carbon; 1 OH.....ester oxygen attached to the same chiral carbon;	-685.986085
trans-OH-7	Both: OH free	Can not be optimized
trans-OH-8	1 OH.....C=O attached to the adjacent chiral carbons; 1 OH.....ester oxygen attached to the adjacent chiral carbon;	-685.989258
trans-H-1	Both: OH.....C=O attached to the same chiral carbon	-685.987905
trans-H-2	Both: OH.....ester oxygen attached to the same chiral carbon	-685.982640
trans-H-3	1 OH.....C=O attached to the same chiral carbon; 1 OH.....OH	-685.989018
trans-H-4	1 OH.....ester oxygen attached to the same chiral carbon; 1 OH.....OH	-685.985202
trans-H-5	1 OH.....ester oxygen attached to the same chiral carbon; 1 OH.....C=O attached to the same chiral carbon;	-685.985739

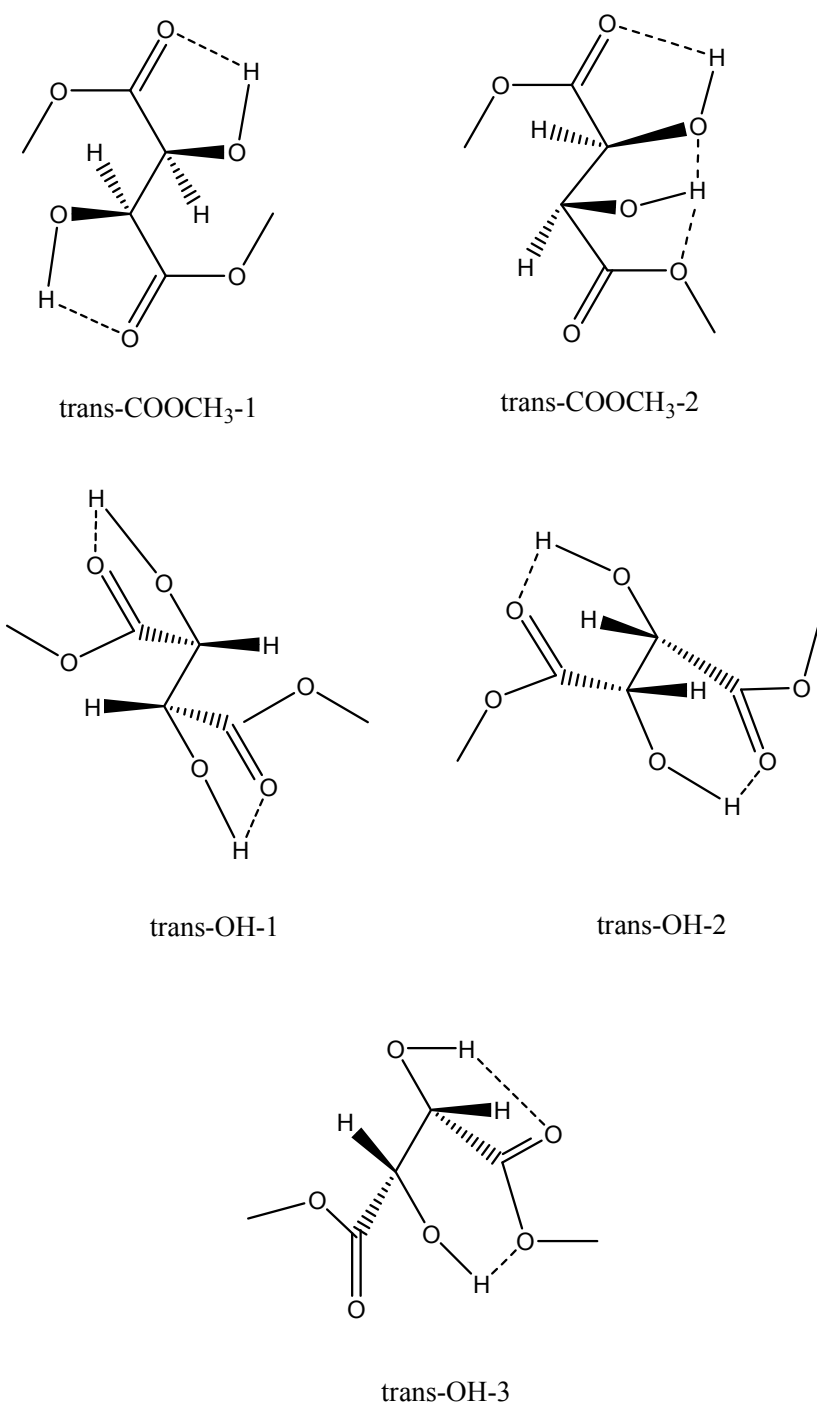


Figure 4-6. The five lowest energy conformers of dimethyl (*S,S*)-tartrate at B3LYP/6-31G\* level in our study

The Gibbs energies, relative populations and specific rotations that are predicted for the five conformers of the isolated molecule using 6-31G\* and aug-cc-pVDZ basis sets in the

Gaussian 98 program are listed in Table 4-2. Trans-COOCH<sub>3</sub>-1 is the predominant conformer for isolated dimethyl (*S,S*)-tartrate. For the specific rotations, only Trans-COOCH<sub>3</sub>-2 has a negative value. The predicted specific rotations, obtained as population weighted sum of specific rotations of different conformers, are 50.4 at the 6-31G\* basis and 38.8 at the aug-cc-pVDZ basis. These two predicted values are close to the experimental intrinsic rotation of dimethyl D-tartrate in CCl<sub>4</sub> (see Table 4-8), especially in the case at the aug-cc-pVDZ basis. (Aug-cc-pVDZ is a higher level basis set compared with 6-31G\*). Our group<sup>18a</sup> also predicted the theoretical optical rotatory dispersion (ORD<sup>18b</sup>, optical rotation as a function of wavelength) for dimethyl (*S,S*)-tartrate at the aug-cc-pVDZ basis set. The predicted ORD was obtained as population weighted data from the two lowest energy conformers of isolated dimethyl (*S,S*)-tartrate: Trans-COOCH<sub>3</sub>-1 and Trans-COOCH<sub>3</sub>-2. The predicted ORD is compared with experimental ORD of dimethyl D-tartrate in CCl<sub>4</sub> in Figure 4-10. A good correlation is found between the predicted ORD and the experimental one.

Table 4-2. B3LYP calculated Gibbs energies; populations, and specific rotations of five conformers of isolated dimethyl (*S, S*)-tartrate

	Trans-COOCH <sub>3</sub> -1	Trans-COOCH <sub>3</sub> -2	Trans-OH-1	Trans-OH-2	Trans-OH-3
	Gibbs Energy (in hartrees)				
6-31G*	-685.86466	-685.86270	-685.86158	-685.86160	-685.86066
aug-cc-pVDZ	-685.98342	-685.98113	-685.97953	-685.97774	-685.97799
	Population(%)				
6-31G*	82.1	10.4	3.1	3.2	1.2
aug-cc-pVDZ	90.2	7.9	1.4	0.2	0.3
	Specific rotation, [ $\alpha$ ] <sub>D</sub>				
6-31G*	65.2	-109.7	222.9	53.5	102.9
aug-cc-pVDZ	47.9	-120.8	209.9	42.2	103.4

The absorption and VCD intensities were calculated for the five conformations at the B3LYP/6-31G\* and B3LYP/aug-cc-pVDZ levels, and all of these conformations were found to have potential energy minima (i.e., all vibrational frequencies are real). The absorption and VCD spectra for all five conformations of dimethyl (*S,S*)-tartrate were simulated with 5 cm<sup>-1</sup> half widths and Lorentzian band shapes. The absorption and VCD spectra at the B3LYP/6-31G\* and B3LYP/aug-cc-pVDZ levels for these five individual conformers and for the isolated molecule, obtained as population weighted sum of the absorption and VCD spectra of individual conformers, are shown in Figures 4-7 ~ 4-8. The calculated frequencies ( $\nu_i$ ), dipole strengths ( $D_i$ ) and rotation strengths ( $R_i$ ) of five conformers of isolated dimethyl (*S, S*)-tartrate at the B3LYP/6-31G\* and B3LYP/aug-cc-pVDZ levels are listed in Table 4-3 and Table 4-4 respectively. The predicted absorption and VCD spectra for the isolated dimethyl (*S,S*)-tartrate (population weighted sum of conformer spectra) at both the B3LYP/6-31G\* and B3LYP/aug-cc-pVDZ levels are compared in the Mid IR region with experimental spectra of diethyl D-tartrate in CCl<sub>4</sub> in

Figures 4-9. Experimental absorption and VCD band positions of diethyl D-tartrate in  $\text{CCl}_4$  and their corresponding B3LYP predicted values of isolated dimethyl (*S, S*)-tartrate are shown in Table 4-7. The predicted absorption and VCD spectra at the B3LYP/6-31G\* level are identical with those at the B3LYP/aug-cc-pVDZ level except that frequencies of absorption and VCD bands of predicted spectra at the B3LYP/aug-cc-pVDZ level are higher by about  $10\text{ cm}^{-1}$  than those of the corresponding bands of predicted spectra at the B3LYP/6-31G\* level. Overall, these predicted absorption and VCD spectra have good correspondence with the experimental spectra of dialkyl tartrates in  $\text{CCl}_4$  in band positions and relative peak intensities. There is just a small disagreement in the VCD spectra: a weak negative-positive doublet is seen in the  $1450\text{-}1350\text{ cm}^{-1}$  region in the predicted VCD spectrum while it does not show up in the experimental spectrum.



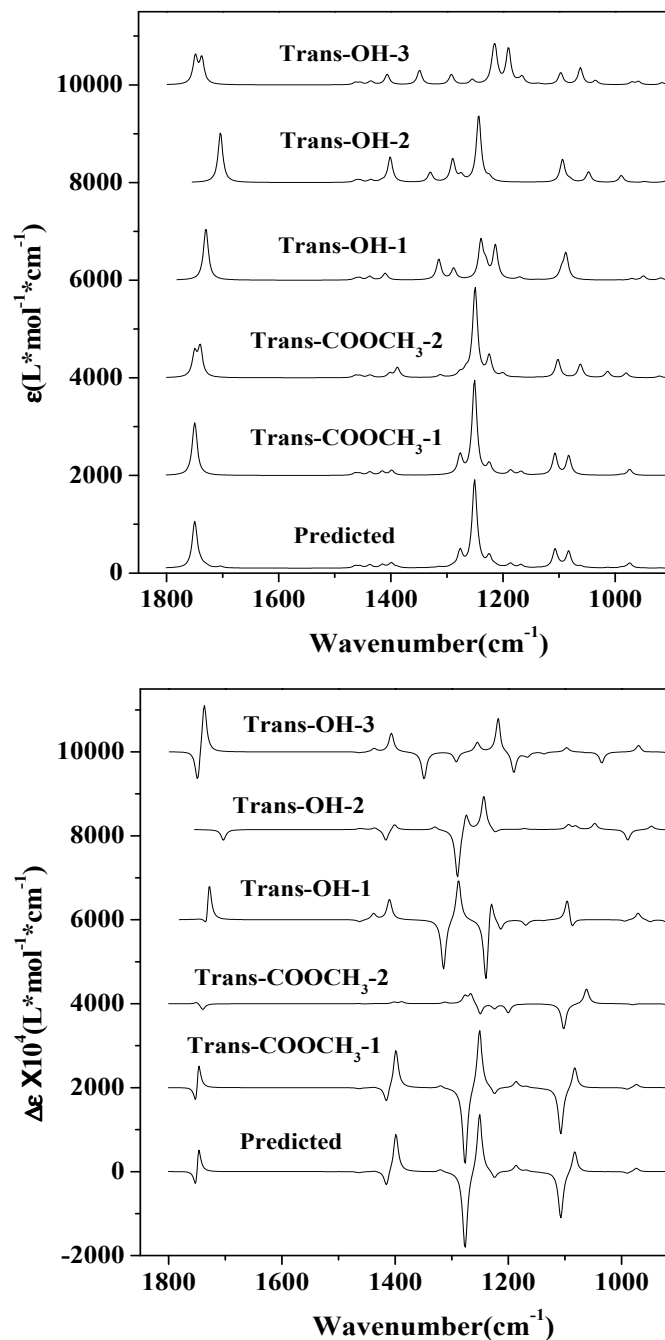


Figure 4-7. The simulated absorption (top) and VCD (bottom) spectra with B3LYP/6-31G\* for individual conformers of isolated dimethyl (*S, S*)-tartrate and for the isolated molecule (population weighted sum of conformer spectra). The 6-31G\* frequencies were scaled by 0.96, and a bandwidth of 5  $\text{cm}^{-1}$  was used in the spectral simulation. Populations determined from the Gibbs energies (Table 2) are used to obtain the predicted spectrum.

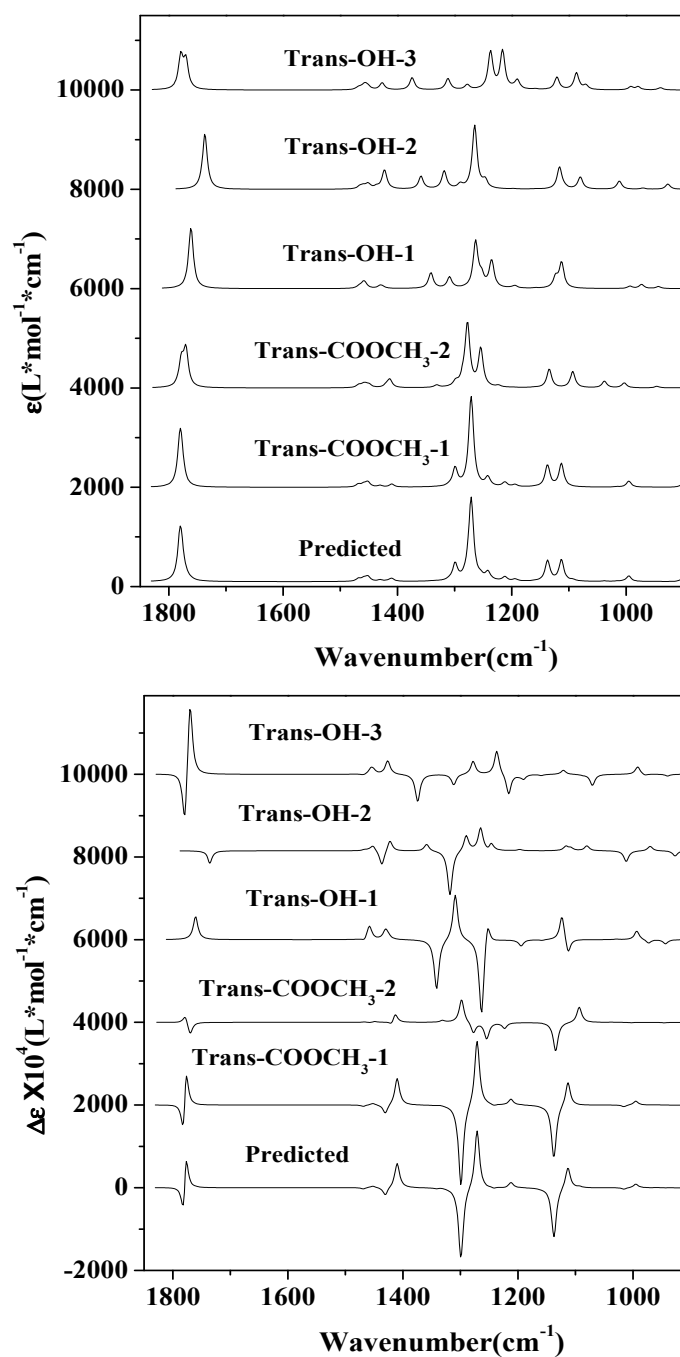


Figure 4-8. The simulated absorption (top) and VCD (bottom) spectra with B3LYP/aug-cc-pVDZ for individual conformers of isolated dimethyl (*S, S*)-tartrate and for the isolated molecule (population weighted sum of conformer spectra). A bandwidth of  $5 \text{ cm}^{-1}$  was used in the spectral simulation. Populations determined from the Gibbs energies (Table 4-2) are used to obtain the predicted spectrum.

Table 4-3. Calculated frequencies<sup>a</sup> ( $\nu_i$ ), dipole strengths ( $D_i$ ) and rotation strengths ( $R_i$ ) of five conformers of isolated dimethyl (*S, S*)-tartrate at B3LYP/6-31G\* level<sup>b</sup>

Trans-COOCH <sub>3</sub> -1			Trans-COOCH <sub>3</sub> -2			Trans-OH-1			Trans-OH-2			Trans-OH-3		
$\nu_i$	$D_i$	$R_i$	$\nu_i$	$D_i$	$R_i$	$\nu_i$	$D_i$	$R_i$	$\nu_i$	$D_i$	$R_i$	$\nu_i$	$D_i$	$R_i$
1750	619.6	-277.6	1750	379.1	11.4	1731	145.9	-290.1	1704	814.4	-139.6	1749	443.5	-172.1
1748	272.9	310.2	1740	480.3	-30.3	1730	720.0	402.0	1401	514.6	36.9	1737	413.1	256.6
1415	79.7	-98.0	1388	206.4	11.8	1410	129.0	113.4	1330	208.3	20.7	1407	188.5	112.3
1399	98.9	239.2	1266	113.8	67.6	1315	441.9	-331.7	1290	500.9	-331.9	1349	306.3	-174.2
1277	52.1	-99.1	1250	2042.8	-75.9	1288	247.4	280.0	1275	133.7	125.9	1292	223.4	-68.0
1276	378.3	-436.6	1225	473.9	-32.7	1240	858.2	-461.6	1243	1533.8	235.3	1218	363.2	285.3
1251	2150.1	416.5	1200	85.3	-64.1	1231	285.6	222.0	1094	598.8	36.6	1214	677.1	-62.7
1225	236.8	-51.7	1102	472.1	-199.6	1213	789.4	-67.3	1048	281.3	50.4	1190	851.9	-155.5
1107	553.2	-367.7	1062	360.9	123.7	1096	212.1	175.5	989	201.4	-93.3	1097	308.1	34.4
1083	509.3	175.4	1014	174.8	0.6	1088	672.9	-93.1	947	26.7	32.5	1062	452.0	-4.1
974	175.5	31.6	981	135.8	-9.0	971	42.4	60.7	903	166.0	-44.4	1035	109.6	-93.1

<sup>a</sup> Calculated frequencies with B3LYP/6-31G\* level were scaled with 0.96. <sup>b</sup> Frequencies are in  $\text{cm}^{-1}$ , dipole strengths are in  $10^{-40} \text{esu}^2\text{cm}^2$ , and rotational strengths are in  $10^{-44} \text{esu}^2\text{cm}^2$ .

Table 4-4. Calculated frequencies ( $\nu_i$ ), dipole strengths ( $D_i$ ) and rotation strengths ( $R_i$ ) of five conformers of isolated dimethyl (*S, S*)-tartrate at B3LYP/ aug-cc-pVDZ level<sup>a</sup>

Trans-COOCH <sub>3</sub> -1			Trans-COOCH <sub>3</sub> -2			Trans-OH-1			Trans-OH-2			Trans-OH-3		
$\nu_i$	$D_i$	$R_i$	$\nu_i$	$D_i$	$R_i$	$\nu_i$	$D_i$	$R_i$	$\nu_i$	$D_i$	$R_i$	$\nu_i$	$D_i$	$R_i$
1781	659.5	-332.6	1778	413.9	41.4	1762	167.4	-338.7	1738	24.2	137.7	1779	522.3	-292.8
1778	373.6	362.9	1770	596.9	-64.4	1761	835.7	450.3	1737	906.1	-195.8	1770	453.5	394.6
1431	31.7	-57.8	1413	165.6	56.4	1458	78.0	79.1	1437	41.5	-92.2	1374	259.4	-174.8
1410	60.6	167.3	1298	106.6	157.6	1431	52.0	53.9	1423	390.4	68.6	1312	248.3	-71.8
1299	403.1	-551.4	1278	1431.0	-75.0	1342	338.0	-326.7	1359	272.6	44.3	1278	107.3	89.6
1271	2063.6	456.2	1254	887.7	-114.1	1309	241.6	309.1	1318	392.6	-296.0	1238	467.6	-0.5
1242	208.4	-10.7	1223	39.7	-40.7	1263	1057.9	-540.5	1290	94.6	106.2	1237	414.6	170.9
1212	105.4	42.9	1135	476.8	-223.1	1253	237.3	170.5	1265	1456.5	156.2	1216	913.6	-148.8
1138	554.6	-411.7	1093	430.4	125.5	1235	642.9	1.0	1117	573.5	32.5	1190	219.8	-32.8
1113	607.9	192.2	1038	183.5	1.8	1123	266.7	198.3	1012	235.1	-93.6	1087	453.9	-5.1
995	176.9	35.3	1003	142.7	-3.3	1113	662.2	-124.8	927	162.0	-49.8	1071	114.2	-91.0

<sup>a</sup> Frequencies are in  $\text{cm}^{-1}$ , dipole strengths are in  $10^{-40} \text{esu}^2 \text{cm}^2$ , and rotational strengths are in  $10^{-44} \text{esu}^2 \text{cm}^2$ .

Using the PCM model that was implemented in the Gaussian 03 program, optimization calculation of the five geometries was performed in CCl<sub>4</sub> solvent. The geometry of Trans-OH-2 is found unstable in CCl<sub>4</sub>. Buffeteau et al<sup>17</sup> also reported that this conformer can not be stabilized in the presence of a solvent before. The specific rotations and absorption and VCD intensities for the other four conformers were calculated at the B3LYP/6-31G\* level with the PCM model.

The Gibbs energies, relative populations and specific rotations predicted for the four conformers of the molecule in CCl<sub>4</sub> using 6-31G\* basis set in the Gaussian 03 program are listed in Table 4-5. Trans-COOCH<sub>3</sub>-1 is still the predominant conformer for dimethyl (*S,S*)-tartrate in CCl<sub>4</sub>. For the specific rotations, only small difference (less than 10%) is found for the value of each conformer in CCl<sub>4</sub> compared with calculation results for isolated molecule. Trans-COOCH<sub>3</sub>-2 still has a negative value. The population-weighted predicted specific rotation is 53.2 at the 6-31G\* basis. This predicted value is close to the experimental intrinsic rotation of dimethyl D-tartrate in CCl<sub>4</sub> and predicted values for the isolated molecule (see Table 4-8).

Table 4-5. B3LYP/ 6-31G\* calculated Gibbs energies; populations, and specific rotations of conformers of dimethyl (*S, S*)-tartrate in CCl<sub>4</sub>

	Trans-COOCH <sub>3</sub> -1	Trans-COOCH <sub>3</sub> -2	Trans-OH-1	Trans-OH-3
Gibbs Energy (in hartrees)	-685.87308	-685.87104	-685.86890	-685.86066
Population(%)	88.4	10.1	1.1	0.4
Specific rotation, [ $\alpha$ ] <sub>D</sub>	70.0	-111.5	241.1	91.2

From the absorption and VCD results of the molecule in CCl<sub>4</sub>, all the four conformers were found to have potential energy minima. The population-weighted predicted absorption and VCD spectra for dimethyl (*S,S*)-tartrate in CCl<sub>4</sub> are shown in Figure 4-9. Experimental absorption and VCD band positions of diethyl D-tartrate in CCl<sub>4</sub> and their corresponding B3LYP Predicted values of dimethyl (*S, S*)-tartrate in CCl<sub>4</sub> are shown in Table 4-7. The predicted absorption and VCD spectra of dimethyl (*S,S*)-tartrate in CCl<sub>4</sub> have a good agreement with predicted spectra of the isolated molecule and correspond well with the experimental spectra of dialkyl tartrate in CCl<sub>4</sub> except that a weak negative-positive doublet is seen in the 1450-1350 cm<sup>-1</sup> region in the predicted VCD spectrum in CCl<sub>4</sub> while it does not show up in the experimental spectrum.

Table 4-6. Calculated frequencies<sup>a</sup> ( $\nu_i$ ), dipole strengths ( $D_i$ ) and rotation strengths ( $R_i$ ) of four conformers of dimethyl (*S, S*)-tartrate in CCl<sub>4</sub> at B3LYP/6-31G\* level<sup>b</sup>

Trans-COOCH <sub>3</sub> -1			Trans-COOCH <sub>3</sub> -2			Trans-OH-1			Trans-OH-3		
$\nu_i$	$D_i$	$R_i$	$\nu_i$	$D_i$	$R_i$	$\nu_i$	$D_i$	$R_i$	$\nu_i$	$D_i$	$R_i$
1740	819.2	-326.8	1734	338.3	208.5	1724	237.6	-313.5	1739	611.7	-198.3
1737	355.9	364.5	1731	789.2	-235.9	1721	872.4	417.2	1729	476.9	280.5
1402	58.7	-55.7	1376	227.1	62.0	1400	117.3	142.6	1400	209.1	104.6
1383	87.9	197.6	1262	266.3	145.6	1309	434.4	-290.5	1344	337.1	-168.2
1266	452.1	-425.9	1247	1969.9	-67.7	1275	302.6	325.6	1291	236.5	-75.9
1242	2345.8	499.8	1224	757.7	-27.5	1233	1199.0	-573.1	1214	488.2	214.8
1222	306.5	-79.4	1193	163.2	-70.3	1230	326.7	218.2	1213	655.4	64.0
1185	105.3	47.7	1099	672.1	-258.3	1210	834.0	-52.7	1187	1087.1	-180.0
1099	766.1	-447.6	1059	469.6	154.1	1091	279.6	217.0	1092	397.2	55.4
1075	659.8	228.1	1008	209.8	2.8	1080	936.2	-117.4	1054	544.5	3.2
968	196.1	41.0	974	152.8	-11.7	966	55.2	78.4	1034	233.4	-143.0

<sup>a</sup> Calculated frequencies with B3LYP/6-31G\* level were scaled with 0.96. <sup>b</sup> Frequencies are in cm<sup>-1</sup>, dipole strengths are in 10<sup>-40</sup> esu<sup>2</sup>cm<sup>2</sup>, and rotational strengths are in 10<sup>-44</sup> esu<sup>2</sup>cm<sup>2</sup>.

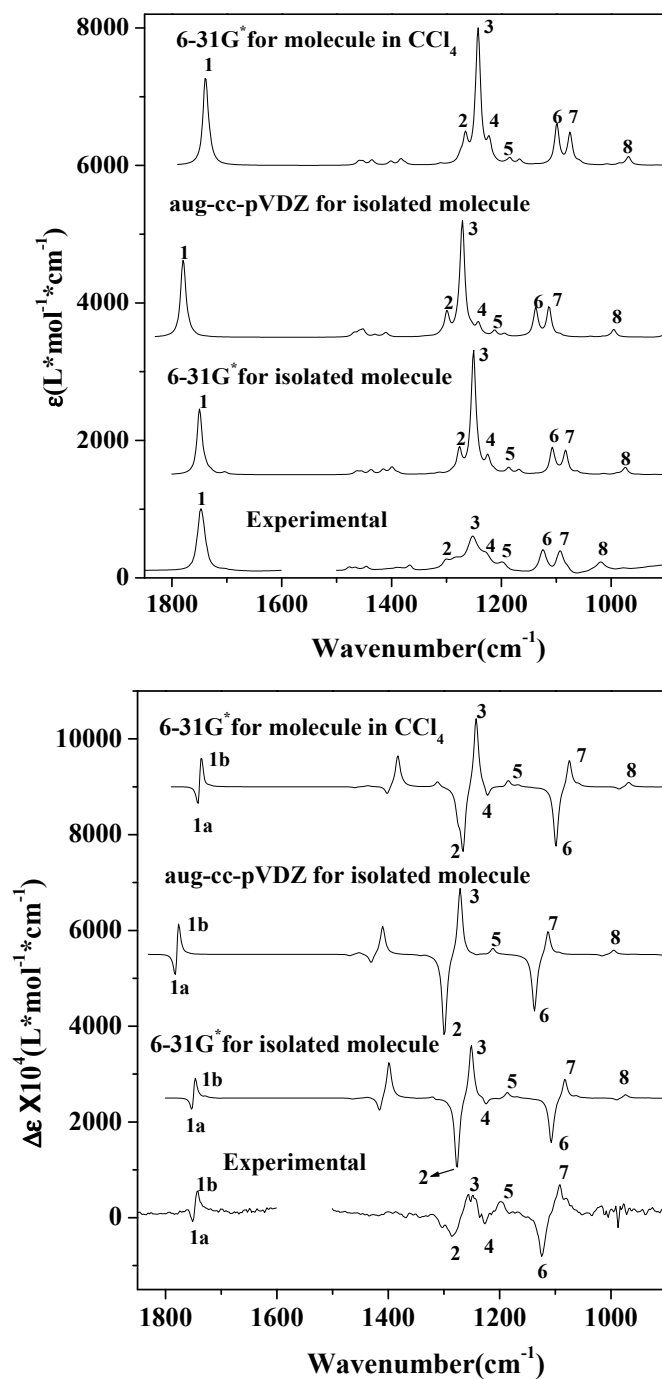


Figure 4-9. Comparison of the experimental absorption (top) and VCD (bottom) spectra of diethyl D-tartrate in  $\text{CCl}_4$  with predicted absorption spectra of isolated dimethyl (*S,S*)-tartrate and the molecule in  $\text{CCl}_4$ . The 6-31G\* frequencies were scaled by 0.96. A bandwidth of  $5 \text{ cm}^{-1}$  was used in all the spectral simulations.



Table 4-7. Experimental absorption and VCD band positions<sup>a</sup> of diethyl D-tartrate in CCl<sub>4</sub> and their correlation to B3LYP predicted values of isolated dimethyl (*S, S*)-tartrate and the molecule in CCl<sub>4</sub>

No	Experimental		Predicted					
			6-31G* for isolated molecule <sup>b</sup>		aug-cc-pVDZ for isolated molecule		6-31G* for molecule in CCl <sub>4</sub> <sup>b</sup>	
	absorption	VCD	absorption	VCD	absorption	VCD	absorption	VCD
1	1746	1750 (-) <sup>c</sup>	1749	1750 (-)	1780	1781 (-)	1739	1740 (-)
		1744(+) <sup>c</sup>		1748(+)		1778(+)		1737(+)
2	1285	1285(-)	1276	1276(-)	1299	1299(-)	1266	1266(-)
3	1252	1252(+)	1251	1251(+)	1271	1271(+)	1242	1242(+)
4	1226	1226(-)	1225	1225(-)	1242	...	1222	1222(-)
5	1200	1200(+)	1200	1200(+)	1212	1212(+)	1185	1185(+)
6	1124	1124(-)	1107	1107(-)	1138	1138(-)	1099	1099(-)
7	1092	1092(+)	1083	1083(+)	1113	1113(+)	1075	1075(+)
8	1019	... <sup>d</sup>	974	974(+)	995	995(+)	968	968(+)

<sup>a</sup> band positions are in cm<sup>-1</sup>; <sup>b</sup> predicted band positions at B3LYP/6-31G\* level were scaled with 0.96; <sup>c</sup>(+) refers to the positive sign of VCD band and (-) refers to the negative sign of VCD band; <sup>d</sup>“...” means that no corresponding VCD band is found.

Table 4-8. B3LYP predicted specific rotation( $[\alpha]_D$ ) of dimethyl (*S, S*)-tartrate and experimental intrinsic rotation( $\{\alpha\}_D$ ) of dimethyl D-tartrate

Method	Value
Predicted Specific Rotation $[\alpha]_D$ for isolated molecule	
6-31G*	50.4
aug-cc-pVDZ	38.8
Predicted Specific Rotation $[\alpha]_D$ in CCl <sub>4</sub>	
6-31G*	53.2
Experimental intrinsic rotation $\{\alpha\}_D$	
CCl <sub>4</sub>	43.0±1.6

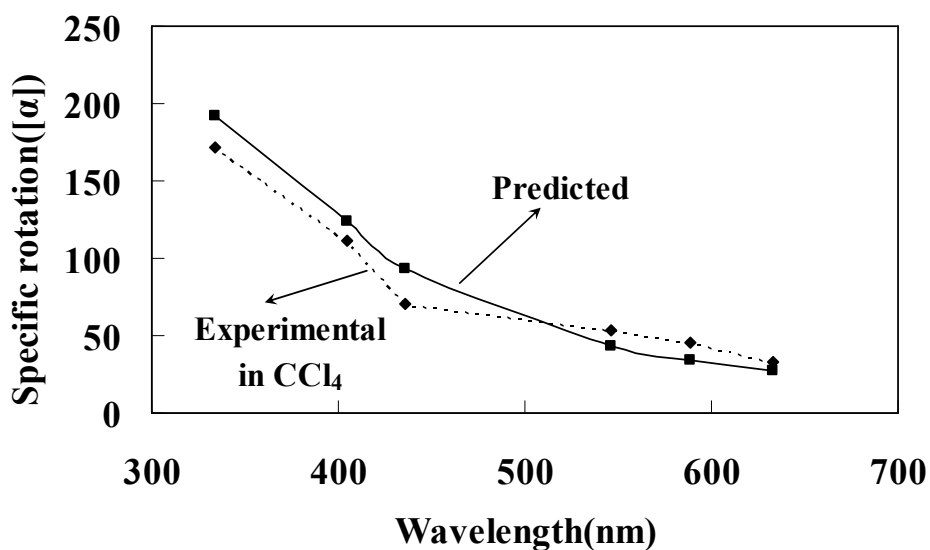


Figure 4-10 Comparison of experimental ORD of dimethyl D-tartrate in CCl<sub>4</sub> and predicted ORD for isolated dimethyl (*S,S*)-tartrate. The predicted ORD was obtained as population weighted data from the two lowest energy conformers of isolated dimethyl (*S,S*)-tartrate: Trans-COOCH<sub>3</sub>-1 and Trans-COOCH<sub>3</sub>-2 at B3LYP/aug-cc-pVDZ basic set.

DFT calculations of dimethyl (*S,S*)-tartrate were continued in DMSO solvent. PCM model in the Gaussian 03 program was used to do the calculation but it turned out conformers of dimethyl (*S,S*)-tartrate can not be optimized in DMSO with PCM model. Then clusters of dimethyl (*S,S*)-tartrate with the solvent molecules were considered to perform the calculation. Proniewicz et al<sup>19</sup> have reported structural study of several hydroxamic acids in DMSO solutions based on the DFT calculations of NMR spectra. In their study they used clusters of the compounds with DMSO molecules in DFT calculation and the computed chemical shifts of these clusters are in good agreement with experimental data.

Dimethyl (*S,S*)-tartrate molecule has two –OH groups which are capable to form hydrogen bonds with DMSO molecules.

Two geometries of clusters of trans-COOCH<sub>3</sub> conformers of dimethyl (*S,S*)-tartrate with 2 DMSO were considered first. Their structures are shown in Figure 4-11. The only difference between these 2 geometries is: in Trans-COOCH<sub>3</sub>-(DMSO)<sub>2</sub>-0, the 2 hydrogen bonds are between OH group and C=O group, which are connected to the same chiral carbon; while in Trans-COOCH<sub>3</sub>-(DMSO)<sub>2</sub>-1, the 2 hydrogen bonds are between OH groups and S=O groups of solvent molecules. Based on their energies after optimization with B3LYP/6-31G\* basis set (shown in Figure 4-11), Trans-COOCH<sub>3</sub>-(DMSO)<sub>2</sub>-1, is much more stable than Trans-COOCH<sub>3</sub>-(DMSO)<sub>2</sub>-0. That means that in DMSO, dimethyl (*S,S*)-tartrate prefers to forming intermolecular hydrogen bonds with solvent molecules compared with forming internal hydrogen bonds.

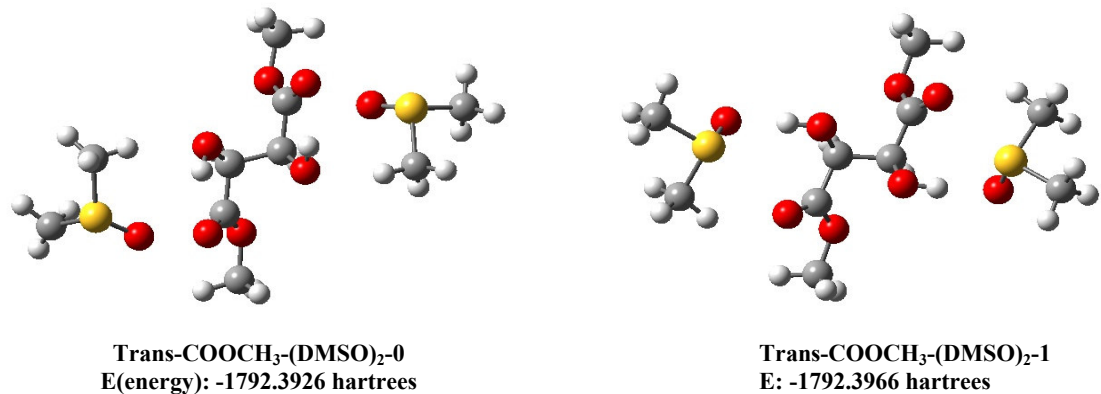


Figure 4-11. Structures and electronic energies(with B3LYP/6-31G\* basis set) of TransCOOCH<sub>3</sub>-(DMSO)<sub>2</sub>-0 and TransCOOCH<sub>3</sub>-(DMSO)<sub>2</sub>-1

Another 5 geometries of clusters of dimethyl (*S,S*)-tartrate with 2 DMSO molecules were considered. Their structures are shown in Figure 4-12. For each of these 5 clusters, the hydrogen bonds are between OH groups and S=O groups of solvent molecules. Based on geometry of dimethyl (*S,S*)-tartrate in the clusters, these clusters can be divided into three groups: trans-COOCH<sub>3</sub>, trans-OH and trans-H conformers of clusters. With Trans-COOCH<sub>3</sub>-(DMSO)<sub>2</sub>-1 included, two geometries of clusters with 2 DMSO were chosen for each group of clusters. For each group of clusters, the only difference between the two geometries is the position of ester groups and C=O groups for dimethyl (*S,S*)-tartrate.

The electronic energies and Gibbs energies were calculated for the 6 conformers of clusters of dimethyl (*S,S*)-tartrate with 2 DMSO molecules at the B3LYP/6-31G\* level. The results are listed in Table 4-9. The absorption and VCD intensities were also calculated for these 6 conformations at the B3LYP/6-31G\* level. All of these conformations except Trans-COOCH<sub>3</sub>-(DMSO)<sub>2</sub>-2 are found to have potential energy minima. For Trans-COOCH<sub>3</sub>-(DMSO)<sub>2</sub>-2, negative vibrational frequencies are found. The absorption and VCD spectra for the 5 conformations with potential energy minima

were simulated with  $5\text{ cm}^{-1}$  half widths and Lorentzian band shapes (shown in Figure 4-13). Based on Gibbs energies, Trans-OH-(DMSO)<sub>2</sub>-1 is the most dominant conformers. But the predicted absorption and VCD spectra (see Figure 4-13) and the predicted optical rotation (150.1 at 589 nm) based on the populations of conformers calculated from Gibbs energies of these conformers (listed in Table 4-9) are far from matching with the experimental ones. A different approach based on the experimental intrinsic rotation and experimental VCD spectrum was used to determine the dominant conformers and populations of the conformers.

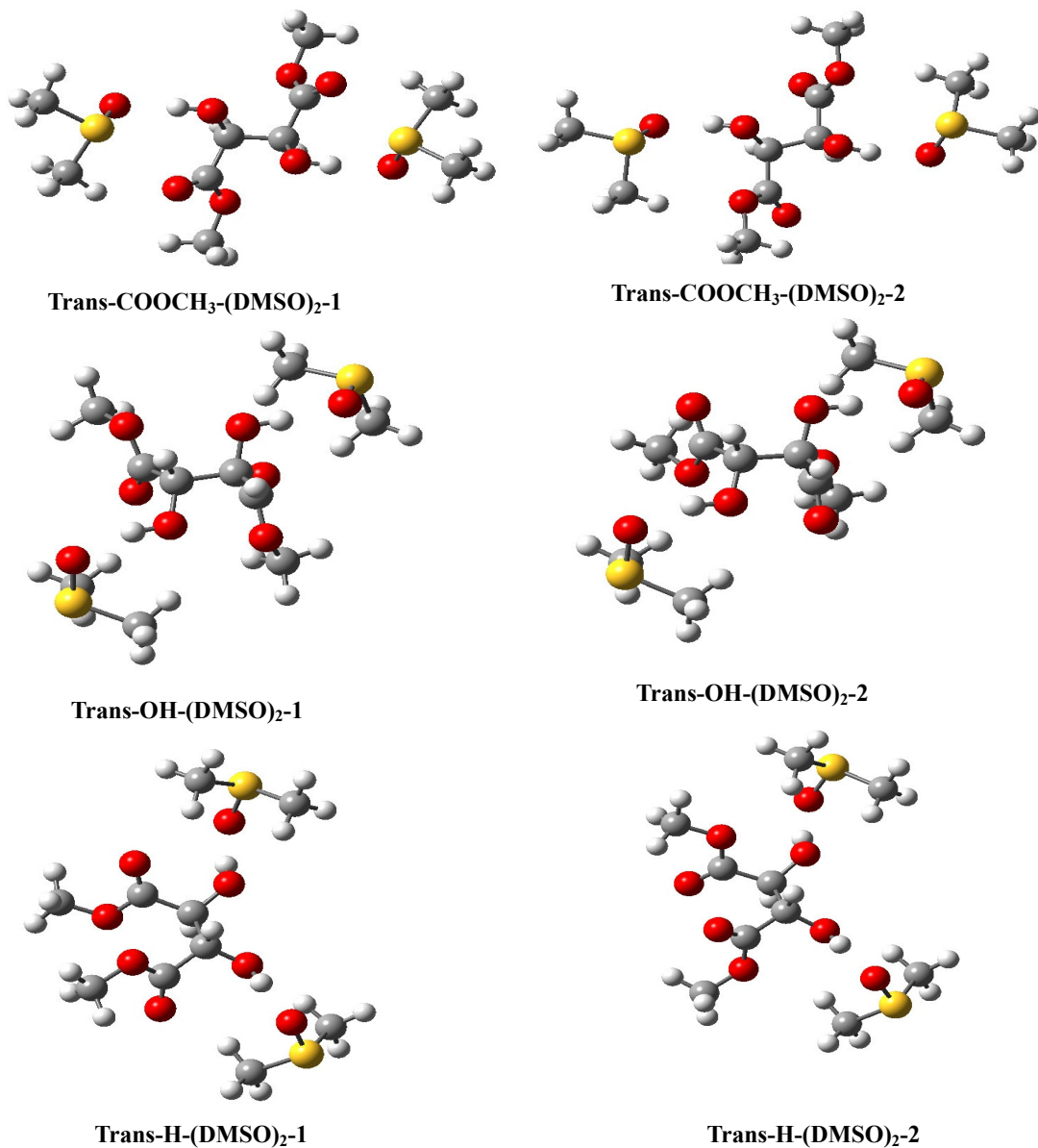


Figure 4-12. Structures of 6 conformers of clusters of dimethyl (*S,S*)-tartrate with 2 DMSO molecules with hydrogen bonds between OH and S=O

Table 4-9 B3LYP/ 6-31G\* calculated Gibbs energies; and specific rotations of conformers of clusters of dimethyl (*S, S*)-tartrate with DMSO

	Gibbs Energy (in hartrees)	Population (%)	Specific rotation, [ $\alpha$ ] (633nm)	Specific rotation, [ $\alpha$ ] (589nm)	Specific rotation, [ $\alpha$ ] (546nm)	Specific rotation, [ $\alpha$ ] (436nm)	Specific rotation, [ $\alpha$ ] (405nm)	Specific rotation, [ $\alpha$ ] (365nm)
Trans-COOCH <sub>3</sub> -(DMSO) <sub>2</sub> -1	-1792.1258	20.7	14.1	18.0	23.8	59.1	81.5	135.2
Trans-COOCH <sub>3</sub> -(DMSO) <sub>2</sub> -2*								
Trans-OH-(DMSO) <sub>2</sub> -1	-1792.1269	66.2	154.2	181.2	215.3	369.3	446.1	591.2
Trans-OH-(DMSO) <sub>2</sub> -2	-1792.1243	4.2	126.2	148.8	177.5	309.8	377.4	508.0
Trans-H-(DMSO) <sub>2</sub> -1	-1792.1250	8.8	194.1	229.0	273.5	479.7	586.0	793.4
Trans-H-(DMSO) <sub>2</sub> -2	-1792.1207	0.1	13.8	17.2	22.0	49.0	65.8	103.7

\*: Trans-COOCH<sub>3</sub>-(DMSO)<sub>2</sub>-2 has no potential energy minima.

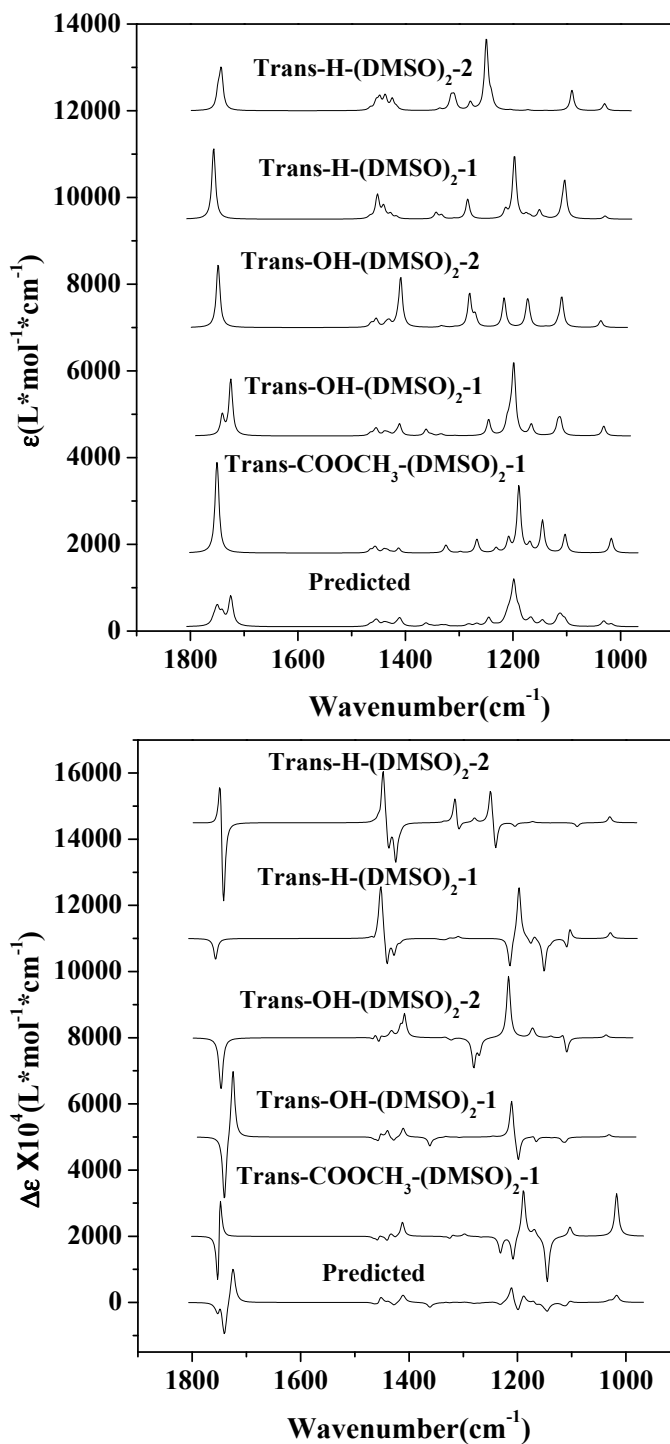


Figure 4-13. The simulated absorption (top) and VCD (bottom) spectra for conformers of cluster of dimethyl (*S,S*)-tartrate with 2 DMSO and for the molecule in DMSO (population weighted sum of conformer spectra) with B3LYP/6-31G\*. The 6-31G\* frequencies were scaled by 0.96, and a bandwidth of 5  $\text{cm}^{-1}$  was used in the spectral simulation.



The experimental intrinsic rotation of dimethyl D-tartrate in DMSO solvent is  $-3.1 \pm 0.2$  at 589nm. This value is very close to zero. When comparing predicted specific rotation value with this experimental intrinsic rotation value, it is really hard to determine they correspond well or not because even with a small difference of 4 between them the sign of optical rotation may change from negative to positive. So it is necessary to measure the experimental intrinsic rotation of dimethyl D-tartrate in DMSO at other wavelengths. So we first measured the specific rotations of dimethyl D-tartrate at 6 wavelengths (633nm ~ 365nm) at the concentration of 0.0064M in DMSO (see Figure 4-15). Specific rotation of dimethyl D-tartrate changes from negative into positive as the wavelength decreases. Dimethyl D-tartrate has anomalous optical rotatory dispersion<sup>18c</sup> in DMSO. It is necessary to measure the intrinsic rotation of dimethyl D-tartrate at a lower wavelength. So intrinsic rotation of dimethyl D-tartrate was also measured at 365nm in DMSO and the intrinsic rotation is  $42.7 \pm 0.4$ .

Specific rotations of these 5 conformations were predicted at 6 wavelengths (633nm ~ 365nm) at the B3LYP/6-31G\* level. The results are shown in Table 4-9. Trans-COOCH<sub>3</sub>-(DMSO)<sub>2</sub>-1 and Trans-H-(DMSO)<sub>2</sub>-2 have the closest specific rotations to the experimental intrinsic rotation both at 589nm and 365nm. When the predicted absorption spectra of these 2 conformers are combined, two bands are formed in the C=O stretching region. These two bands correspond well with the experimental absorption bands in this region for dialkyl D-tartrates in DMSO-d<sub>6</sub>. When the predicted VCD spectra of these 2 conformers are combined, a negative-positive-negative triplet is formed in the C=O stretching region, which has also a good agreement with the experimental VCD sign in this region. Based on the fact that the intensities of two negative bands of this triplet are

almost the same in the experimental VCD spectra of dialkyl tartrates, populations of these two conformers were predicted. It is found that when populations of Trans-COOCH<sub>3</sub>-(DMSO)<sub>2</sub>-1 and Trans-H-(DMSO)<sub>2</sub>-2 are 62.5% and 37.5% respectively, the two negative bands of predicted VCD spectrum of dimethyl (*S,S*)-tartrate are almost the same. The empirically predicted absorption and VCD spectra of dimethyl (*S,S*)-tartrate (population weighted sum of spectra of Trans-COOCH<sub>3</sub>-(DMSO)<sub>2</sub>-1 and Trans-H-(DMSO)<sub>2</sub>-2) are compared with the experimental spectra of dimethyl D-tartrate in DMSO-d<sub>6</sub> solvent and shown on Figure 4-14. Experimental absorption and VCD band positions of dimethyl D-tartrate in DMSO-d<sub>6</sub> and their corresponding values in the empirically predicted spectra are shown in Table 4-10. For the absorption spectra, a good agreement is seen for major bands in the comparison between the empirically predicted and the experimental spectra. Overall the bands in the experimental absorption spectrum are broader than those in the empirically predicted spectrum and several small bands which show up in the 1300-1180 cm<sup>-1</sup> region in the empirically predicted spectrum have not been observed in the experimental spectra possibly because of their overlapping with other bands. For the VCD spectra, there is a good agreement in the C=O stretching region (1850-1600 cm<sup>-1</sup>) and the C-O stretching region (1250-1100 cm<sup>-1</sup>) between the VCD bands in the empirically predicted spectrum and those in experimental spectrum. Several bands with relatively low intensities are observed in the 1500-1250 cm<sup>-1</sup> region in the empirically predicted VCD spectrum but these VCD bands did not show up in the experimental spectrum. A similar discrepancy was also seen for the spectra in CCl<sub>4</sub>(Figure 4-9). The empirically predicted specific rotations (population weighted sum of specific rotations of Trans-COOCH<sub>3</sub>-(DMSO)<sub>2</sub>-1 and Trans-H-(DMSO)<sub>2</sub>-2) are listed

on Table 4-11. At 589 nm, the experimental intrinsic rotation is close to zero. Even though the empirically predicted value (17.7) is close to the experimental one ( $-3.1 \pm 0.2$ ), they differ in the sign. At 365 nm, the difference between the empirically predicted optical rotation and experimental intrinsic rotation is bigger than that at 589nm but the empirically predicted optical rotation and experimental value match in the sign. The empirically predicted optical rotatory dispersion (ORD) for dimethyl (*S,S*)-tartrate in DMSO , which was obtained as population weighted data from Trans-COOCH<sub>3</sub>-(DMSO)<sub>2</sub>-1 and Trans-H-(DMSO)<sub>2</sub>-2 , is compared with experimental ORD of dimethyl D-tartrate in DMSO in Figure 4-15. There is a gap between empirically predicted ORD and experimental ORD. But overall there is a good correlation between the predicted ORD and the experimental one.

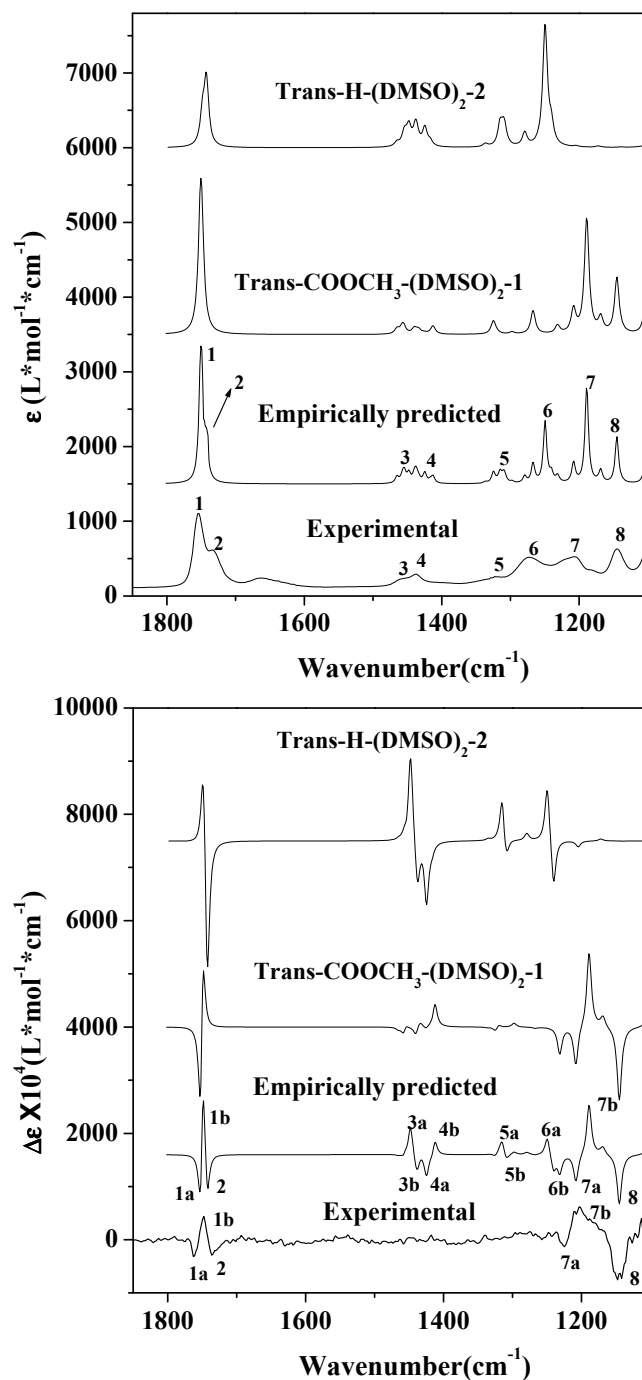


Figure 4-14. Comparison of the experimental absorption (top) and VCD (bottom) spectra of dimethyl D-tartrate in DMSO- $d_6$  with the simulated absorption spectra of Trans-COOCH<sub>3</sub>-(DMSO)<sub>2</sub>-1 and Trans-H-(DMSO)<sub>2</sub>-2 conformers and the predicted absorption spectra of dimethyl (*S,S*)-tartrate in DMSO (population weighted sum of conformer spectra). The 6-31G\* frequencies were scaled by 0.96, and a bandwidth of 5  $cm^{-1}$  was used in the spectral simulation.

Table 4-10. Experimental absorption and VCD band positions<sup>a</sup> of dimethyl D-tartrate in DMSO-d<sub>6</sub> and their correlation to predicted values of dimethyl (*S, S*)-tartrate in DMSO

No	Experimental		Predicted <sup>b</sup>	
	absorption	VCD	absorption	VCD
1	1753	1763 (-) <sup>c</sup>	1748	1750 (-)
		1747(+) <sup>c</sup>		1745(+)
2	1736	1736(-)	1737	1737 (-)
3	1457	... <sup>d</sup>	1445	1447(+)
				1437(-)
4	1437	...	1420	1422(-)
				1410(+)
5	1324	...	1311	1313(+)
				1306(-)
6	1273	...	1246	1248(+)
				1234(-)
7	1207	1224(-)	1188	1207(-)
		1201(+)		1186(+)
8	1146	1146(-)	1142	1142(-)

<sup>a</sup> band positions are in cm<sup>-1</sup>; <sup>b</sup> predicted band positions at B3LYP/6-31G\* level were scaled with 0.96; <sup>c</sup>(+) refers to the positive sign of VCD band and (-) refers to the negative sign of VCD band; <sup>d</sup>“...” means that no corresponding VCD band is found.

Table 4-11. B3LYP/6-31G\* empirically predicted specific rotation( $[\alpha]_D$ ) of dimethyl (*S, S*)-tartrate and experimental intrinsic rotation( $\{\alpha\}_D$ ) of dimethyl D-tartrate in DMSO

Wavelength	Value
Empirically predicted specific rotation $[\alpha]_D$ for isolated molecule	
589 nm	17.7
365 nm	123.4
Experimental intrinsic rotation $\{\alpha\}_D$	
589 nm	-3.1±0.2
365 nm	42.7±0.4

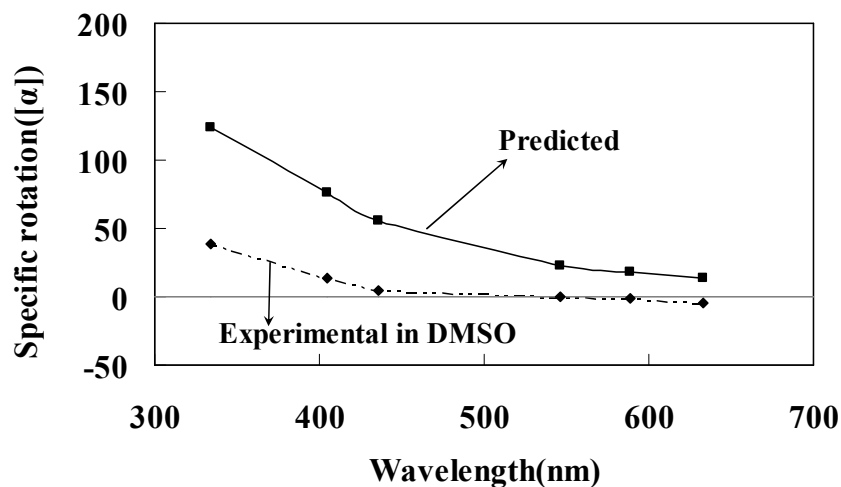


Figure 4-15 Comparison of experimental ORD of dimethyl D-tartrate in DMSO and predicted ORD for dimethyl (*S,S*)-tartrate in DMSO. The predicted ORD was obtained as population weighted data from the two conformers of cluster of dimethyl (*S,S*)-tartrate with 2 DMSO: Trans-COOCH<sub>3</sub>-(DMSO)<sub>2</sub>-1 and Trans-H-(DMSO)<sub>2</sub>-2 at B3LYP/6-31G\* basic set.

We could not perform calculation about dimethyl (*S, S*)-tartrate in H<sub>2</sub>O successfully because great difficulties exist in the prediction of absorption and VCD spectra and optical rotation for dimethyl (*S, S*)-tartrate in H<sub>2</sub>O. Hydrogen bonding between dimethyl (*S, S*)-tartrate and solvent molecules is a very important factor in investigation of conformations of dimethyl (*S, S*)-tartrate in H<sub>2</sub>O. PCM model in the Gaussian 03 program does not considerate hydrogen bonding in the calculation. Clusters of dimethyl (*S, S*)-tartrate with H<sub>2</sub>O molecules were also tried in the calculation but the number of H<sub>2</sub>O molecules in the clusters is hard to determine because H<sub>2</sub>O molecules are both hydrogen bond donors and acceptors while DMSO molecules are just hydrogen bond acceptors.

#### 4. Study of dialkyl tartrate cyclodextrin complexes

Dialkyl tartrate cyclodextrin complexes were prepared using coprecipitation method and characterized by  $^1\text{H}$  NMR. From the integration result in the NMR spectra, the complexation ratios for these complexes are confirmed to be 1:1.

The vibrational absorption and VCD spectra of dialkyl tartrate-cyclodextrin complexes were measured in  $\text{DMSO-d}_6$  and  $\text{D}_2\text{O}$  solvents in the Mid IR region (see Figures 4-16 ~ 4-17). The absorption and VCD bands in the region below  $1600\text{ cm}^{-1}$  originate from vibrational modes of both dialkyl tartrate and cyclodextrin molecules in the complex while bands in the  $\text{C}=\text{O}$  stretching region ( $1850\text{-}1600\text{ cm}^{-1}$ ) only come from ester groups in dialkyl tartrate. By direct comparison between absorption and VCD bands the  $\text{C}=\text{O}$  region of dialkyl tartrates and those of their corresponding complexes, effects of complexation with cyclodextrin on dialkyl tartrate can be investigated. The absorption and VCD signs in the  $\text{C}=\text{O}$  region for these complexes are identical with those shown in the spectra of dialkyl tartrates: in  $\text{DMSO-d}_6$ , there are two absorption bands and three VCD bands (negative-positive-negative triplet for D enantiomer complexes); in  $\text{D}_2\text{O}$ , one broader absorption band and no VCD signs are found. The frequencies of these bands for the complexes in the  $\text{C}=\text{O}$  region are almost the same as those for dialkyl tartrates.

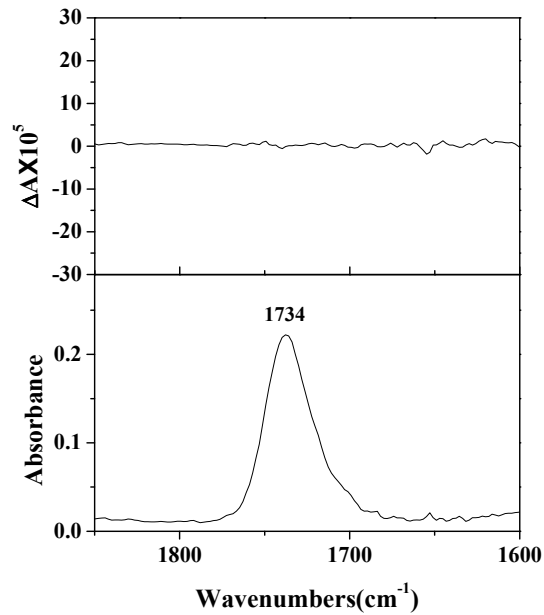


Figure 4-16. Vibrational absorption(bottom) and VCD(top) spectra in the C=O region in D<sub>2</sub>O solution of diethyl L-tartrate  $\alpha$ -CD complex(0.044M).

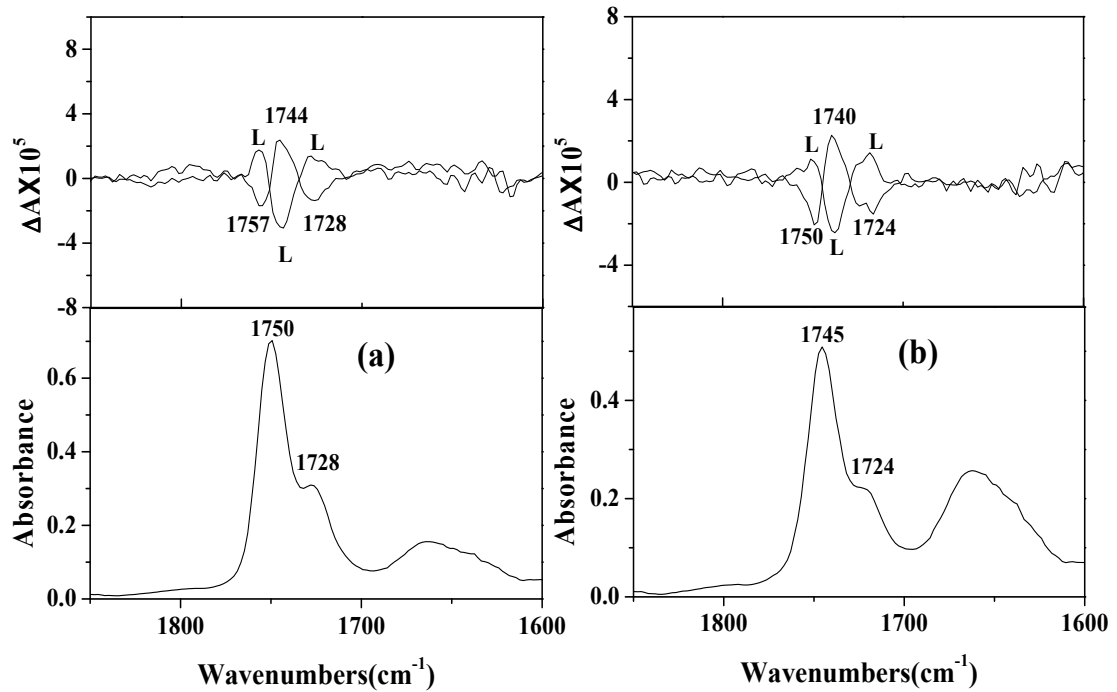


Figure 4-17. Vibrational absorption(bottom) and VCD(top) spectra in the C=O stretching region in DMSO-d<sub>6</sub> solution of (a)diethyl tartrate  $\beta$ -CD complex(0.040M); (b)diisopropyl tartrate  $\beta$ -CD complex(0.040M ). L enantiomer complexes are labeled with L.



The intrinsic rotations of dialkyl tartrates-cyclodextrin complexes were measured in H<sub>2</sub>O. They were compared with the intrinsic rotations of 1:1 ratio mixtures of dialkyl tartrate and cyclodextrin in Table 4-12. The intrinsic rotations of these 1:1 ratio mixtures were calculated using equation 4-1, which is derived in CHAPTER VI.

$$\{\alpha\}_{\text{mixture}} = \{\alpha\}_{\text{guest}} * \frac{M_{\text{guest}}}{(M_{\text{guest}} + M_{\text{host}})} + \{\alpha\}_{\text{host}} * \frac{M_{\text{host}}}{(M_{\text{guest}} + M_{\text{host}})} \quad (4-1)$$

{ $\alpha$ }: intrinsic rotation; M: molar mass; dialkyl tartrate molecules are guest molecules and cyclodextrin molecules are host molecules.

Table 4-12. Comparison of intrinsic rotations between dialkyl tartrate- cyclodextrin complexes and their corresponding 1:1 ratio mixtures

Guest	Host	Intrinsic rotation( $\{\alpha\}_D$ for the complex	Intrinsic rotation( $\{\alpha\}_D$ of 1:1 ratio mixture
Diethyl L-tartrate	$\alpha$ -CD	120.9 $\pm$ 0.7	129.5 $\pm$ 0.4
Diethyl D-tartrate	$\beta$ -CD	126.0 $\pm$ 0.9	130.6 $\pm$ 0.4
Diethyl L-tartrate	$\beta$ -CD	128.1 $\pm$ 1.2	138.9 $\pm$ 0.4
Diisopropyl D-tartrate	$\beta$ -CD	126.0 $\pm$ 0.9	126.7 $\pm$ 0.4
Diisopropyl L-tartrate	$\beta$ -CD	132.4 $\pm$ 1.2	136.9 $\pm$ 0.4

The intrinsic rotations of dialkyl tartrate-cyclodextrin complexes are close to the values of 1:1 ratio mixtures of dialkyl tartrates and cyclodextrin in H<sub>2</sub>O. The differences between intrinsic rotation of the complexes and their corresponding mixtures are less than 10% in all cases.

From the comparison between VA and VCD spectra of dialkyl tartrate-cyclodextrin complexes and those of dialkyl tartrate in the C=O stretching region and the comparison

of intrinsic rotations of dialkyl tartrate-cyclodextrin complexes with those of 1:1 ratio mixtures of dialkyl tartrates and cyclodextrin, it is indicated that in the solution of DMSO and H<sub>2</sub>O, the interaction between dialkyl tartrates and cyclodextrin is very weak and cyclodextrin does not change the VA, VCD and intrinsic rotation properties of dialkyl tartrates significantly.

To prove the weak interaction between dialkyl tartrates and cyclodextrin in solutions, it is very important to measure the binding constants of dialkyl tartrates and cyclodextrin in solutions. Quantitative NMR method<sup>20</sup> was tried to measure the binding constants of dialkyl tartrates in DMSO and H<sub>2</sub>O, but big errors are found from the results. Isothermal titration calorimetry (ITC) is a thermodynamic technique that allows the study of the interactions of two species.<sup>14</sup> When these two species interact, heat is either generated or absorbed. By measuring these interaction heats, binding constants ( $K$ ), reaction stoichiometry ( $n$ ), and thermodynamic parameters including enthalpy ( $\Delta H$ ) and entropy ( $\Delta S$ ) can be accurately determined. ITC is a direct, accurate and highly sensitive method to measure binding constants and other thermodynamic parameters. ITC has found widespread applicability in the study of biological systems<sup>21</sup> involving protein-ligand, protein-nucleic acid and protein-protein interactions and also in supramolecular chemistry, most notably for cyclodextrins (CDs)<sup>22</sup> and crown ethers<sup>23</sup>.

For each titration, a curve of heat pulse ( $dQ/dt$ ) over time was recorded as raw data. Heat pulse ( $dQ/dt$ ) can be calculated by equation 4-2<sup>24</sup>, where  $\Delta T$  is the temperature difference between sample cell and reference cell, and  $k$  is the calibration constant.

$$dQ/dt = k\Delta T \quad (4-2)$$

Then a binding curve between integrated heat ( $Q$ ) and mole ratio of two species (ligand : macromolecules) can be obtained from raw data. The integrated heat ( $Q$ ) is related to the molar ratio as shown in equation 4-3<sup>14</sup>, where  $V$  is the reaction volume, and  $[L_B]$ ,  $[L]$  and  $[M]$  are molarities of bound ligand, total ligand and total macromolecules in the sample cell respectively. Molar ratio of ligand to macromolecules is equal to  $[L]/[M]$ .

$$Q = V\Delta H[L_B] = V\Delta H[M] \frac{nK[L]}{1 + K[L]} = V\Delta H[M] \frac{nK\left(\frac{[L]}{[M]}\right)}{\frac{1}{[M]} + K\left(\frac{[L]}{[M]}\right)} \quad (4-3)$$

For single site interaction cases,  $n$  is equal to 1. With ORIGIN software, best fits can be found for binding curves based on equation 4-3 and  $\Delta H$  and  $K$  can be obtained.  $\Delta G$  (free energy) and  $\Delta S$  can be obtained from equation 4-4 and 4-5 respectively.

$$\Delta G = -RT \ln K \quad (4-4)$$

$$\Delta S = (\Delta H - \Delta G)/T \quad (4-5)$$

Calorimetric titrations were made for  $\alpha$ -CD and  $\beta$ -CD with diethyl L-tartrate in both  $H_2O$  and DMSO. The calorimetric titrations of diethyl L-tartrate with  $\alpha$ -CD and  $\beta$ -CD in  $H_2O$  and DMSO are shown in Figure 4-18. The binding constants of diethyl L-tartrate complexes of  $\alpha$ -CD and  $\beta$ -CD in  $H_2O$  and DMSO solvents are listed in Table 4-13.

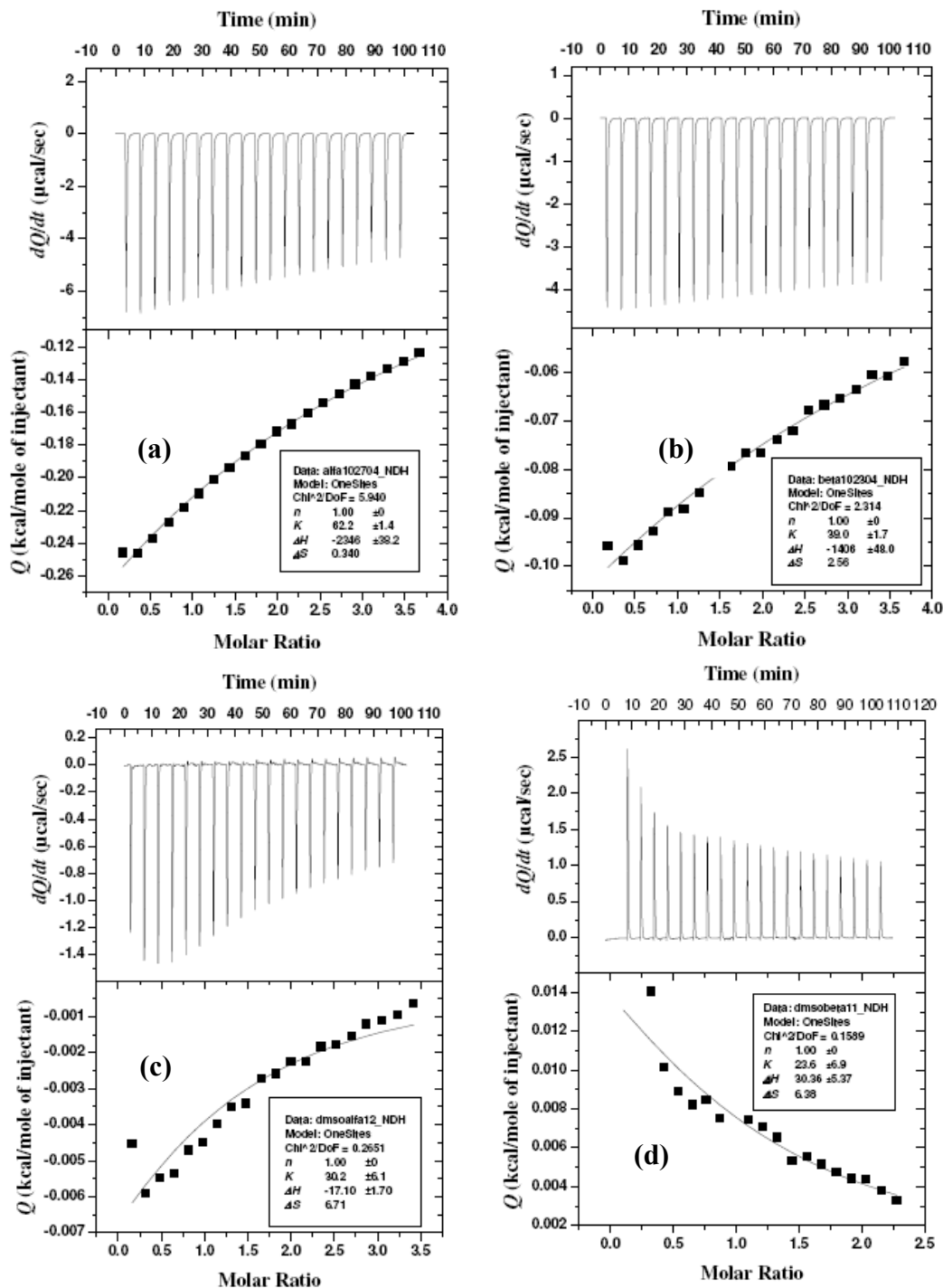


Figure 4-18. Calorimetric titrations of (a) diethyl L-tartrate (100 mM) with  $\alpha$ -CD (2 mM) in  $\text{H}_2\text{O}$ ; (b) diethyl L-tartrate (100 mM) with  $\beta$ -CD (2 mM) in  $\text{H}_2\text{O}$ ; (c) diethyl L-tartrate (450 mM) with  $\alpha$ -CD (20 mM) in DMSO; (d) diethyl L-tartrate (150 mM) with  $\beta$ -CD (20 mM) in DMSO. Raw data (**top**) was obtained for 20 ejections with each of 5  $\mu\text{L}$  of diethyl L-tartrate solution in  $\text{H}_2\text{O}$  or with each of 10  $\mu\text{L}$  of diethyl L-tartrate solution in DMSO; the binding curves (**bottom**) were obtained in best fit with binding constants and other thermodynamic parameters shown in the window.

Table 4-13. Binding constants of diethyl L-tartrate and cyclodextrin in solutions

Host	Solvent	Binding constant( $K$ , $M^{-1}$ )*
$\alpha$ -CD	H <sub>2</sub> O	62.2±1.4
$\alpha$ -CD	DMSO	30.2±6.1
$\beta$ -CD	H <sub>2</sub> O	39.0±1.7
$\beta$ -CD	DMSO	23.6±6.9

The binding constants between diethyl L-tartrate and cyclodextrin ( $\alpha$ -CD or  $\beta$ -CD) in DMSO are smaller than their corresponding binding constants in H<sub>2</sub>O. Generally, these binding constants are very small ( $< 100 M^{-1}$ ) in both H<sub>2</sub>O and DMSO. It can be concluded that in the solutions of H<sub>2</sub>O and DMSO, interaction between diethyl L-tartrate and cyclodextrin( $\alpha$ -CD or  $\beta$ -CD) is very weak. This can explain why absorption and VCD spectra, and optical rotation properties of dialkyl tartrate are not affected significantly by cyclodextrin in solution states.

### Conclusion

Dialkyl tartrates show different VA and VCD spectra in the Mid IR region and different intrinsic rotation values in different solvents. The DFT calculations for dimethyl (*S,S*)-tartrate, a representative compound among these tartrates, were performed in isolated state and in different solvents. The trans COOR conformer with hydrogen bonding between OH and C=O groups attached to the same chiral carbon is dominant (population is more than 80%) for isolated dimethyl (*S,S*)-tartrate and the molecule in CCl<sub>4</sub>. The population weighted VA and VCD spectra and specific rotations for isolated dimethyl (*S,S*)-tartrate and the molecule in CCl<sub>4</sub> correspond well with the experimental

spectra and intrinsic rotations in CCl<sub>4</sub>. In DMSO, dimethyl (*S,S*)-tartrate molecules are in favor of forming intermolecular hydrogen bonding with DMSO solvent molecules and clusters of dimethyl (*S,S*)-tartrate with 2 DMSO molecules were used to perform DFT calculation of dimethyl (*S,S*)-tartrate in DMSO. Based on experimental results, there are two dominant conformers of cluster including a Trans COOR cluster conformer and a Trans H one in DMSO solvent and the corresponding predicted VA and VCD spectra and specific rotations are in good agreement with experimental spectra and intrinsic rotations of dimethyl D-tartrate in DMSO solvent.

For dialkyl tartrate-cyclodextrin complexes, cyclodextrin does not change the VA, VCD and intrinsic rotation properties of dialkyl tartrates significantly in the complexation because of weak interaction between cyclodextrin and dialkyl tartrate molecules in the solution state.

Combined use of VA, VCD, optical rotation techniques with DFT calculations is a powerful tool to study chiral molecules in solutions. VA, VCD and optical rotation techniques are also quite useful to study the effects of cyclodextrins on guest molecules in cyclodextrin complexes.

## References

1. (a) Wang, F.; Polavarapu, P. L.; Drabowicz, J.; Kielbasinski, P.; Potrzebowski, M. J.; Mikolajczyk, M.; Wieczorek M. W.; Majzner, W. W.; Lazewska, I. *J. Phys. Chem. A* **2004**, *108*, 2072-2079; (b) He, J. T.; Petrovich, A.; Polavarapu, P. L. *J. Phys. Chem. A* **2004**, *108*, 1671-1680; (c) Wang, F.; Polavarapu, P. L.; Lebon, F.; Giovanna, L.; Abbate, S.; Catellani, M. *J. Phys. Chem. A* **2002**, *106*, 12365-12369; (d) Wang, F.; Wang, Y.; Polavarapu, P. L.; Li, T.; Drabowicz, J.; Pietrusiewicz, K. M.; Zygo, K. *J. Org. Chem.* **2002**, *67*, 6539-6541.; (e) Wang, F.; Polavarapu, P. L.; Drabowicz, J.; Mikoajczyk, M.; Lyzwa, P. *J. Org. Chem.*, **2001**, *66*, 9015-9019.

2. Becke, A. D.; *J. Chem. Phys.* **1993**, *98*, 5648.
3. Cheeseman, J. R.; Frisch, M. J.; Devlin, F. J.; Stephens, P. J. *Chem. Phys. Lett.* **1996**, *252*, 211.
4. Frisch, M. J.; Trucks, G. W.; Schlegel, H. B.; Scuseria, G. E.; Robb, M. A.; Cheeseman, J. R.; Zakrzewski, V. G.; Montgomery, Jr., J. A.; Stratmann, R. E.; Burant, J. C.; Dapprich, S.; Millam, J. M.; Daniels, A. D.; Kudin, K. N.; Strain, M. C.; Farkas, O.; Tomasi, J.; Barone, V.; Cossi, M.; Cammi, R.; Mennucci, B.; Pomelli, C.; Adamo, C.; Clifford, S.; Ochterski, J.; Petersson, G. A.; Ayala, P. Y.; Cui, Q.; Morokuma, K.; Malick, D. K.; Rabuck, A. D.; Raghavachari, K.; Foresman, J. B.; Cioslowski, J.; Ortiz, J. V.; Stefanov, B. B.; Liu, G.; Liashenko, A.; Piskorz, P.; Komaromi, I.; Gomperts, R.; Martin, R. L.; Fox, D. J.; Keith, T.; Al-Laham, M. A.; Peng, C. Y.; Nanayakkara, A.; Gonzalez, C.; Challacombe, M.; Gill, P. M. W.; Johnson, B.; Chen, W.; Wong, M. W.; Andres, J. L.; Gonzalez, C.; Head-Gordon, M.; Replogle, E. S.; Pople, J. A. *Gaussian 98/03*; Gaussian, Inc.: Pittsburgh, PA.
5. (a) Bose, P. K.; Polavarapu, P. L. *Carbonhydr. Res.* **2000**, *323*, 63-72; (b) Setnicka, V.; Urbanova, M.; Kral, V.; Volka, K. *Spectr. Acta A* **2002**, *58*, 2983-2989.
6. Polavarapu, P. L. *Mol. Phys.* **1997**, *91*, 551-554.
7. Polavarapu, P. L. *Chirality* **2002**, *14*, 768-781.
8. Polavarapu, P. L.; Petrovic, A.; Wang, F.; *Chirality* **2003**, *15*, S143-S149
9. Gawronski, J.; Gawronska, K. *Tetrahedron Letters* **1989**, *30*, 6071.
10. (a) Johnson, R. A.; Sharpless, K. B. In *Catalytic Asymmetric Synthesis*, 2nd ed.; Ojima, I., Ed.; Wiley-VCH: New York, 2000; Chapter 6A, pp 231; (b) Seebach, D.; Beck, A. K.; Heckel, A. *Angew. Chem., Int. Ed.* **2001**, *40*, 92.
11. (a) Keiderling, T. A.; Stephens, P. J.; *J. Am. Chem. Soc.* **1977**, *99*, 8061-8062; (b) Su, C. N.; Keiderling, T. A.; *J. Am. Chem. Soc.* **1980**, *102*, 511-515.
12. Polavarapu, P. L.; Ewig, C. S.; Chandramouly, T.; *J. Am. Chem. Soc.* **1980**, *102*, 511-515.
13. Hedges, A. R. *Chem. Rev.* **1998**, *98*, 2035-2044.
14. Freire, E.; Mayorga, O.L.; Straume, M. *Anal. Chem.* **1990**, *62*, 950A-959A.
15. (a) Gawronski, J.; Gawronska, K.; Rychlewska, U.; *Tetrahedron Letters* **1989**, *44*, 6071; (b) Hoffmann, M.; Rychlewski, J.; Rychlewska, U. *Computational Methods in Science and Technology* 1996, *2*, 51; (c) Gawronski, J.; Gawronska, K.; Skowronek, P.; Rychlewska, U.; Warzajtis, B.; Rychlewski, J.; Hoffmann, M.; Szarecka, A. *Tetrahedron* **1997**, *53*, 6113.
16. Rychlewska, U.; Warzajtis, B.; Hoffmann, M.; Rychlewski, J. *Molecules* **1997**, *2*, 106.

17. Buffeteau, T.; Ducasse, L.; Brizard, A.; Huc, I.; Oda, R. *J. Phys. Chem. A* **2004**, *108*, 4080-4086.
18. (a) Polavarapu, P. L.; Petrovic A. G.; Zhang P. Accepted by *Chirality*; (b). Polavarapu, P. L. *Chirality* **2006**, *18*, 348-356. (c) Polavarapu, P. L.; Zhao, X. *J. Am. Chem. Soc.* **1999**, *121*, 246-247.
19. (a). Kaczor, A. J.; Proniewicz, L. M. *Molecular Structure* **2003**, *640*, 133-41; (b). Kaczor, A. J.; Proniewicz, L. M. *Molecular Structure* **2004**, *704*, 189-96.
- 20 Andini, S.; Castronuovo, G.; Elia, V.; Gallotta, E. *Carbonhydr. Res.* **1991**, *217*: 87-97.
21. (a) Cooper, A. *Curr. Opin. Chem. Biol.* **1999**, *3*, 557-563. (b) Haq, I. Ladbury, J. E. *J. Mol. Recognit.* **2000**, *13*, 188-197. (c) Leavitt, S.; Freire, E. *Curr. Opin. Struct. Biol.* **2001**, *11*, 560-566. (d) Weber, P. C.; Salemme, F. R. *Curr. Opin. Struct. Biol.* **2003**, *13*, 115-121.
22. Rekharsky, M. V.; Inoue, Y. *Chem. Rev.* **1998**, *98*, 1875-1917.
23. (a) Izatt, R. M.; Terry, R. E.; Haymore, B. L.; Hansen, L. D.; Dalley, N. K.; Avondet, A. G.; Christensen, J. J. *J. Am. Chem. Soc.* **1976**, *98*, 7620-7630. (b) Ozutsumi, K.; Ishiguro, S.-I. *Bull. Chem. Soc. Jpn.* **1992**, *65*, 1173-1175.
24. Jones, C.; Mulloy, B.; Thomas A. H. *Methods in molecular biology*, vol.22; Humana Press Inc.: Totowa, NJ, 2000; Chapter 11, pp 137.



## CHAPTER V

### VIBRATIONAL CIRCULAR DICHROISM OF MATRIX ASSISTED AMINO ACID FILMS IN THE MID-INFRARED REGION

#### Introduction

Vibrational Circular Dichroism (VCD) is the measurement of differential absorbance of left and right circularly polarized light in the infrared region resulting from molecular vibrational transitions.<sup>1</sup> In recent years, VCD is being used extensively for determining the absolute configuration and predominant conformations of chiral molecules.<sup>2</sup> Furthermore, VCD has also been used successfully in the conformational analysis of biological molecules, such as proteins, peptides, nucleic acids, and even viruses.<sup>3</sup>

The conformations of amino acids in aqueous solutions are of considerable interest owing to the role that these molecules play in the determination of structure and function of peptides and proteins. Nafie and coworkers<sup>4</sup> have reported VCD spectra in the C-H stretching region (3100-2800  $\text{cm}^{-1}$ ) for several amino acids in  $\text{D}_2\text{O}$ . But in the mid infrared region (2000-900  $\text{cm}^{-1}$ ), VCD spectra were reported for only two amino acids in aqueous solution. VCD spectra of L-alanine were reported<sup>5</sup> by Diem in  $\text{D}_2\text{O}$  in the 1700-1500  $\text{cm}^{-1}$ , 1500-1250  $\text{cm}^{-1}$  and 1150-900  $\text{cm}^{-1}$  regions; VCD spectra of L-alanine were also measured<sup>5</sup> by Diem in  $\text{H}_2\text{O}$  in the 1500-1250  $\text{cm}^{-1}$  and 1250-1000  $\text{cm}^{-1}$  regions. Nafie and coworkers reported<sup>4c</sup> the VCD spectra of L-alanine in the methine bending region (1400-1250  $\text{cm}^{-1}$ ) both in  $\text{D}_2\text{O}$  and  $\text{H}_2\text{O}$ . They have also measured<sup>4c</sup> the VCD spectra of L-proline in  $\text{D}_2\text{O}$  in the 1400-1250  $\text{cm}^{-1}$  region. Although the strong absorption of  $\text{H}_2\text{O}$  in the C-H stretching and C=O stretching regions is avoided by substituting  $\text{D}_2\text{O}$

for H<sub>2</sub>O, Diem found<sup>5</sup> that in D<sub>2</sub>O, the frequencies and VCD intensities can be significantly altered because of the exchange of N-H protons with deuterium.

Nafie and coworkers adapted<sup>4a</sup> the mull sampling technique in halocarbon oil and reported the VCD spectra in the 3600-1900 cm<sup>-1</sup> region for alanine and serine. They have also reported<sup>4d</sup> the VCD spectra for solid state samples in the mid-infrared region. However, a direct correlation between the solid- and solution-phase VCD data was not observed because of significant perturbations for crystalline samples.

VCD measurements in the mid-infrared region for simple amino acids in aqueous solution are difficult to undertake because of two reasons. First, interfering water absorption requires the use of high concentrations and low pathlengths; second, the solubilities of most simple amino acids in water at neutral pH are not sufficient enough for undertaking VCD measurements in solution. The interfering water absorption can be avoided if the measurements can be undertaken on films prepared from aqueous solutions. Film technique was successfully used in our laboratory to measure the VCD spectra of peptides<sup>6</sup>, proteins<sup>7</sup>, carbohydrates<sup>8a</sup>, nucleic acids<sup>8b</sup> and viruses<sup>3e</sup>. VCD spectra of these peptide, protein, carbohydrate and nucleic acid films compared well with the corresponding spectra measured for aqueous solutions. Also, VCD spectra of films were found to have better signal to noise ratio than those of corresponding aqueous solutions.

However, when aqueous solutions of amino acids are dried to make films, amino acids tend to form microcrystalline deposits which are not suitable for artifact free VCD measurements. For such cases, investigations in our laboratory revealed that the matrix assisted film formation<sup>9,8b</sup> can avoid crystalline deposits. Since different samples work better with different matrices, it is necessary to investigate and find a suitable matrix for

the samples of interest. For amino acid films we found that  $\alpha$ -cyclodextrin ( $\alpha$ -CD) serves as a suitable matrix. Even though  $\alpha$ -CD provides a chiral environment, the interaction between  $\alpha$ -CD and amino acids is weak<sup>10</sup> and therefore the VCD spectra of parent amino acids are unlikely to be perturbed. Furthermore,  $\alpha$ -CD is water-soluble, chemically stable and does not have strong interfering absorption bands in the region of 2000-1200  $\text{cm}^{-1}$ . Utilizing these advantages, we report here VCD measurements for matrix assisted amino acid films, with  $\alpha$ -CD serving as the matrix to facilitate the film formation. Wherever possible, VCD spectra for aqueous solutions were also measured and compared to the film state measurements. For those amino acids whose VCD spectra could not be measured in solution, the absorption spectra of films and solutions are compared. Advantages and limitations of the film method are also discussed.

### Experimental

The samples of L-alanine, L-proline, L-methionine, DL-methionine, and L-valine were obtained from Mann Research Lab. L-tyrosine and DL-valine were obtained from Nutritional Biochemical Corp. Racemic alanine was obtained from Sigma. The remaining amino acids and  $\alpha$ -cyclodextrin were obtained from Acros Chemicals. These samples were used as received. The amino acids studied, their solubilities<sup>11</sup> and concentrations used in the present measurements are listed in Table 5-1.

All VCD spectra were recorded on a commercial ChiralIr spectrometer (Bomem-Biotoools, Canada) modified as described previously<sup>6-9</sup> to minimize the artifacts using the double polarization modulation method<sup>12</sup>. All VCD spectra were recorded at 4  $\text{cm}^{-1}$

resolution. The data collection time was 3 hr, except for the solution state VCD spectra of methionine, histidine, and valine where 6 hr data collection time was used.

For the absorption and VCD measurements on films, stock solutions containing amino acid and  $\alpha$ -CD with molar ratio of 1:1 or 2:1 were prepared. The concentration of  $\alpha$ -CD in these stock solutions is between 9.7 mg/mL (0.010 M) and 48.5 mg/mL (0.050 M). The concentration of amino acids in these stock solutions is between 1.6 mg/mL and 11.5 mg/mL (see Table 5-1). For stock solution containing tyrosine (L or racemic) and  $\alpha$ -CD, the concentration of  $\alpha$ -CD is about 0.01M but the concentration of tyrosine is much less than 0.01M because of low solubility of tyrosine in water at neutral pH. A portion, usually in the range of 100-660  $\mu$ L, of stock solution (containing the desired amino acid and  $\alpha$ -CD) was cast onto a 2.5 cm diameter BaF<sub>2</sub> window. Evaporation was continued at room temperature in a fume hood until dry films were formed. VCD spectra were measured for these dried films. The absorption spectrum of  $\alpha$ -CD film was subtracted from those of the films containing amino acid and  $\alpha$ -CD. The VCD spectra of films containing racemic amino acid +  $\alpha$ -CD were subtracted from the corresponding spectra of films containing L-amino acid and  $\alpha$ -CD. In the case of alanine, however, the VCD spectra were also obtained for D-alanine +  $\alpha$ -CD. By subtracting the VCD spectrum of racemic alanine +  $\alpha$ -CD from the individual VCD spectra of L-alanine +  $\alpha$ -CD and D-alanine +  $\alpha$ -CD, the required mirror image features for L-alanine and D-alanine have been verified. For the amino acids investigated here, the film VCD measurements were repeated with different levels of absorbance (by varying the solution amount deposited) and the VCD features were reproduced in these measurements except for the films of L-valine +  $\alpha$ -CD.

For the solution state absorption and VCD measurements, spectra were measured for water solutions, using either a demountable cell with  $\sim 6$  (or  $\sim 15$ )  $\mu\text{m}$  spacer or a variable pathlength cell set to give a minimum of  $\sim 6$   $\mu\text{m}$  pathlength. Both cells used  $\text{BaF}_2$  windows. The concentrations of solutions and the solution volumes used are summarized in Table 5-1. The absorption spectra of  $\text{H}_2\text{O}$  solvent were subtracted from the corresponding spectra of amino acid solutions. The presented VCD spectra in  $\text{H}_2\text{O}$  solution are the raw spectra as obtained, except for L-proline in the  $1800\text{-}1550\text{ cm}^{-1}$  region where VCD of racemic proline was subtracted.

Table 5-1. Amino acids, their solubilities, concentrations and volumes of stock solutions used for solution and film VCD studies

amino acid	Solubility <sup>a</sup> (g/100g, H <sub>2</sub> O, 25°C)	Concentration and volume used for solution VCD studies <sup>b</sup>			Concentration and volume used for film VCD studies		
		Concentration		Volume ( $\mu$ L)	Concentration		Volume ( $\mu$ L)
		mg/mL	mol/L		mg/mL	mol/L	
Alanine <sup>c</sup>	16.65	151	1.7	600	1.6	0.018	400
Proline	162.30	230	2.0	25	2.9	0.025	200
		115	1.0	600	11.5	0.10	200
Valine <sup>c</sup>	8.85	84	0.71	25	2.1	0.018	330
Methionine <sup>c</sup>	3.38	30	0.20	25	2.0	0.014	400
							660
Histidine <sup>c</sup>	4.19	40	0.26	25	1.9	0.012	200
					3.8	0.024	200
Phenylalanine <sup>c</sup>	2.96	28	0.17	25	4.0	0.024	100
							200
Tryptophan <sup>c</sup>	1.14	11	0.05	25	3.8	0.019	160
							420
Tyrosine <sup>d</sup>	0.04	saturated	saturated	25	saturated	saturated	540

<sup>a</sup> Solubility data was obtained from reference 11; <sup>b</sup> variable pathlength cell with  $\sim 6 \mu\text{m}$  pathlength whenever 600  $\mu\text{L}$  volume was used; demountable cell with  $\sim 6$  or 15  $\mu\text{m}$  spacer in other cases; <sup>c</sup> nearly saturated solutions were used for solution state VCD measurement; <sup>d</sup> Saturated solutions (after filtration) were used for both solution and film state measurements.

## Results and discussion

For  $\alpha$ -CD film (Figure 5-1), its characteristic absorption originating from C-O/C-C stretching modes appear in the 1200-900  $\text{cm}^{-1}$  region. Three major absorption bands at 1152  $\text{cm}^{-1}$ , 1078  $\text{cm}^{-1}$  and 1034  $\text{cm}^{-1}$  can be noted for  $\alpha$ -CD in this region. For films of L-proline +  $\alpha$ -CD, the absorption spectra (Figure 5-1) in the 1200-900  $\text{cm}^{-1}$  region are similar to the corresponding spectra of  $\alpha$ -CD film. This observation indicates that the absorption signals originating from proline in the 1200-900  $\text{cm}^{-1}$  region are very weak and also that L-proline has very weak interaction with  $\alpha$ -CD in the film state. These observations, illustrated in Figure 5-1 for proline as an example, also apply for other simple amino acids studied here, except valine. The absorption spectra of L-proline +  $\alpha$ -CD film are also compared to those of racemic proline +  $\alpha$ -CD film in Figure 5-1. The absorption spectra of racemic amino acid +  $\alpha$ -CD films are quite similar to the corresponding spectra of L-amino acid +  $\alpha$ -CD films. For the reasons mentioned above, the absorption spectra of  $\alpha$ -CD films were subtracted from those of amino acid +  $\alpha$ -CD films to obtain the absorption spectra of amino acids in the film state (see Figure 5-1).

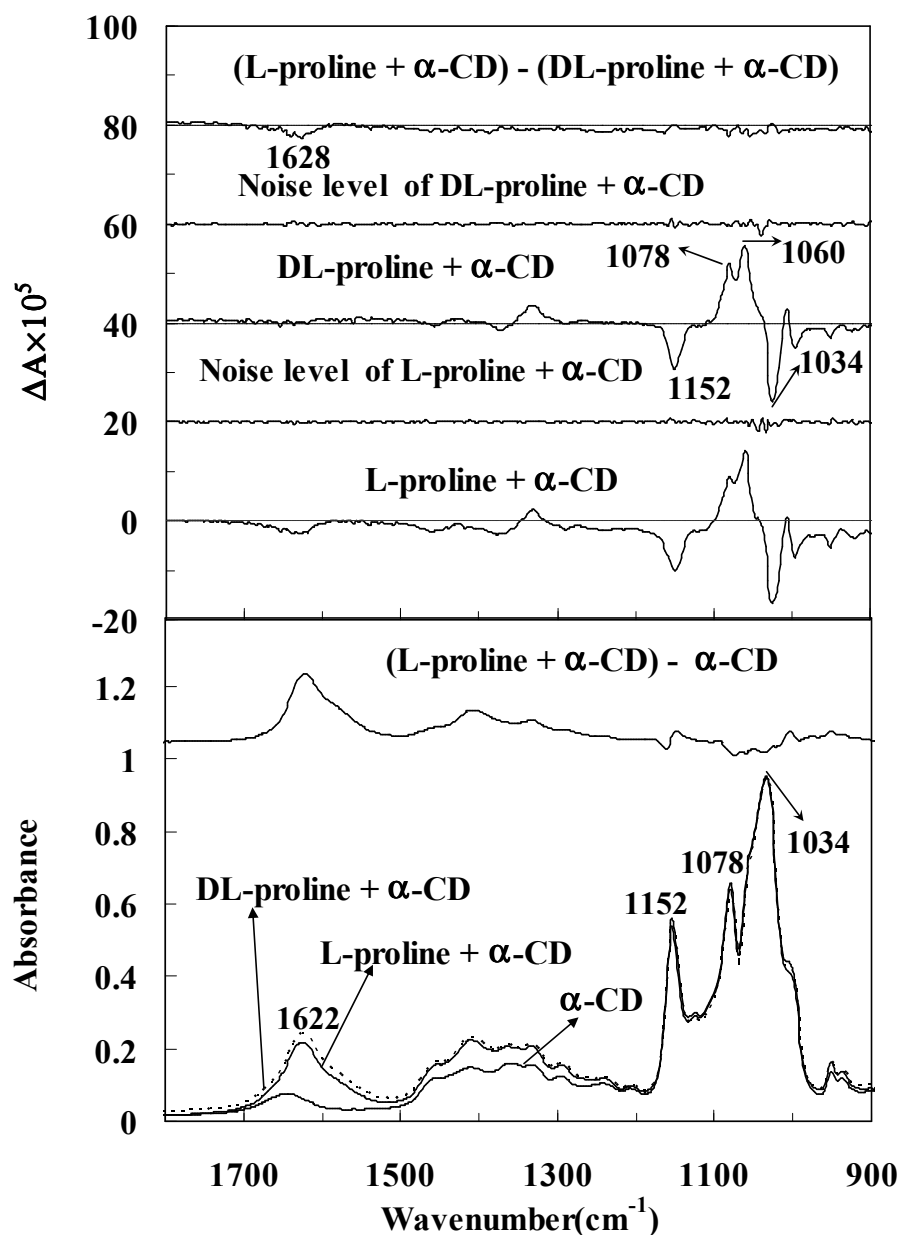


Figure 5-1. Absorption and VCD spectra of L-proline at lower absorption.  $\alpha$ -CD film was prepared from 200  $\mu\text{L}$  solution of  $\alpha$ -CD (0.025M) in  $\text{H}_2\text{O}$ ; DL-proline +  $\alpha$ -CD film was prepared from 200  $\mu\text{L}$  solution of DL-proline +  $\alpha$ -CD (molar ratio: 1:1, 0.025M for  $\alpha$ -CD) in  $\text{H}_2\text{O}$ ; L-proline +  $\alpha$ -CD film was prepared from 200  $\mu\text{L}$  solution of L-proline +  $\alpha$ -CD (molar ratio: 1:1, 0.025M for  $\alpha$ -CD) in  $\text{H}_2\text{O}$ .



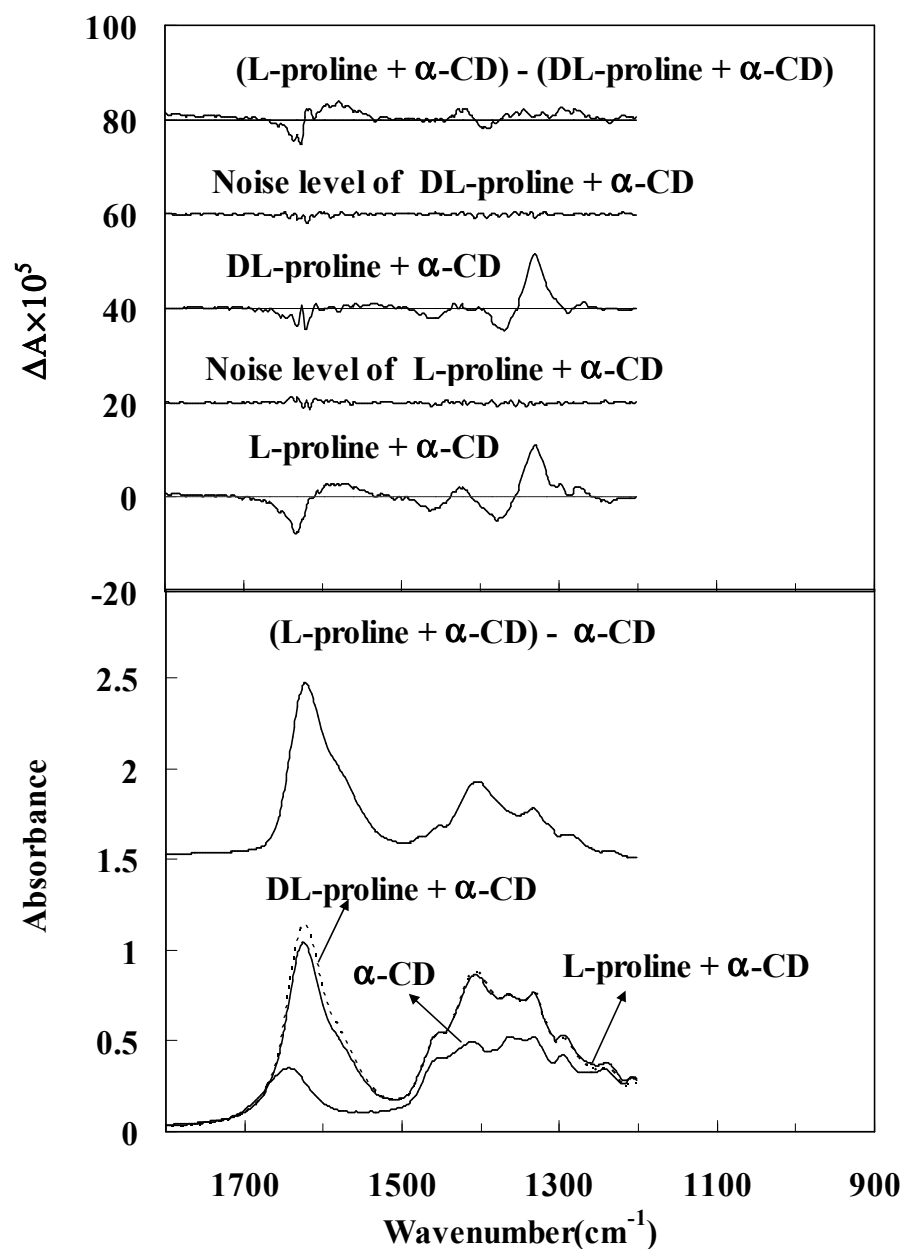


Figure 5-2. Absorption and VCD spectra of L-proline at higher absorption.  $\alpha$ -CD film was prepared from 200  $\mu$ L solution of  $\alpha$ -CD (0.050M) in H<sub>2</sub>O; DL-proline +  $\alpha$ -CD film was prepared from 200  $\mu$ L solution of DL-proline +  $\alpha$ -CD (molar ratio: 2:1, 0.050M for  $\alpha$ -CD) in H<sub>2</sub>O; L-proline +  $\alpha$ -CD film was prepared from 200  $\mu$ L solution of L-proline +  $\alpha$ -CD (molar ratio: 2:1, 0.050M for  $\alpha$ -CD) in H<sub>2</sub>O.

From the comparison between the VCD spectra of racemic amino acid +  $\alpha$ -CD films and L-amino acid +  $\alpha$ -CD films, it is seen that the position, sign and intensities of VCD bands of  $\alpha$ -CD in the region of 1200-900  $\text{cm}^{-1}$  remain essentially unchanged (see Figure 5-1 as an example). The VCD spectra of racemic amino acid +  $\alpha$ -CD films were subtracted from those of L-amino acid +  $\alpha$ -CD films to obtain the VCD spectra of L-amino acids in the film state. Racemic amino acids are not expected to yield any VCD signals, and accordingly racemic amino acid +  $\alpha$ -CD films give the same VCD patterns as  $\alpha$ -CD films. The VCD spectra of racemic amino acid +  $\alpha$ -CD films match better (than  $\alpha$ -CD films) in the baseline with the corresponding VCD spectra of L-amino acid +  $\alpha$ -CD films. For this reason, VCD spectra of the racemic amino acid +  $\alpha$ -CD films, instead of those of  $\alpha$ -CD films, were chosen in the subtraction process to obtain the VCD spectra of L-amino acids. When available, VCD spectra of D-amino acid +  $\alpha$ -CD films are better choices to subtract from the spectra of L-amino acid +  $\alpha$ -CD films because this process can double the magnitude of the intensities of VCD bands, thereby yielding better signal to noise ratio. But D-amino acids are generally more expensive than racemic amino acids. In the present study, VCD spectra of D-amino acid +  $\alpha$ -CD films are also measured only in the case of alanine (*vide infra*).

A negative VCD band at 1628  $\text{cm}^{-1}$ , associated with the absorption band at 1622  $\text{cm}^{-1}$ , is present for L-proline in the subtracted spectrum (Figure 5-1). However, no VCD bands are seen in the 1550-1200  $\text{cm}^{-1}$  region because of low absorption of L-proline in this region. To investigate the VCD signals of L-proline in the 1550-1200  $\text{cm}^{-1}$  region, the stock solutions of higher concentration and higher molar ratio for L-proline and  $\alpha$ -CD have been prepared to obtain the films. Spectra for the films of higher absorbance are

shown in Figure 5-2. Since the absorbance of bands in the 1200-900  $\text{cm}^{-1}$  region for films in Figure 5-2 is above 1.5, and therefore the corresponding VCD bands are not reliable in this region, the spectra in Figure 5-2 are presented only in the 1800-1200  $\text{cm}^{-1}$  region. VCD bands in the 1550-1200  $\text{cm}^{-1}$  region can now be seen in the subtracted spectra. Also a negative-positive doublet (Figure 5-2) in the 1650-1550  $\text{cm}^{-1}$  region is clearly seen in the subtracted VCD spectrum for L-proline. All these VCD signals are also seen in the solution spectrum (vide infra).

For alanine, the film measurements were undertaken for both of the enantiomers as well as the racemic mixture (Figure 5-3). As before, the absorption spectra were obtained by subtracting the absorption spectrum of  $\alpha$ -CD from those of alanine +  $\alpha$ -CD. The absorption spectra obtained in this manner for both enantiomers and racemic mixture of alanine are identical except for a small difference in the intensity of the band at 1610  $\text{cm}^{-1}$ . The VCD spectra of enantiomers of alanine were obtained by subtracting the VCD spectrum of racemic alanine +  $\alpha$ -CD from that of individual enantiomer +  $\alpha$ -CD. VCD spectra obtained in this manner displayed excellent mirror image features (Figure 5-3) for L- and D-alanine, which supports our hypothesis that interactions of amino acids with  $\alpha$ -CD are weak enough for not perturbing the VCD of native amino acids. VCD spectrum of L-alanine was also obtained (Figure 5-3) as one-half of the difference between the raw VCD spectra of L-alanine +  $\alpha$ -CD and D-alanine +  $\alpha$ -CD, which provided better signal to noise ratio as expected.

Eight amino acids of different solubilities in water (Table 5-1) were chosen for the present study. Among the amino acids studied, L-alanine and L-proline have high enough solubility in  $\text{H}_2\text{O}$  to obtain the VCD spectra in solution state in the 1800-1200  $\text{cm}^{-1}$

region (Figure 5-3). For the remaining amino acids, which have low solubility in water, very low absorption intensities (less than 0.10) in the 1550-1200  $\text{cm}^{-1}$  region are obtained for saturated or nearly saturated solutions. As a result, very weak VCD bands are found for L-methionine, L-histidine and L-valine and no VCD bands are seen for L-phenylalanine, and L-tryptophan in the solution measurement. For L-tyrosine, even the absorption spectra could not be obtained in the solution state because of extremely low solubility. For four amino acids, L-alanine, L-proline, L-methionine and L-histidine, whose VCD spectra could be measured in solution, the absorption and VCD spectra in the film state are compared with their corresponding spectra in the solution state (Figures 5-3~5-4). For L-phenylalanine and L-tryptophan, whose VCD spectra could not be obtained in solution, the absorption spectra of films are compared to those of corresponding solutions (Figure 5-5).

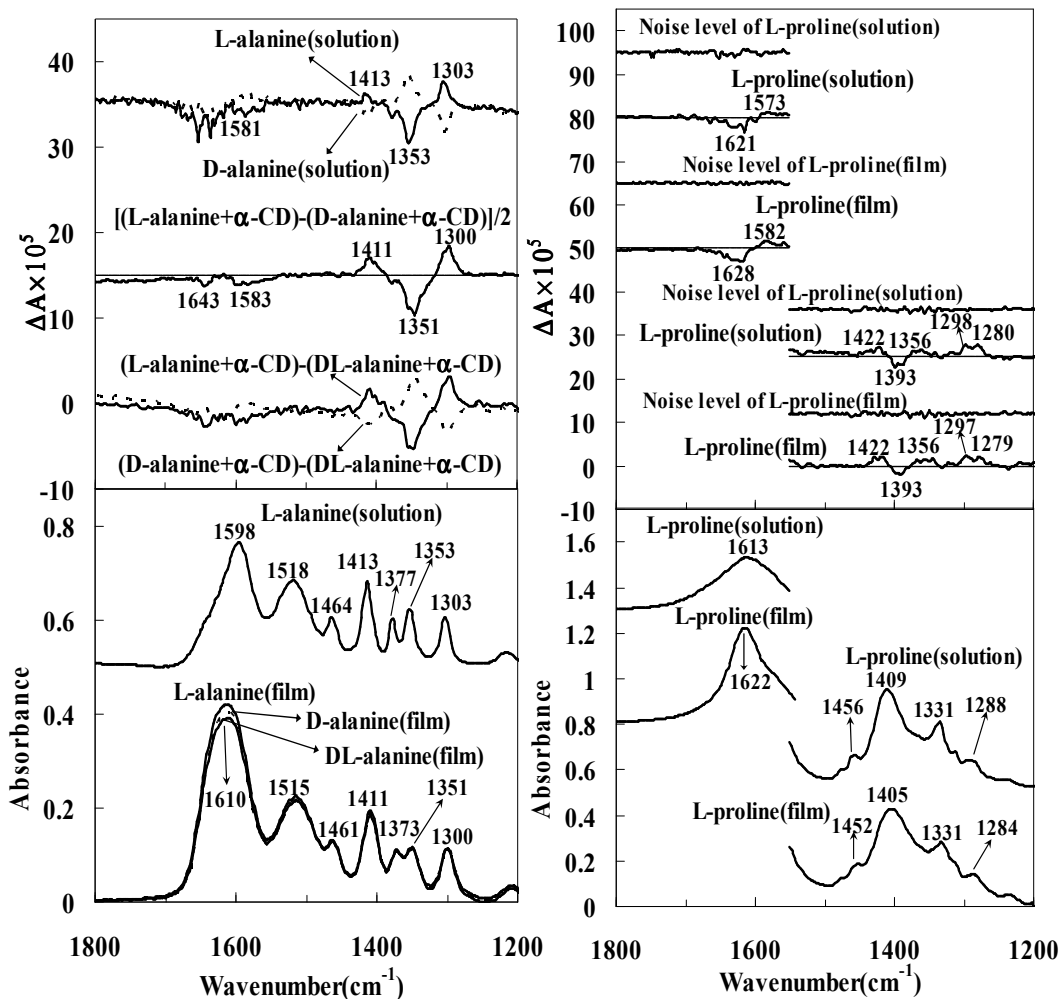


Figure 5-3. Absorption and VCD spectra of films and of aqueous solutions (Left panel: alanine; right panel: proline). Films of L-alanine, D-alanine and DL-alanine were obtained respectively from their corresponding 400  $\mu\text{L}$  solutions of alanine +  $\alpha\text{-CD}$  (molar ratio: 1:1, 0.018M) in  $\text{H}_2\text{O}$ . Films of proline for investigating the 1550-1200  $\text{cm}^{-1}$  region are same as those described in Figure 2; for investigating the 1800-1550  $\text{cm}^{-1}$  region, films of proline were obtained from 1:1 molar ratio mixture of proline: $\alpha\text{-CD}$ . Solution spectra of L-alanine were obtained with saturated solutions using a variable pathlength cell ( $\sim 6 \mu\text{m}$  pathlength). Solution spectra of proline in the 1800-1550  $\text{cm}^{-1}$  region were obtained at 1.0 M using a variable pathlength cell ( $\sim 6 \mu\text{m}$  pathlength), and those in the 1550-1200  $\text{cm}^{-1}$  region were obtained at 2.0 M using a demountable cell ( $\sim 6 \mu\text{m}$  path length). For alanine, expected mirror image VCD features for the enantiomers are shown in both film and solution states.

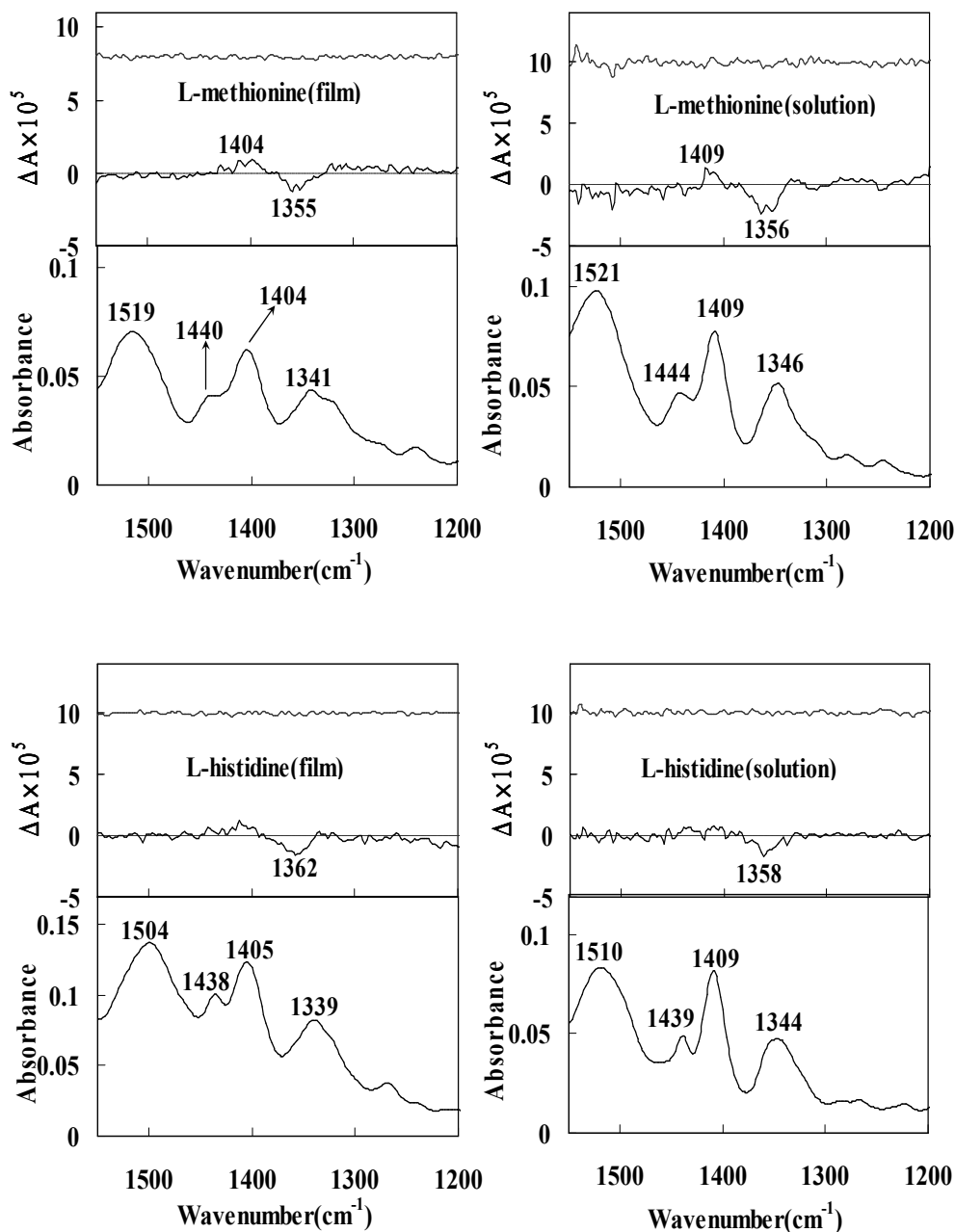


Figure 5-4. Absorption and VCD spectra of films (left panels) and of aqueous solutions (right panels) for L-methionine and L-histidine. The topmost traces represent the noise levels in the corresponding VCD spectra. Film of L-methionine was obtained from 400 $\mu$ L solution of L-methionine +  $\alpha$ -CD (0.014M) in H<sub>2</sub>O. Film of L-histidine was obtained from 200  $\mu$ L solution of L-histidine +  $\alpha$ -CD (0.012M) in H<sub>2</sub>O. Solution spectra of L-methionine and L-histidine were obtained respectively at 0.20M and 0.26M using a 15  $\mu$ m path length demountable cell. Solution VCD spectra were obtained with 6 hr data collection time.

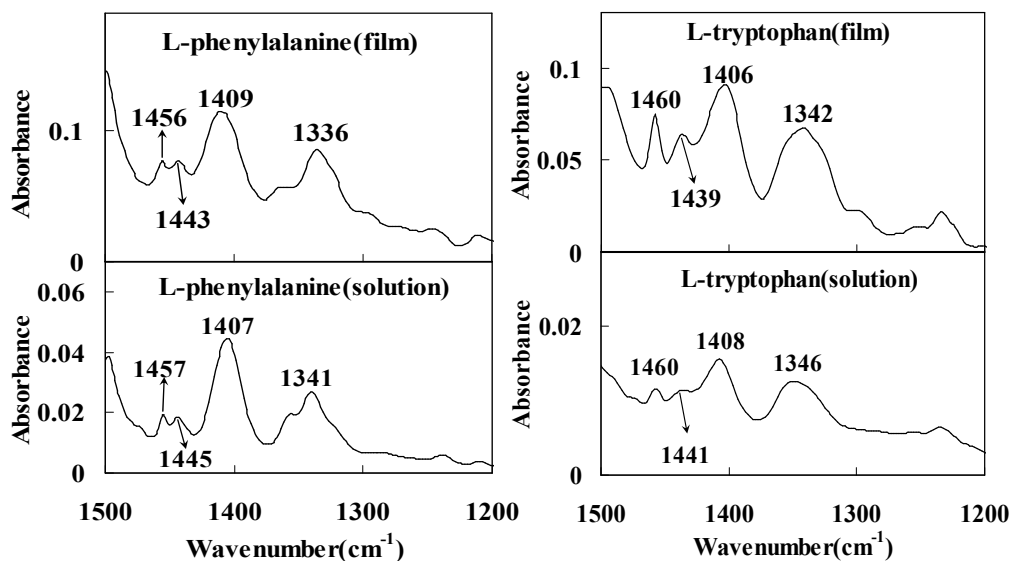


Figure 5-5 Absorption spectra of films (top) and of aqueous solutions (bottom) for L-phenylalanine and L-tryptophan. 100  $\mu\text{L}$  solution of L-phenylalanine +  $\alpha\text{-CD}$  (0.024M) and 160  $\mu\text{L}$  solution of L-tryptophan +  $\alpha\text{-CD}$  (0.019M) in  $\text{H}_2\text{O}$  were used respectively to make the films. The solution spectra of these two amino acids were obtained from nearly saturated solutions (Table 1) using a demountable cell with  $\sim 15 \mu\text{m}$  path length.

The 1800-1200  $\text{cm}^{-1}$  region (Figure 5-3) is the common region accessible to both film and solution samples of L-alanine and L-proline, while the 1550-1200  $\text{cm}^{-1}$  region (Figure 5-4) is the common region accessible to both film and solution samples of L-methionine and L-histidine. For L-alanine, L-proline, L-methionine and L-histidine in the film state, films were prepared to give comparable absorption intensity with that in solution measurement. For each of these four amino acids, whose VCD could be measured in both film and solution states, the VCD patterns observed for solutions match with those observed for films (see Figures 5-3~5-4). These VCD patterns for L-alanine (Figure 5-3) in the solution state include two weak negative bands, at  $\sim 1640$  and  $1581 \text{ cm}^{-1}$  in the  $1650\text{-}1500 \text{ cm}^{-1}$  region and a positive-negative-positive pattern at  $1413$ ,  $1353$ , and  $1303 \text{ cm}^{-1}$  in the  $1450\text{-}1250 \text{ cm}^{-1}$  region. The corresponding VCD patterns for L-

alanine (Figure 5-3) in the film state include two weak negative bands, at  $\sim 1643$  and  $1583\text{ cm}^{-1}$  in the  $1650\text{-}1500\text{ cm}^{-1}$  region and a positive-negative-positive pattern at  $1411$ ,  $1351$ , and  $1300\text{ cm}^{-1}$  in the  $1450\text{-}1250\text{ cm}^{-1}$  region. Note that the negative VCD band at  $\sim 1640\text{ cm}^{-1}$  for L-alanine in solution is dominated by noise coming from interference of water absorption. For L-proline (Figure 5-3) in the solution state, the observed VCD bands include a negative-positive doublet at  $1621$  and  $1573\text{ cm}^{-1}$  in the  $1650\text{-}1500\text{ cm}^{-1}$  region and a positive-negative-positive triplet at  $1422$ ,  $1393$  and  $1356\text{ cm}^{-1}$  in the  $1450\text{-}1300\text{ cm}^{-1}$  region and two positive bands at  $1298$  and  $1280\text{ cm}^{-1}$  in the  $1300\text{-}1250\text{ cm}^{-1}$  region. The corresponding bands observed for L-proline (Figure 5-3) in the film state include a negative-positive doublet at  $1628$  and  $1582\text{ cm}^{-1}$  in the  $1650\text{-}1500\text{ cm}^{-1}$  region and a positive-negative-positive triplet at  $1422$ ,  $1393$  and  $1356\text{ cm}^{-1}$  in the  $1450\text{-}1300\text{ cm}^{-1}$  region and two positive bands at  $1297$  and  $1279\text{ cm}^{-1}$  in the  $1300\text{-}1250\text{ cm}^{-1}$  region. For L-methionine (Figure 5-4) in the solution state, a positive-negative VCD doublet at  $1409$  and  $1356\text{ cm}^{-1}$  is seen in the  $1450\text{-}1300\text{ cm}^{-1}$  region, with corresponding bands in the film state seen at  $1404$  and  $1355\text{ cm}^{-1}$ . For L-histidine (Figure 5-4) in the solution state a negative band at  $1358\text{ cm}^{-1}$  is seen in the  $1400\text{-}1300\text{ cm}^{-1}$  region with the corresponding band in the film state at  $1362\text{ cm}^{-1}$ . There is a small frequency shift (of  $2\text{-}12\text{ cm}^{-1}$  to lower frequency) for band positions in the spectra of solutions compared to those in the spectra of films. Overall only minor differences are found in the comparison of spectra for solution and film samples of these amino acids. Thus the interactions between amino acids and  $\alpha$ -CD in the film state are not considered significant enough to perturb the native VCD of amino acids.



For the case of L-valine, a positive VCD band at  $1416\text{ cm}^{-1}$  and a negative VCD band at  $1356\text{ cm}^{-1}$  in the  $\sim 1450\text{-}1300\text{ cm}^{-1}$  region are found in the solution measurement (not shown). However, the films L-valine formed with  $\alpha$ -CD are cloudy and artifacts were found in the film VCD spectra. So a comparison could not be made between solution and film spectra for L-valine. For L-tyrosine, both absorption and VCD spectra could not be obtained in the solution state because of extremely low solubility. Also, VCD spectrum could not be obtained for L-tyrosine in the film state, although it was possible to obtain its absorption spectrum (not shown) with low intensity.

The absorption and VCD spectra in the  $1800\text{-}1200\text{ cm}^{-1}$  region for L-methionine, L-histidine, L-phenylalanine and L-tryptophan films at higher absorption intensities than those shown in Figures 5-4~5-5 are shown in Figure 5-6. Here higher absorption intensity was obtained by depositing a larger volume of the stock solution, or using a higher concentration solution, during the preparation of films. We have also considered the pH dependence as a means to improve the solubility of tyrosine, but found<sup>14</sup> that its solubility remains essentially the same in the pH range of 3-11. In the  $1800\text{-}1550\text{ cm}^{-1}$  region, two negative VCD bands for L-tryptophan (Figure 5-6) at  $1635$  and  $1592\text{ cm}^{-1}$ , and a positive-negative VCD couplet for L-phenylalanine at  $1627$  and  $1587\text{ cm}^{-1}$  (Figure 6) are found. No VCD bands are seen in the  $1800\text{-}1550\text{ cm}^{-1}$  region for L-methionine and L-histidine. The vibrations responsible for the amino acids in the  $1800\text{-}1550\text{ cm}^{-1}$  region are the stretching motions of  $\text{-COO}^-$ . The weak VCD intensities of amino acids in this region indicate that the rotational strengths of stretching modes of  $\text{-COO}^-$  in amino acids are small. In the  $1500\text{-}1200\text{ cm}^{-1}$  region, both L-phenylalanine and L-tryptophan show one negative VCD band each at  $1336$  and  $1342\text{ cm}^{-1}$  respectively. A positive VCD band at

1328  $\text{cm}^{-1}$  for L-methionine, and at 1405  $\text{cm}^{-1}$  for L-histidine, which were not as clearly seen in the low absorption measurements (Figure 4), are clearly seen in the higher absorption measurements (Figure 5-6). All of the VCD bands observed for amino acid films are summarized in Table 5-2.

The amount of amino acid sample used in the present measurements for obtaining sufficient absorption (for VCD measurements) in the film spectra is lower than that used for obtaining the solution-based spectra. For example, to obtain the same level of absorbance in solution and film studies for L-alanine, 600  $\mu\text{L}$  solution at a concentration of saturated ( $\sim 151\text{ mg/mL}$ ) solution was used for the solution measurement (which amounts to 90.6 mg sample) with a variable pathlength cell, while 400  $\mu\text{L}$  solution at a concentration of 1.6 mg/mL was used for the film measurement (which amounts to 0.6 mg sample). In the case of L-proline, 600  $\mu\text{L}$  solution at a concentration of 115 mg/mL was used for the solution measurement (which amounts to 69 mg sample) with a variable pathlength cell, while 200  $\mu\text{L}$  solution at a concentration of 11.5 mg/mL was used for the film measurement (which amounts to 2.3 mg sample). However, a significant portion of the 600  $\mu\text{L}$  volume used for solution measurements with variable pathlength cell is wasted in dead volume (those parts of the cell that light does not probe). With special etched cells<sup>13</sup>, the sample volume requirement can be lowered to about 5  $\mu\text{L}$  and in such instances the amounts of sample needed for film and solution measurements become comparable.

Table 5-2. VCD bands of amino acid films in the 1800-1200  $\text{cm}^{-1}$  region

amino acid	band position <sup>a</sup>	$\Delta A/A$ <sup>b</sup>
L-Alanine	1643	-0.9
	1583	-0.6
	1411	+1.4
	1351	-1.7
	1300	+3.0
L-Proline	1628	-0.6
	1582	+0.9
	1422	+0.8
	1393	-0.4
	1356	+0.7
	1297	+1.7
	1279	+1.7
L-methionine	1404	+1.2
	1355	-1.3
	1328	+1.6
L-histidine	1405	+1.0
	1362	-1.7
L-phenylalanine	1627	+0.4
	1587	-0.6
	1336	-1.6
L-tryptophan	1635	-0.5
	1592	-0.5
	1342	-2.9

<sup>a</sup> Frequencies in  $\text{cm}^{-1}$ . <sup>b</sup> The numbers listed under  $\Delta A/A$  are to be multiplied by  $10^{-4}$ .

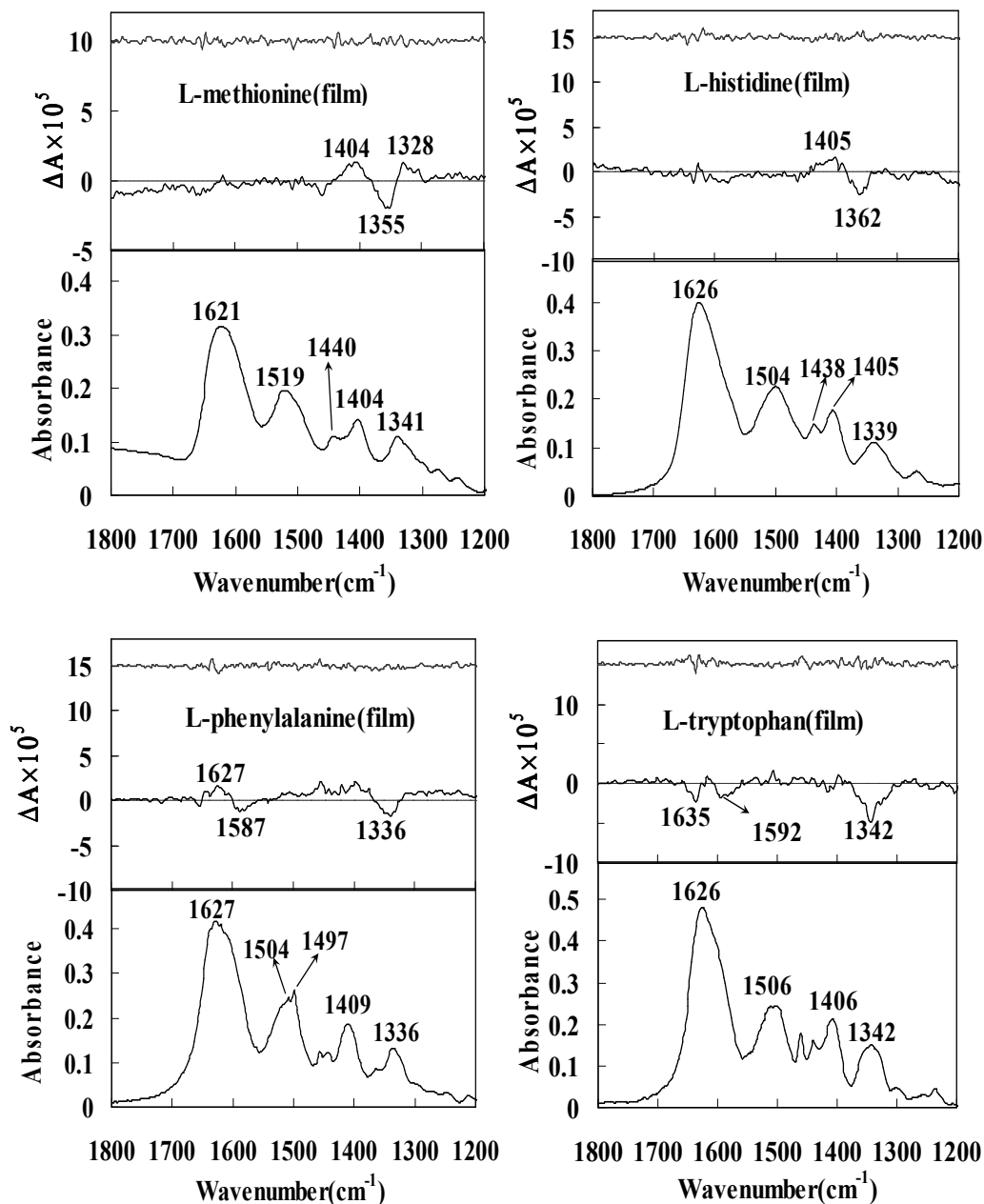


Figure 5-6. Absorption (bottom) and VCD (top) spectra of L-methionine, L-histidine L-phenylalanine and L-tryptophan in the film state. The topmost traces represent the noise levels in the VCD spectra. Films were prepared from their corresponding stock solutions of L-amino acid +  $\alpha$ -CD. The spectra for methionine and histidine were obtained at higher absorbances than those in Figure 4. 660  $\mu$ L solution of L-methionine +  $\alpha$ -CD (molar ratio: 1:1, 0.014M), 200  $\mu$ L solution of L-histidine +  $\alpha$ -CD (molar ratio: 1:1, 0.024M), 200  $\mu$ L solution of L-phenylalanine +  $\alpha$ -CD (molar ratio: 1:1, 0.024M) and 420  $\mu$ L solution of L-tryptophan +  $\alpha$ -CD (molar ratio: 1:1, 0.019M) in  $H_2O$  were used respectively to obtain the VCD spectra of these amino acids in the film state.

The matrix assisted film method, with  $\alpha$ -CD as the matrix, improves greatly the role of VCD technique in the chiral analysis of amino acid samples. The film method presented here provides practical convenience for VCD measurements, and also avoids the absorption interference in the 1800- 1550  $\text{cm}^{-1}$  region from water solvent. Film method is advantageous for obtaining the VCD spectra for amino acids, even with low solubility in water. The film method for VCD measurement can be applied in the field of environmental analysis, such as detection and analysis of samples containing low level of amino acids. This film method also offers a means to obtain the VCD spectra of other types of compounds, such as pharmaceuticals which have limited solubility in water, or are only available in very limited amounts. To make a successful VCD measurement with the matrix assisted film method, target molecules should have either no, or only weak, interaction with the matrix and should form a uniform amorphous film. Another limitation with the matrix assisted film method is that the strong absorption bands of matrix can limit the useful region for measuring the VCD spectra of target molecules.

### **Conclusion**

Matrix assisted amino acid films, with  $\alpha$ -cyclodextrin serving as the matrix, are shown to be useful means for obtaining their VCD spectra. Using this film method, VCD spectra in the 1800-1200  $\text{cm}^{-1}$  region were successfully measured for six amino acids. The absorption and VCD spectra for films are found to have a good correlation with the corresponding spectra obtained for aqueous solutions. The film method is advantageous, compared to the solution measurements, in obtaining the VCD spectra for amino acids in the mid-IR region, especially for those with low solubility in water. The VCD spectra of

L-methionine, L-histidine, L-phenylalanine and L-tryptophan are reported here in the mid infrared region for the first time. The matrix assisted film method greatly improves the role of VCD spectroscopy in the analysis of amino acids with low solubility in water and in obtaining the structural information of amino acids.

## References

1. (a) Barron, L. D. *Molecular Light Scattering and optical activity*; Cambridge Univ. Press, Second Edition, 2004; (b). Polavarapu, P. L. *Vibrational Spectra: Principles and Applications with emphasis on optical activity*; Elsevier:New York, 1998.
2. (a) Polavarapu, P. L.; He, J. *Analytical Chem.* **2004**, *76*, 61A-67A; (b). Freedman, T. B.; Cao, X.; Dukor, R. K.; Nafie, L. A. *Chirality* **2003**, *15*, 743-758; (c). Stephens, P. J.; Devlin, F. J. *Chirality* **2000**, *12*, 172-179.
3. (a) Polavarapu, P. L.; Zhao, C. *Fresenius' J. Anal. Chem.* **2000**, *366*, 727-734. (b) Keiderling, T. A.; Xu, Q. *Advances in protein chem.* **2002**, *62* 111-161; (c).Polyanichko, A. M.; Andrushchenko, V. V.; Chikhirzhina, E. V.; Vorob'ev, V. I.; Wieser, H. *Nucleic Acids Research* **2004**, *32*, 989-996; (d) Taniguchi, T.; Miura, N.; Nishimura, S.; Monde, K. *Mol. Nutr. Food Res.* **2004**, *48*, 246-54; (e). Shanmugam, G.; Polavarapu, P. L.; Kendall A.; Stubbs, G. *J. Gen. Virology* **2005**, *86*, 2371-2377.
4. (a) Diem, M.; Photos, E.; Khouri, H.; Nafie, L. A. *J. Am. Chem. Soc.* **1979**, *101*, 6829-37. (b) Nafie, L. A.; Oboodi, M. R.; Freedman, T. B. *J. Am. Chem. Soc.* **1983**, *105*, 7449-50. (c) Freedman, T. B.; Chernovitz, A. C.; Zuk, W. M.; Paterlini, M. G. ; Nafie, L. A. *J. Am. Chem. Soc.* **1988**, *110*, 6970-4; (d). Lombardi, R. S.; Cao, X.; Nafie, L. A. Poster #270, 16<sup>th</sup> International Symposium on Chirality, New York, **2004**.
5. Diem, M. *J. Am. Chem. Soc.* **1988**, *110*, 6967-70.
6. (a) Shanmugam G.; Polavarapu, P. L. *Biophys. J.* **2004**, *87*, 622-630; (b). Shanmugam, G.; Polavarapu, P. L.; Gopinath, D.; Jayakumar, R. *Biopolymers: Peptide Science* **2005**, *80*, 636-642.
7. (a) Shanmugam G.; Polavarapu, P. L. *Biophys. Chem.* **2004**, *111*, 73-77. (b) Shanmugam G.; Polavarapu, P. L. *J. Am. Chem. Soc.* **2004**, *126*, 10292-295.
8. (a). Petrovic, A. G.; Bose, P. K.; Polavarapu, P. L. *Carbohydrate Res.* **2004**, *339*, 2713-20; (b). Petrovic, A. G.; Polavarapu, P. L. *J. Phys. Chem.B* **2005**, *109*, 23698-23705.

9. Shanmugam G.; Polavarapu, P. L. *Applied Spectroscopy* **2005**, *59*, 673-681.
10. (a) Lewis, E. A.; Hansen, L. D. *J. Chem. Soc., Perkin Trans. 2*, **1973**, *15*, 2081-86;  
(b) Rekharsky, M. V.; Schwarz, F. P.; Tewari, Y. B.; Goldberg, R. N. *J. Phys. Chem.*, **1994**, *98*, 282-88. (c) Terekhova, I. V.; Parfenyuk, E. V.; Kulikov, O. V. *Russian J. General Chem.* **2002**, *72*, 1090-92.
11. "Handbook of Chemistry and Physics", 85<sup>th</sup> ed.; CRC Press: Cleveland, **2004**; p 7-1~2.
12. Nafie, L. A. *Appl. Spectrosc.* **2000**, *54*, 1634-45.
13. Biocell from BioTools Inc.; [www.btools.com](http://www.btools.com)
14. Carta R.; Tola, G. *J. Chem. Eng. Data*, **1996**, *41*, 414-417.

## CHAPTER VI

### EXPERIMENTAL VERIFICATION OF THE VALIDITY OF VAN'T HOFF'S PRINCIPLE OF OPTICAL SUPERPOSITION

#### **Introduction**

In 1875, van't Hoff referred<sup>1</sup> to a molecule made up of two similar asymmetric groups and stated that the optical rotation that each of these asymmetric carbon atoms contributes to the whole will be equal with either the same or opposite signs. In other words, the optical rotation contribution from a given asymmetric carbon atom is assumed to be independent of the other asymmetric carbon atom in the molecule. Thus the optical rotation of a molecule can be visualized as the sum of contributions from individual chiral centers. Later, in 1894, van't Hoff extended this assumption to molecules with several different asymmetric carbon atoms.<sup>2</sup> This concept is referred to as the principle of optical superposition (POS). Several researchers<sup>3-16</sup> have either assumed, or offered evidence for, the validity of POS in molecules made up of two or more asymmetric carbon atoms. Rosanoff<sup>6,7</sup>, however, questioned the validity of the POS. This controversy was attributed to the ignorance of vicinal action<sup>8</sup>. Thus the validity of POS has not yet been clearly established in the literature.

One approach to test the POS is to compare the optical rotation of a given molecule with the sum of the optical rotations of molecules that represent the fragments of that molecule. Since optical rotation is influenced by experimental conditions such as concentration and solvent, it is necessary to use the same experimental conditions for measuring the optical rotations of all different molecules involved. However, little attention was paid in the



past to maintain the same experimental conditions in testing or assuming the validity of POS. To rectify this situation we report here the first carefully designed systematic investigation of the POS.

To verify the validity of the POS we have synthesized (+)-ketoconazole **1**, the enantiomers **2** and **3** of 3,3,3-trifluoro-2-methoxy- 2-phenyl-1-piperidin-1-yl-propan-1-one, and the epimers **4** and **5** (see figure 6-1), which are very good candidates to examine the POS. Compound **4** can be thought as the assembled structure from **1** and **2** while its epimer **5** as the assembled structure from **1** and **3**. The chiral center of **2** or **3** is far away from chiral carbons of **1** in the assembled structure of **4** or **5**. We have chosen the same concentration, solvent, temperature and wavelength in the optical measurements of these compounds. To avoid the influence of solute-solute interactions, the limiting value of specific rotation at zero concentration of solute, referred as the “intrinsic rotation”, was measured and used for the investigation of the POS.

## Experimental

Compound **1**, **2**, **4** and **5** were synthesized and provided by Gal group (University of Colorado). These compounds were characterized by MS and NMR<sup>17</sup>. Peeters reported the crystal structure and absolute configuration for compound **1** and **4** recently.<sup>18</sup>

For optical rotation measurement, an Autopol IV polarimeter with a resolution of 0.001° (reproducibility of 0.002°) and analytic balances with accuracy of 0.00001 g were used. Optical rotations were measured at the wavelength of 589 nm.

Four compounds(**1**, **2**, **4** and **5**) were dissolved in CH<sub>2</sub>Cl<sub>2</sub> to obtain original solutions ( [c]=5mg/mL) for measurement of optical rotations. Then series of dilutions were done

from the original solution (dilution factor is 0.75 for compound **1** and 0.5 for compound **2**, **4** and **5**). After each dilution, optical rotation was measured. Each time the solution was transferred to a 1.0 dm cell and optical rotation was measured three different times to check for consistency. The averages of these measurements were used to calculate specific rotation. This procedure ensured that no unusual data scatter was present in the measurements.

Based on experimental results for compound **1**, **2**, **4** and **5**, plots of  $c$ (concentration) Vs.  $\alpha$ (observed rotation) and  $c$ (concentration) Vs.  $[\alpha]$ (specific rotation) were made and equation fittings were performed for each case. Normal least-squares fitting is appropriate for  $\alpha$  vs.  $c$  data, weighted least-squares fitting is needed for fitting the  $[\alpha]$  vs.  $c$  data. Intrinsic rotation ( $[\alpha]_{c=0}$  or  $\{\alpha\}$ ) can be obtained from these equations.

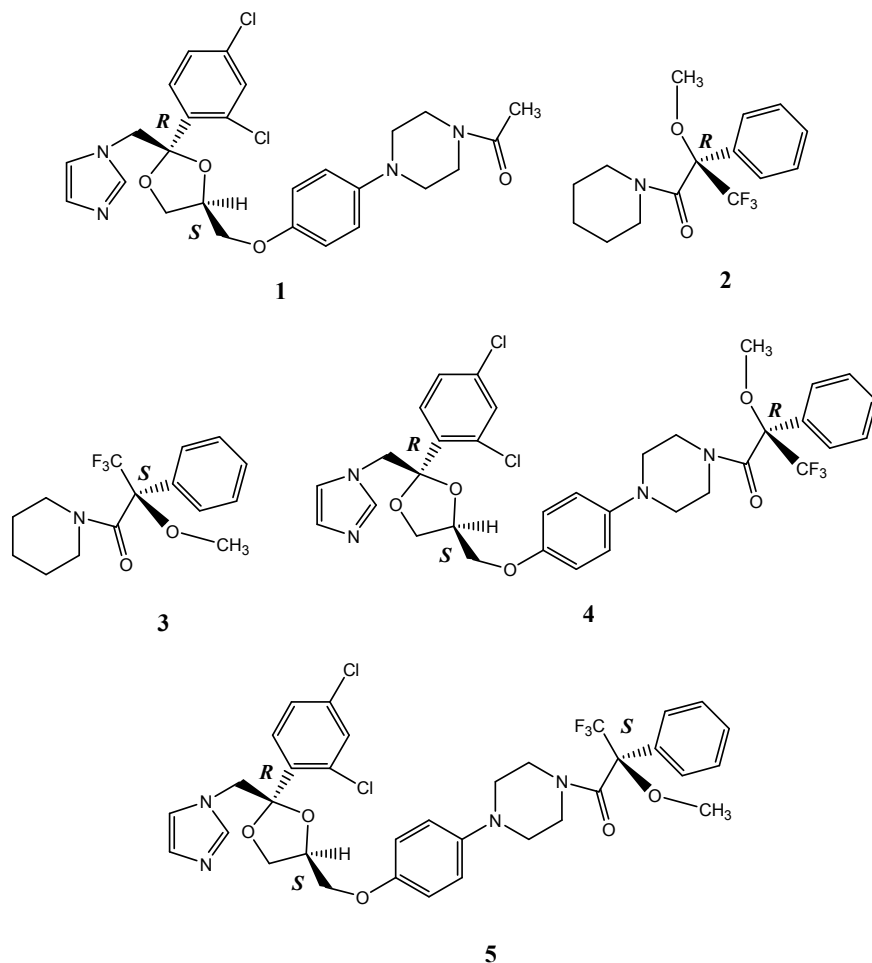


Figure 6-1. Structures of compounds 1-5.

## Results and discussion

Optical rotations were measured for **1**, **2**, **4** and **5** at exactly the same experimental conditions: room temperature, sodium D line, and concentration of 5 mg/mL in  $\text{CH}_2\text{Cl}_2$  solvent for their original solutions. For each case, intrinsic rotation was obtained by measuring specific rotation as a function of finite concentration and extrapolating the data to zero concentration (shown in Figure 6-2). The results of intrinsic rotations and their corresponding molar rotations are listed in Table 6-1.

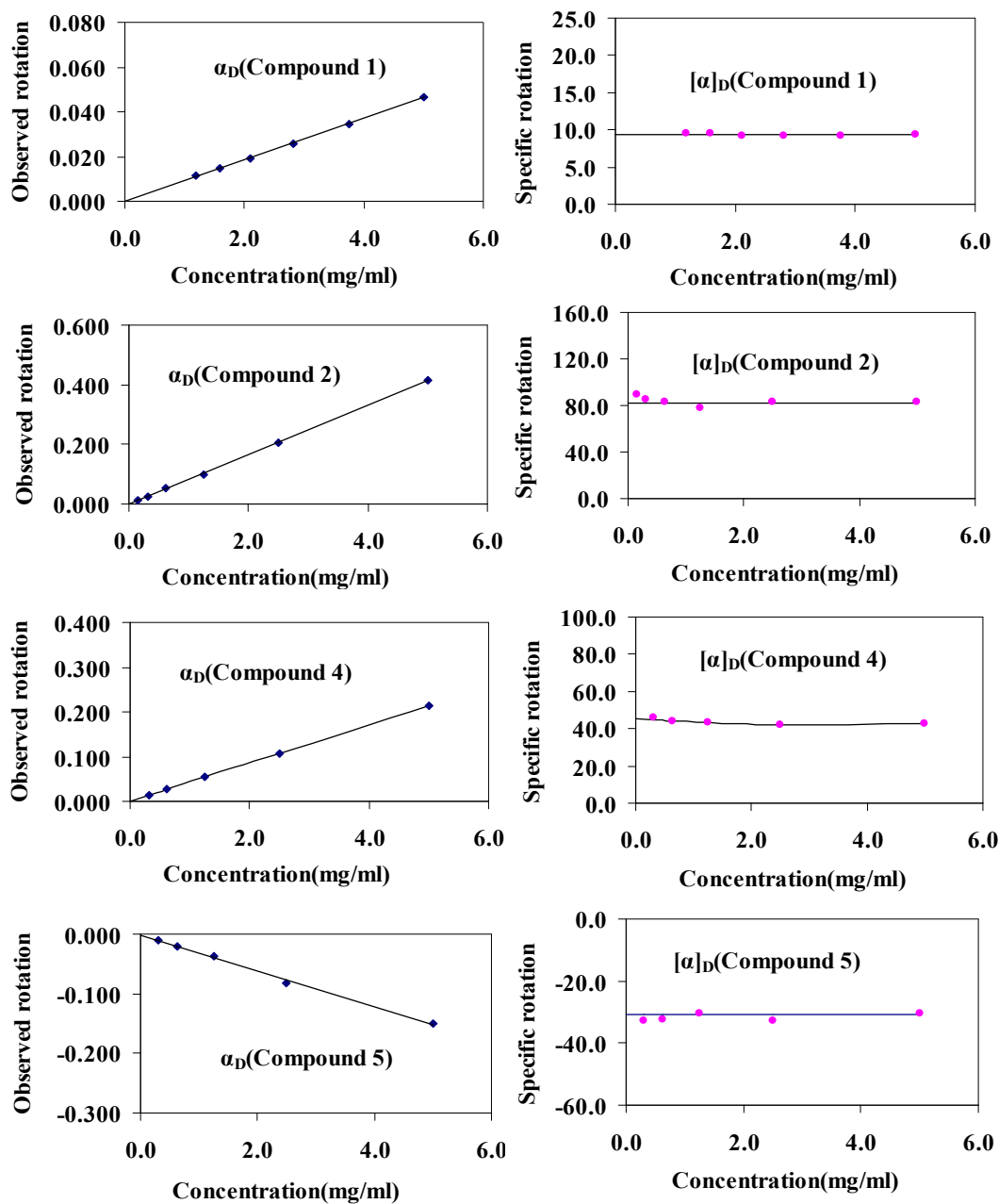


Figure 6-2. Observed rotation ( $\alpha_{589}$ ) and specific rotation ( $[\alpha]_{589}$ ) of compound **1**, **2**, **4** and **5**, as a function of concentration in  $\text{CH}_2\text{Cl}_2$  solutions. For compound **1**, a plot of  $\alpha_{589}$  versus concentration was fit to  $\alpha_{589} = 0.0093c$  and  $[\alpha]_{589}$  versus concentration is a constant;  $[\alpha]_{589} = 9.3$ . For compound **2**, a plot of  $\alpha_{589}$  versus concentration was fit to  $\alpha_{589} = 0.0826c$  and  $[\alpha]_{589}$  versus concentration is a constant;  $[\alpha]_{589} = 82.6$ . For compound **4**, a plot of  $\alpha_{589}$  versus concentration was fit to  $\alpha_{589} = 0.0452c - 0.00174c^2 + 0.000244c^3$  and  $[\alpha]_{589}$  versus concentration was fit to  $[\alpha]_{589} = 45.2 - 1.74c + 0.244c^2$ . For compound **5**, a plot of  $\alpha_{589}$  versus concentration was fit to  $\alpha_{589} = -0.0308c$  and  $[\alpha]_{589}$  versus concentration is a constant;  $[\alpha]_{589} = -30.8$ .

The POS can be interpreted to suggest that, at a given wavelength  $\lambda$ , the intrinsic molar rotation  $\{\phi\}_\lambda$  of a given molecule is equal to the sum of molar rotations of fragments that constitute the chemical structure of that molecule. That is,  $\{\phi\}_\lambda = \sum_i \{\phi_i\}_\lambda$ , where subscript  $\{\phi_i\}_\lambda$  represents intrinsic molar rotation at wavelength  $\lambda$  for  $i$ th fragment in the chemical structure of the molecule. For example, the intrinsic molar rotation of **4** can be viewed as the sum of those for the fragments A and B. Using the definition for molar rotation,  $\{\phi_i\}_\lambda = \{\alpha_i\}_\lambda \times M_i/100$  where  $\{\alpha_i\}_\lambda$  is the intrinsic rotation of fragment  $i$  at wavelength  $\lambda$  and  $M_i$  is the molar mass of that fragment, it follows that,  $\{\alpha\}_\lambda = \sum_i \{\alpha_i\}_\lambda \times M_i/M$  where  $M$  is the molar mass of the molecule of interest. The intrinsic rotations of fragments cannot be measured because fragments may not exist as such. However the intrinsic rotation for the parent molecules of those fragments can be measured. A necessary condition here is that a given fragment and its parent molecule exist in the same conformations and possess the same chiral elements. For example the parent molecules for fragments A and B of **4** are **1** and **2**, respectively. Then the intrinsic rotation of the fragment  $i$  can be cast in terms of that for its parent molecule  $p$  as,  $\{\alpha_i\}_\lambda M_i = \{\alpha_p\}_\lambda M_p$ . Thus,  $\{\alpha\}_\lambda = \sum_p \{\alpha_p\}_\lambda \times M_p/M$  or equivalently,  $\{\phi\}_\lambda = \sum_p \{\phi_p\}_\lambda$ . The experimental intrinsic optical rotations and those determined with the POS at 589 nm are summarized in table 6-1. For compounds **4** and **5**, the differences between the values predicted with the POS and the experimental values are found to be

less than 10%. This observation supports the validity of the POS for the molecules investigated.

Table 6-1 Comparison of the experimental rotations with those predicted with the principle of optical superposition

	Experimental		Predicted <sup>b</sup>		Error(%) <sup>b</sup>
	intrinsic rotation $\{\alpha\}_D(\text{obs.})$	intrinsic Molar rotation $\{\phi\}_D(\text{obs.})$	intrinsic rotation $\{\alpha\}_D(\text{calc.})$	intrinsic Molar rotation $\{\phi\}_D(\text{calc.})$	
<b>1</b> <sup>a</sup>	9.3	49.42			
<b>2</b>	82.6	248.88			
<b>4</b>	45.2	318.9	42.3	298.3	6.5
<b>5</b>	-30.8	-217.31	-28.3	-199.5	8.2

<sup>a</sup>molar masses of compounds **1**, **2**, **4** and **5** are, respectively, 531.44, 301.31, 705.56 and 705.56.

<sup>b</sup> $\{\alpha\}_D(\text{calc.})$  of compound **4** =  $(M_1/M_4) * \{\alpha_1\}_D + (M_2/M_4) * \{\alpha_2\}_D$ ; similarly,  $\{\alpha\}_D(\text{calc.})$  of compound **5** =  $(M_1/M_5) * \{\alpha_1\}_D - (M_2/M_5) * \{\alpha_2\}_D$ ;  $\{\phi\}_D(\text{calc.})$  of compound **4** =  $\{\phi_1\}_D + \{\phi_2\}_D$ ;  $\{\phi\}_D(\text{calc.})$  of compound **5** =  $\{\phi_1\}_D - \{\phi_2\}_D$ ; fragments A and B of compound **4** are shown in figure 6-3.

<sup>c</sup>error (%) = 100% \* ((obs.) - (calc.)) / (obs.)

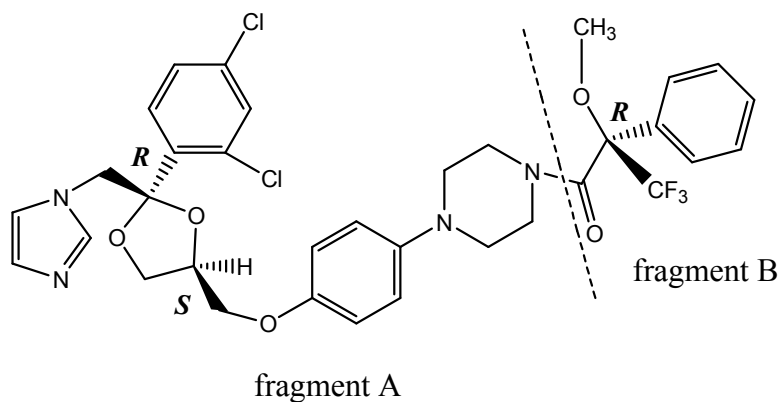


Figure 6-3. Two fragments of compound **4**.

## Conclusion

van't Hoff's principle of optical superposition (POS) was examined in a more careful and scientific way using using compounds **1**, **2**, **4** and **5**. The same experimental conditions were used for optical rotation measurements in all cases. By comparison between calculated molar rotations or intrinsic rotations based on the POS and their corresponding experimental values in both cases of **4** and **5**, it can be concluded that the POS is valid. And the POS will enable optical rotation technique to play more important roles in stereochemical analysis, especially in determination of absolute configuration of chiral centers in molecules.

## References

1. van't Hoff, G. H. *Bull. Soc. Chim. Fr.* **1875**, *23*, 295-301.
2. van't Hoff, G. H. *Die lagerung der Atome in Raum*; Branschweig: Vieweg, 1908.
3. Walden, P. *Z. Physik. Chem.* **1894**, *15*, 638-655.
4. Walden, P. *Z. Physik. Chem.* **1895**, *17*, 705-724.
5. Guye, A.; Goudet, M. C.P. *Acad. Sci. Paris.* **1895**, *121*, 827-829.
6. Rosanoff, M. A. *J. Am. Chem. Soc.* **1906**, *28*, 525-533.
7. Rosanoff, M. A. *J. Am. Chem. Soc.* **1907**, *29*, 536-539.
8. Eliel E. L.; Willen S. H. *Stereochemistry of carbon compounds*; McGraw-Hill: New York, 1962, pp110-114.
9. Carman, R. M. *Aust. J. Chem.* **1966**, *19*, 629-643.
10. Kondru, R. K.; Wipf, P.; Beratan, D. N. *J. Am. Chem. Soc.* **1998**, *120*, 2204-2205.
11. Shallenberger R. S. *Advanced sugar chemistry principles of sugar stereochemistry*, Ellis Horwood: Chichester, 1982; pp162-166.

12. (a) Hudson, C.S. *J. Am. Chem. Soc.* **1909**, *31*, 66-86. (b) Lowry, T.M. *Optical rotation power*. Longmans, Green and Co.:London. (c) Isbell, H S *J. Res. Natl. Bur. Stand.* **1937**, *18*, 505-534.
13. (a) Capon, R. J.; Ghisalberti, E. L.; Jefferies, P. R. *Aust. J. Chem.* **1981**, *34*, 1775-1778. (b) Capon, R. J.; Ghisalberti, E. L.; Jefferies, P. R. *Tetrahedron* **1982**, *38*, 1699-1703. (c) Butler, M. S.; Capon, R. J. *Aust. J. Chem.* **1992**, *45*, 1705-1743. (d) Capon, R. J. *Aust. J. Chem.* **1991**, *44*, 77-85.
14. (a) Kondru, R. K.; Beratan, D. N.; Friestad, G. K.; Smith, A. B.; Wipf, P. *Org. Lett.* **2000**, *2*, 1509-1512. (b) Wipf, P.; Uto, Y.; Yoshimura, S. *Chem. Eur. J.* **2002**, *8*, 1670-1681.
15. Hecker, S. J.; Heathcock, C. H. *J. Am. Chem. Soc.* **1986**, *108*, 4586-4594.
16. Kondru, R. K.; Lim, S.; Wipf, P.; Beratan, D. N. *Chirality* **1997**, *9*, 469-477.
17. NMR and Mass spectra are presented in the appendix.
18. (a) Peeters, O. M.; Blaton, N. M.; Gerber, J. G.; Gal, J. *Acta Crystallogr. E.* **2004**, *60*, O367-O369. (b) Peeters, O. M.; Polavarapu, P. L.; Zhang, P.; Gera, L.; Gal, J. *Acta Crystallogr. E.* **2006**, *62*, O191-O192.



## APPENDIX A

### MASS SPETRA

High resolution mass spectra of compounds **1**, **2**, **4**, and **5** in chapter VI were acquired at Vanderbilt University using a 4700 Proteomics Analyzer (Applied Biosystems, Framingham, MA) equipped with a Nd:Yag laser operating in reflector mode.

The compounds were mixed in equal parts with internal standards (10 pmol each of tubocurarine (MW=610.3) and the peptide AcGGGGKGGGR (MW=743.3) and the MALDI matrix, 2,5-dihydroxybenzoic acid (10mg/mL in 50:50:0.1 Acetonitrile/water/TFA). A 10 pmol aliquot of compounds **1**, **4** and **5** were analyzed and a 100 pmol aliquot of compound **2**.

Each sample was analyzed using 12 independent measurements. The resulting spectra were smoothed (Gaussian, 5pt), internally calibrated, and the peak of interest used for statistical analysis. The results are shown in the following:

	Compound <b>1</b>	Compound <b>2</b>	Compound <b>4</b>	Compound <b>5</b>
Theoretical mass	531.156	302.1362	705.1853	705.1853
Experimental	531.1544	302.1333	705.1856	705.186
	± 0.0024	± 0.0032	± 0.0037	± 0.0042
	-3.0311245ppm	-9.6976122ppm	0.4254201 ppm	0.9926469ppm

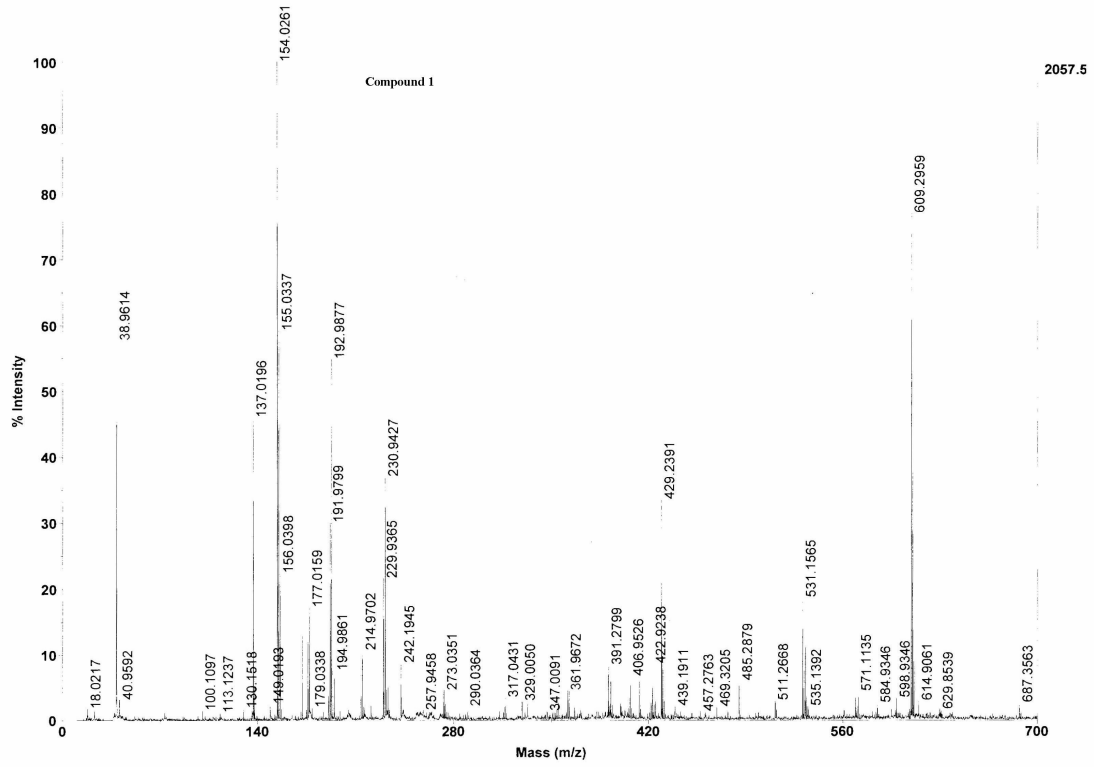


Figure A-1. Mass spectrum of Compound 1.

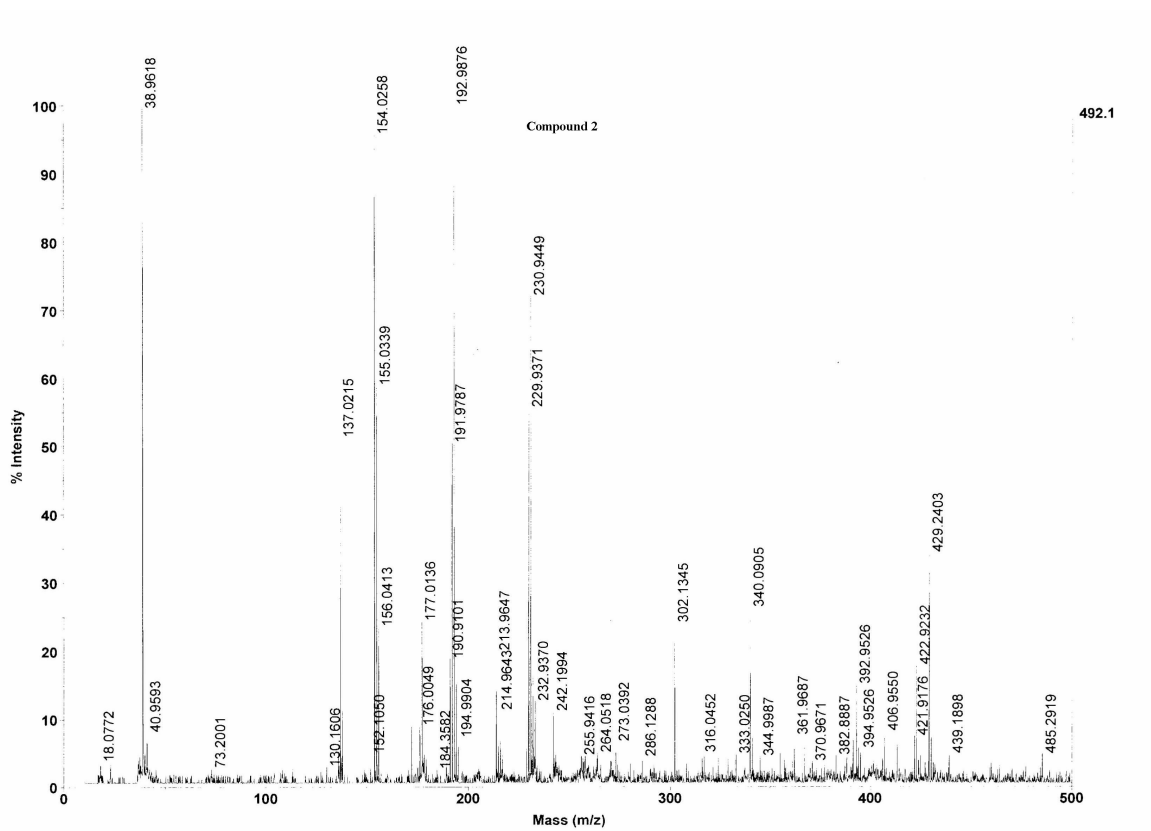


Figure A-2. Mass spectrum of Compound 2.

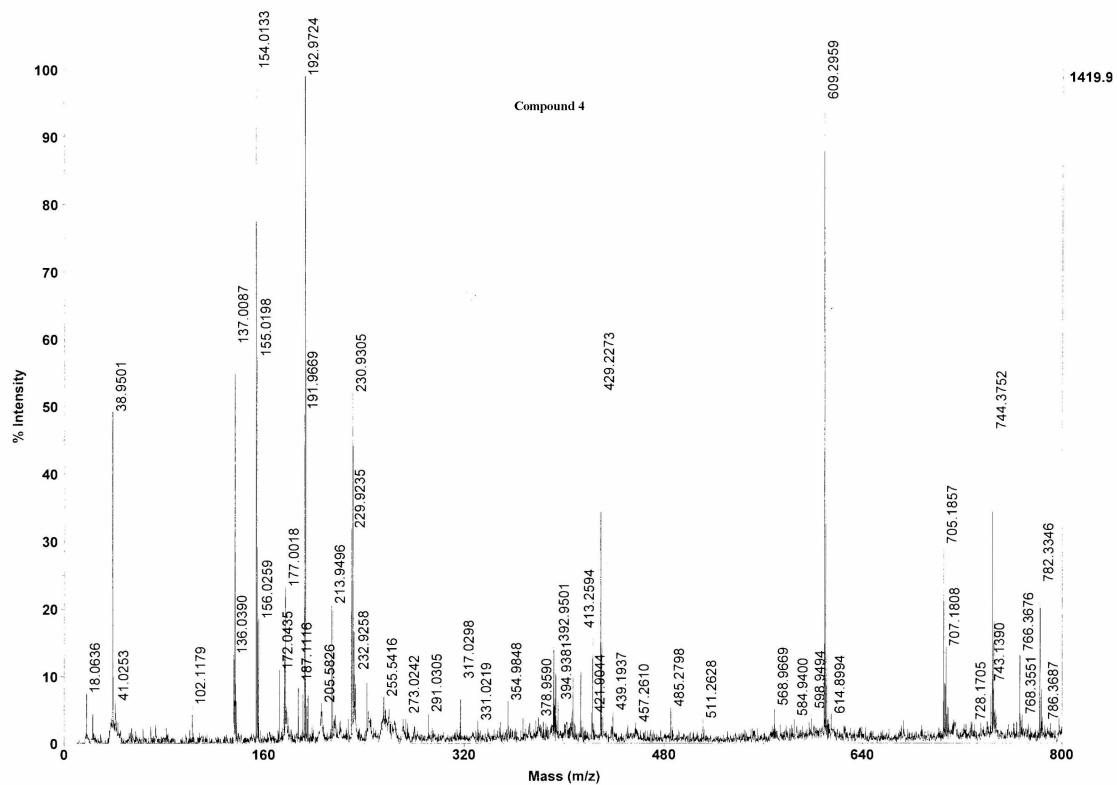


Figure A-3. Mass spectrum of Compound 4.

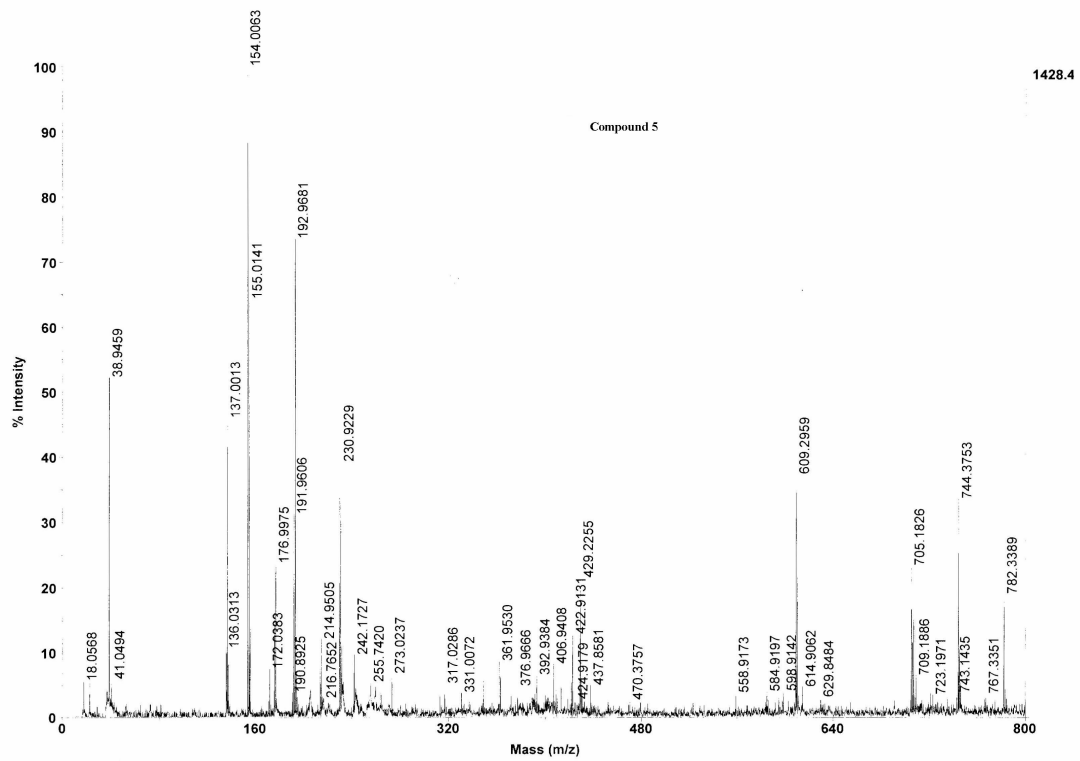


Figure A-4. Mass spectrum of Compound 5.

# APPENDIX B

## NMR SPECTRA

Proton NMR spectra of compounds **1**, **2**, **4**, and **5** in CHAPTER VI at the concentration of 1mg/mL in CDCl<sub>3</sub> were acquired at Vanderbilt University using 300 MHz Bruker Spectrometer.

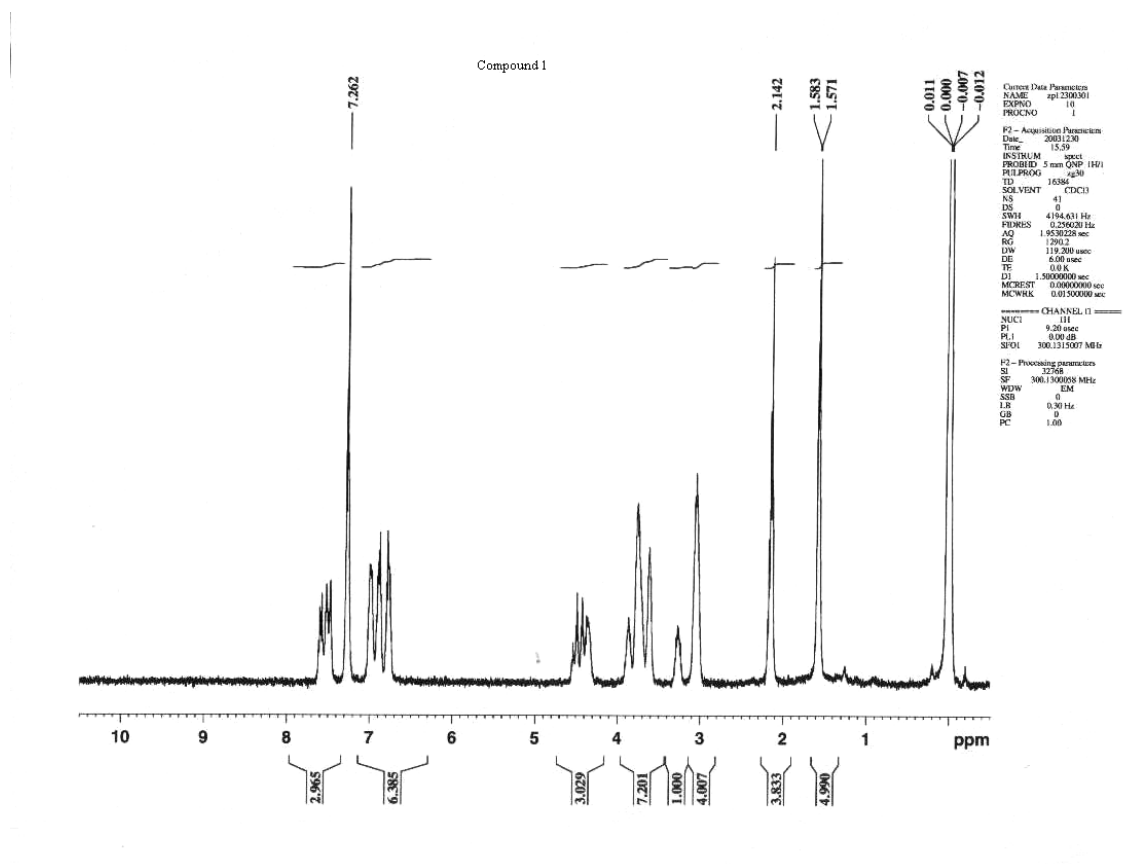


Figure B-1. NMR spectrum of Compound 1.

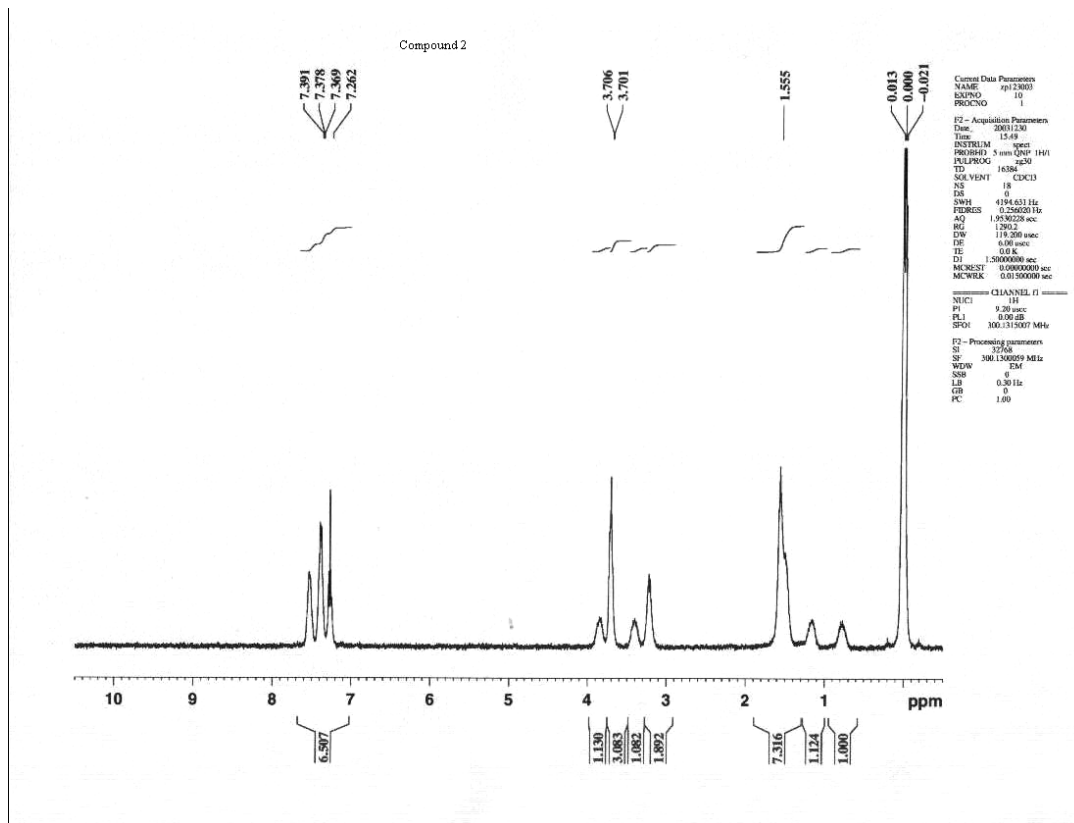


Figure B-2. NMR spectrum of Compound 2.

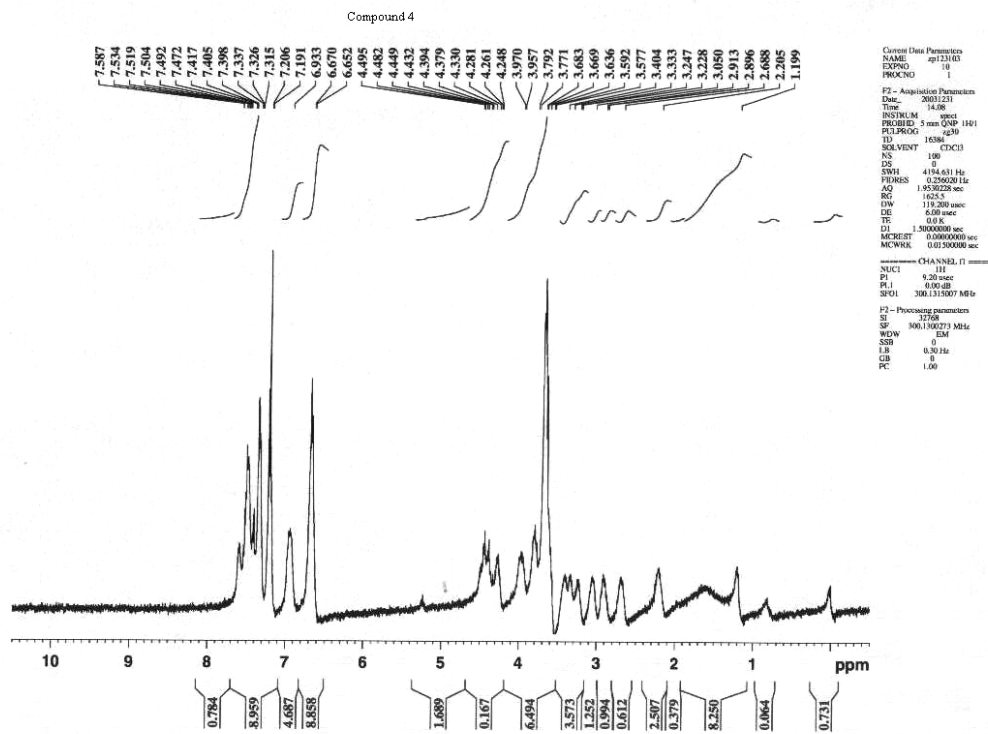


Figure B-3. NMR spectrum of Compound 4.



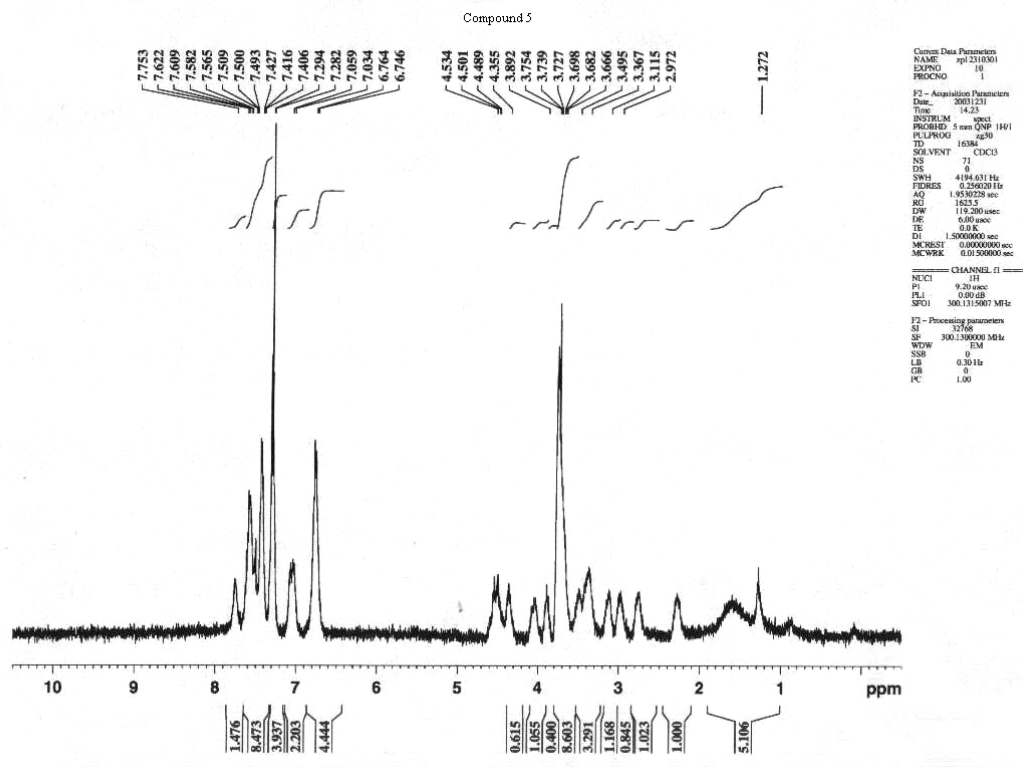


Figure B-4. NMR spectrum of Compound 5